Experimental and Computational Investigations on Fracture Behaviour of Extra Deep Drawn Steel Sheets in General Yield Regime

THESIS

Submitted in partial fulfillment
of the requirements for the degree of
DOCTOR OF PHILOSOPHY

by

CHAUDHARI VIKAS VINAYAK

Under the supervision of
PROF. D. M. KULKARNI

BIRLA INSTITUTE OF TECHNOLOGY AND SCIENCE, PILANI

2013

BIRLA INSTITUTE OF TECHNOLOGY AND SCIENCE, PILANI

CERTIFICATE

This is to certify that the thesis entitled **"Experimental and Computational Investigations on Fracture Behaviour of Extra Deep Drawn Steel Sheets in General Yield Regime"** and submitted by **CHAUDHARI VIKAS VINAYAK** ID No **2004PHXF446G** for award of Ph. D. Degree of the Institute embodies original work done by him under my supervision.

Signature of the Supervisor: _____

Name in capital block letters: **PROF. D. M. KULKARNI**

Designation: **Associate Professor,**

Mechanical Engineering Department.

In- charge, Computer Center,

BITS Pilani- KK Birla Goa Campus

Date:

ACKNOWLEDGEMENTS

ABSTRACT

Sheet metals have wide applications such as pressure vessels, auto components and aircrafts. Sheet forming processes are among the most important processes in manufacturing. Particularly these processes are important in the field of car body and auto components manufacturing, due to the fact that the tools are very expensive and any failure or redesign procedure dramatically increases the price of the products. Fracture phenomenon is one of the main obstacles affecting sheet metal forming as accurate prediction of fracture initiation is difficult in the forming processes. Numerous efforts are to predict accurate fracture limits of sheet metals by using formability approach. However, even today to prevent crack formation during forming process is a challenging task.

The phenomena of crack initiation and crack propagation are dealt within the discipline of fracture mechanics. Significant deformation ahead of crack tip plays an important role in crack initiation and crack propagation process. Extensive deformation ahead of a crack tip region has emerged a new discipline in fracture mechanics called general yielding fracture mechanics (GYFM).

Present study aims to evaluate fracture behaviour of Extra deep drawn (EDD) steel sheets using fracture mechanics approach to predict fracture limits accurately which will be beneficial to both, sheet metal manufacturer and their industrial users (product manufacturers). Amongst sheet metals, EDD steel sheets are widely used in auto components. There is an increasing demand in ensuring consistency in quality and avoid wastage of material during forming operations. Formability approach is being utilized to predict fracture limits (load at crack initiation and critical forming rate) for so many decades with numerous attempts made in improving the quality and ensuring the consistency in quality of EDD steel sheets.

Fracture mechanics approach is suggested to EDD steel sheet manufacturer to build a complete framework in which new methodologies of investigations correlating mechanical and fracture properties are used to determine fracture limits. In order to find out the fracture limits, fracture test and finite-element (cohesive zone model) simulation tool are proposed. With the help of the sophisticated fracture test and / or fracture simulation tool, manufacturers will be able to give data on the load at which crack initiates as well as critical forming rate, apart from basic

(mechanical and metallurgical) properties. This data would help the industrial user to ensure the consistency in quality and avoid wastage of material. In present work, TATA steel Jamshedpur has sponsored the EDD steel sheets, mechanical properties and data related to formability parameters.

The present attempt aims to generate more information and understanding on fracture behaviour of EDD steel sheets based on fracture parameters. In the present work, information on conventional indicators of formability parameters is obtained to study good deep drawing qualities. The fracture behaviour of EDD steel sheets is studied which falls in the regime of general yield.

After successive experimental attempts, 'load drop technique' is used as a fracture criterion. A few specimens are checked before load drop to verify the fracture criterion using thermal shock treatment. The J-integral is measured using area under load – load-line displacement curve obtained from fracture test. As the plastic load-line displacement is high in case of EDD steel sheets, crack flank opening angle (CFOA) method is proposed to find plastic crack tip opening displacement ($CTOD$), in addition to existing plastic hinge model (PHM) and FE analysis. CFOA method accounts for nonlinearities in the relationship between plastic $CTOD$ and plastic load-line displacements.

Finite element analysis incorporating cohesive elements used to verify experimental results. Cohesive zone model (CZM) is formulated to represent EDD steel sheets using compact tension (CT) specimens to verify planned objectives. The procedure to calibrate cohesive parameters in general yield regime is formulated. An alternative constant traction separation law is proposed to account for maximum load and large load line displacements. The results from proposed constant traction separation law are found to be close with the experimental findings. By using proposed traction separation law, the maximum load is overestimated only by 1.44% and corresponding J_i–integral based on load vs load line displacement (LLD) is 2.14% more than experimental value. The proposed constant traction separation law is found suitable in general yield regime.

The critical $CTOD$ values are found to increase with increase in thickness, this observation is found to be unlike that of thick plates (LEFM and EPFM regime). Influence of

notch radius on fracture toughness is studied. The fracture toughness remains independent of notch radius value up to 0.15 mm. However fracture toughness increases linearly with notch radius beyond 0.15 mm. With this study, it is recommended that fatigue pre-cracking, which is costly and time consuming job, is not essential in case of EDD steel sheets. The wire electric discharge machining (WEDM) process can be successively used for pre-cracking. Experimental findings as well as CZM shows that the strain rate has no significant effect on fracture toughness till the strain rate is 0.4 mm/min at room temperature; however, there is a sharp decrease in fracture toughness beyond 0.4 mm/min. Thus, it is concluded that the forming of the EDD steel sheet should be done at lower strain rates for high formability. Effect of a_0/W ratio on fracture toughness of EDD steel sheets is studied. It has been observed that as a_0/W ratio increases, the location of plastic hinge shifts towards the crack tip (i.e. size of tensile plastic zone reduces), which reduces fracture toughness. That is, the material is less resistant to crack growth for deeper cracks.

It is concluded that conventional indicators of formability alone are not sufficient to characterize the fracture behaviour of EDD steel sheets. The fracture mechanics approach enhances the understanding of the fracture behaviour.

TABLE OF CONTENTS

CHAPTER- 4

CHAPTER- 5

CHAPTER- 6

LIST OF FIGURES

LIST OF TABLES

LIST OF SYMBOLS

a_0	initial crack length
b	unbroken ligament length
A_{pl}	plastic area under load – load-line displacement curve
B	thickness of specimen
J	J-integral, a fracture parameter
J_i	J-integral at crack initiation
E	elastic modulus
J_{el}	elastic J integral
J_{pl}	plastic J integral
J_c	critical J integral
K	stress intensity factor
K_I	mode I, stress intensity factor
K_{Ic}	critical stress intensity factor
P_c	critical load
S_Y	yield strength
V_{el}	elastic load line displacement
V_{ll}	load line displacement
V_{pl}	plastic load line displacement
W	width of specimen
m	strain rate sensitivity index

n	strain hardening exponent.
r_0	strain ratio along 0° to rolling direction
r_{45}	strain ratio along 45° to rolling direction
r_{90}	strain ratio along 90° to rolling direction
$\bar{r}$	normal anisotropy factor
r_{pl}	plastic rotational factor
r_{pz}	plastic zone size
α	a_0/W ratio
β	factor to calculate plastic rotational factor (r_{pl})
η	geometry factor
δ_{el}	elastic CTOD
δ_{CI}	crack initiation *CTOD*
δ_{pl}	plastic *CTOD*
δ_c	critical *CTOD*
ε_u	ultimate strain
ρ	notch radius
v	Poisson's ratio
θ_{CT}	crack tip opening angle measured at current crack tip
σ_0	cohesive strength
k_P	penalty stiffness
Γ_0	fracture energy

δ_f separation distance

σ_{true} true stress

σ_{nom} nominal stress

ε_{nom} nominal strain

$\varepsilon_{ln}{}^{pl}$ logarithmic plastic strain

δ_1 separation distance at damage initiation

T_C thickness of cohesive elements

D damage variable

t^i_S separation distance

t^i_t stress component predicted by elastic-separation behaviour

t_0 elastic traction equal to cohesive strength

LIST OF ABBREVIATIONS

ASTM   American Society of Testing and Materials

BLD   before load drop

CI   crack initiation

CT   compact tension

CFOA   crack flank opening angle

CMOD   crack mouth opening displacement

CTOA   crack tip opening angle

CTOD   crack tip opening displacement

DD	deep drawn
EDD	extra deep drawn
EPFM	elastic plastic fracture mechanics
FC	fatigue pre-cracked
FE	finite element
FEA	finite element analysis
FLC	forming limit curve
GYFM	general yielding fracture mechanics
LEFM	liner elastic fracture mechanics
LLD	load-line displacement
RD	rolling direction
YS	yield strength
UTS	ultimate tensile strength
WEDM	wire electric discharge machine
CZM	cohesive zone model
TSL	traction separation law

LIST OF SUBSCRIPTS

CZM	cohesive zone model
CFOA	Crack Flank Opening Angle
PHM	Plastic Hinge Model

CHAPTER- 1

INTRODUCTION

The regimes of linear elastic fracture mechanics (LEFM) and elastic–plastic fracture mechanics (EPFM) are well developed for the proactive design of mechanical components and civil structures. However mechanical components made out of sheet metals are manufactured using deep drawn (DD) or extra deep drawn (EDD) steel sheets and by forming processes (like bending, stretching, drawing etc.). Numerous efforts have been taken to predict accurate fracture limits of sheet metals by using formability approach, however even today to prevent crack formation during forming process is a challenging task. With the help of the present characterization, there is no assurance in the consistency of quality control of components. The phenomena of crack initiation and crack propagation are dealt within the discipline of fracture mechanics. Significant deformation ahead of crack tip plays an important role in crack initiation and crack propagation process. Extensive deformation ahead of a crack tip has emerged a new discipline in fracture mechanics called general yielding fracture mechanics (GYFM). Mechanical components used in automobile industries, usually made out of EDD steel sheets involving simple to complex shapes which require high formability. EDD steel sheets because of their geometry and material property, fall into a regime of GYFM. Present work aims to evaluate fracture behaviour of EDD steel sheets using fracture mechanics approach to predict fracture limits accurately which will be beneficial to both, sheet metal manufacturer and their industrial users (product manufacturers).

1.1   Introduction to EDD Steel Sheets

Steel is one of the most commonly used metals in sheet metal industry because of its low price, excellent reliability and compatibility with most manufacturing techniques. Among the steel sheets, extra deep drawn (EDD) steel sheet is widely used in industrial applications. EDD steel has superior formability and non–ageing characteristics. These steels are low carbon, Al–killed steels. EDD steel is the most widely used material for automotive applications involving simple to complex products, which require very high formability. Exterior components such as car body, starter, end-covers, petrol tanks, etc. are made of EDD grade steel sheets. Apart from automobile industries, the EDD steel sheets are extensively used in enameling applications such

as bath sink units, kitchenware, cooker, washing machine and refrigerator bodies, etc. EDD steel sheets account for a sizable proportion of the manufactured goods produced and used by industries. In order to ensure the consistency in quality and avoid wastage of material, characterization of EDD steel sheet is important.

1.2   Present Practice of Quality Control of EDD Steel Sheets

The goal of every industry is to increase the performance of the manufactured product and reduce the manufacturing cost by reducing the wastage. Quality control of the EDD steel sheets is presently dependent on formability characterization approach. Steel sheets used for such applications are subjected to various types of forming operations depending on the desirable shapes. In industry, the performance of such operations is assessed in terms of formability indices. The formability characterization tests can be broadly classified into two groups namely: simulative tests and intrinsic tests. The simulative tests are empirical in nature whereas the intrinsic tests are fundamental or semi empirical in nature. In the simulative tests, the formability characterization can be accomplished by the employment of Erichsen cup test, hole-expansion test and Olsen cup test. In the intrinsic tests, the formability characterization can be accomplished by determination of either one or the combination of strain hardening exponent, strain rate sensitivity index, normal anisotropy factor and formability limit curves (FLC).

1.3   Need for Alternative Method

Forming processes are important in the field of car body and auto components manufacturing, due to the fact that the tools are very expensive and any failure or redesign procedure dramatically increases the price of the products. Fracture phenomenon is one of the main obstacles affecting the successful forming as accurate prediction of fracture initiation is very difficult in the forming processes of auto components. As a consequence, it is very important to avoid the failure situations from the design stage. This task can be achieved by adopting the most accurate and realistic procedures to find fracture limits. The realistic prediction of fracture limits can reduce the occurrence of failure during manufacturing as well as during the life period in application of product.

There is a need to understand the fracture behaviour in EDD steel sheets from the fracture mechanics point of view as fracture mechanics approach is a comprehensive solution addressing material, geometry, and 3 modes of fracture which are observed in forming operations.

1.4   Fracture Mechanics Approach

In the modern materials science, fracture mechanics is an important tool in improving the mechanical performance of materials and components [Cotterell (2002)]. Crack initiation and crack propagation phenomena are well described in fracture mechanics. Number of trials are required to find out maximum load and critical forming rate for crack initiation by using a formability approach. Industrial users (product manufacturers) are more concerned with the formation of cracks in thin sheets during as well as after the forming operations. The objective of the present investigation is to study the application feasibility of fracture mechanics in characterizing the quality of EDD steel sheets through experimental and finite element analysis.

1.5   Definition of the Problem

Forming operations like stretching, bending and drawing are used to manufacture complex shaped components out of EDD steel sheets which require high formability. During such operations, different locations of the component are subjected to tensile (mode-I) or shear (mode-II) or tear (mode-III) kind of fracture. There is an increasing demand from industrial users for an accurate assessment of crack initiation load and forming rate. Therefore, fracture resistance is an important issue from the perspective of wastage of material, consistency in quality of manufactured components out of EDD steel sheets. In the domain of fracture mechanics insufficient attention on studies related to fracture behaviour of EDD steel sheet metals originates from the fact that engineering materials with thinner sections are not considered as load bearing structural parts. Therefore, the problem of crack initiation and its subsequent propagation in thin steel sheets is not well defined in the domain of fracture mechanics.

Therefore, EDD steel sheets are now required to be characterized with the aid of data obtained from laboratory experiments that enable the fracture behaviour of sheet metals to be reliably predicted. Understanding of fracture behaviour of EDD steel sheet will help the

manufacturer as well as user for the successful production of quality products and reduce the wastage of raw material. Keeping above points in mind the present work is proposed.

1.6 Scope and Objectives of Present Work

Presently EDD steel sheet is characterized by formability approach. Good amount of improvements and research is observed in order to achieve better results on formability following formability techniques. Formability approach has well established procedures; however research is still going on using experiments and simulations to avoid wrinkles and cracks. There are certain limitations to predict fracture limits using this approach.

Based on the existing industrial practice, industrial demand and suggested alternative approach, following objectives are framed in order to ensure consistency in quality of EDD steel sheets.

1. To study the deep drawing qualities of EDD steel sheets from the formability point of view.
2. To present a simple experimental technique and study the fracture criteria for various combinations of material, geometry, loading and verify using FE analysis.
3. To examine the effect of thickness of EDD steel sheets on fracture toughness.
4. Predict most accurate data and realistic limits on load and forming rate in extra deep drawn steel sheets.
5. To examine the effect of notch root radius of EDD steel sheets on fracture toughness.
6. To examine the effect of a_0/W ratio of EDD steel sheets on fracture toughness.

1.7 Organization of Thesis

In order to present the subject matter in a logical order, present work is discussed in six chapters.

Chapter–1 addresses the importance of sheet metal characterization and need of fracture mechanics approach to characterize sheet metals, which fall in the regime of general yield. It also serves for the understanding of the present industrial practice to characterize fracture behaviour in EDD steel sheets and consequently defines the scope and objectives of research work. This Chapter also discusses the logical order of presentation of the thesis work in six chapters.

Chapter–2 reports the major aspects of the background pertaining to the present research work from recently published literatures. The content of this chapter is grouped under five major sections. The first section demonstrates the introduction and development of general yielding fracture mechanics. Second section covers the present characterization of thin sheets which fall into the regime of general yield. The same section also covers drawbacks of the present characterization. Third section discusses the status of characterization of thin sheets from the fracture mechanics point of view. Gap areas are defined in the fourth section in order to define the research problem. Fifth section deals with the selection of fracture parameters, test methods, their applicability and limits from the perspective of the characterization of fracture behaviour in the regime of general yield. This section also covers a literature on FE analysis.

Chapter–3 discusses about experimental procedures adopted to characterize fracture behaviour of EDD steel sheets which fall in general yield regime. Subsequent topics focus on investigation of fracture parameters with existing standards, methods and proposed methods to fulfill the planned objectives. The specimen specifications for various objectives are tabulated in details.

Chapter–4 presents the procedure adopted to perform the finite element analysis. It discusses about the formulation of suitable cohesive zone model (CZM) to characterize the fracture behaviour of EDD steel sheets loaded in Mode–I and to establish the main finite element attributes to be used in general yield regime. CZM is formulated with the help of finite element analysis software ABAQUS 6.7 to verify experimental results. CZM for the compact tension (CT) specimen is used to study the effect of the type of softening and cohesive parameters on the load versus load line displacement response in general yield regime.

Chapter–5 discusses determination of cohesive parameters and validation of cohesive zone model (CZM) with experimental observations. Subsequent topic focuses on the results obtained from the experiment and cohesive zone model (CZM) analysis. The results are summarized in tabular and graphical form. The discussion follows the results for various objectives. The results are discussed on formability indices and fracture behaviour. These results are discussed with reference to previously published journal papers, technical reports and conference proceedings.

Summary, conclusions, advantages of the present work and suggestions in design are discussed in Chapter–6. A few suggestions for future scope of work are also mentioned at the end of Chapter-6.

The List of Tables, List of Figures, List of Symbols, List of Abbreviations and List of Subscripts are presented after Contents. The References are cited in the text by author(s) name(s) with year of publication in parenthesis. In Reference section, the references are listed alphabetically by author's names, followed by initials, title of the article, name of the journal, year of publication, volume number, and numbers of first and last pages. The list of publications is shown after the Reference section. Appendices are labeled as A, B, C … etc. Various results on tensile tests, validation of CZM, additional observations and specifications of equipment and machines are included in Appendices. The brief biography of the supervisor and the student is given in the last two pages.

CHAPTER- 2

LITERATURE SURVEY

Introduction

This chapter reports the major aspects of the background pertaining to the present research work from recently published literatures. The content of this chapter is grouped under five major sections. Section 1 demonstrates the introduction and development of general yielding fracture mechanics. Section 2 covers the present characterization of thin sheets which fall into the regime of general yield. The same section also covers limitations of the present characterization. Section 3 discusses the status of characterization of thin sheets from the fracture mechanics point of view. Section 4 deals with the selection of fracture parameters, test methods, their applicability and limits from the perspective of the characterization of fracture behaviour in the regime of general yield. Section 4 also covers a literature on FE analysis. Gap areas are defined in section 5 in order to define the research problem.

2.1   Development of General Yielding Fracture Mechanics

Fracture mechanics provides a tool for assessing the criticality of flaws in structures. Linear elastic fracture mechanics (LEFM) is the basic theory of fracture, originated by Griffith and completed by Irwin, Rice and Riveros [Anderson (2005)]. In this regime, the crack driving force is measured by a parameter called stress intensity factor (K_I), is a function of applied stress, crack size and geometry of the component. One basic assumption in Irwin's linear elastic fracture mechanics is that size of the plastic zone is small compared to crack length. However, most engineering materials show some inelastic behaviour under operating conditions that involve large loads (e.g low carbon steel is not perfectly elastic but undergo significant plastic deformation at the tip of a crack). In such materials, the assumptions: LEFM breaks down and plastic deformation has to be considered in detail. Shortcomings of the LEFM approach led to efforts to seek other techniques that are suitable for materials with extensive plastic yielding. Two major approaches have been developed: crack tip opening displacement (*CTOD*) and *J*-integral under the new theory of fracture mechanics called elastic–plastic fracture mechanics (EPFM).

Fig 2.1 show broad regimes of fracture mechanics; LEFM, EPFM and general yielding. LEFM demonstrates basic theory of fracture mechanics and huge literature is available in this regime. Extensive literature is available for EPFM however there are some areas like driving force in weldments, residual stresses, three-dimensional effects, crack tip constraint, gross-section yielding and general yielding are unresolved in EPFM regime [Brighton and Christopherb (2012)].
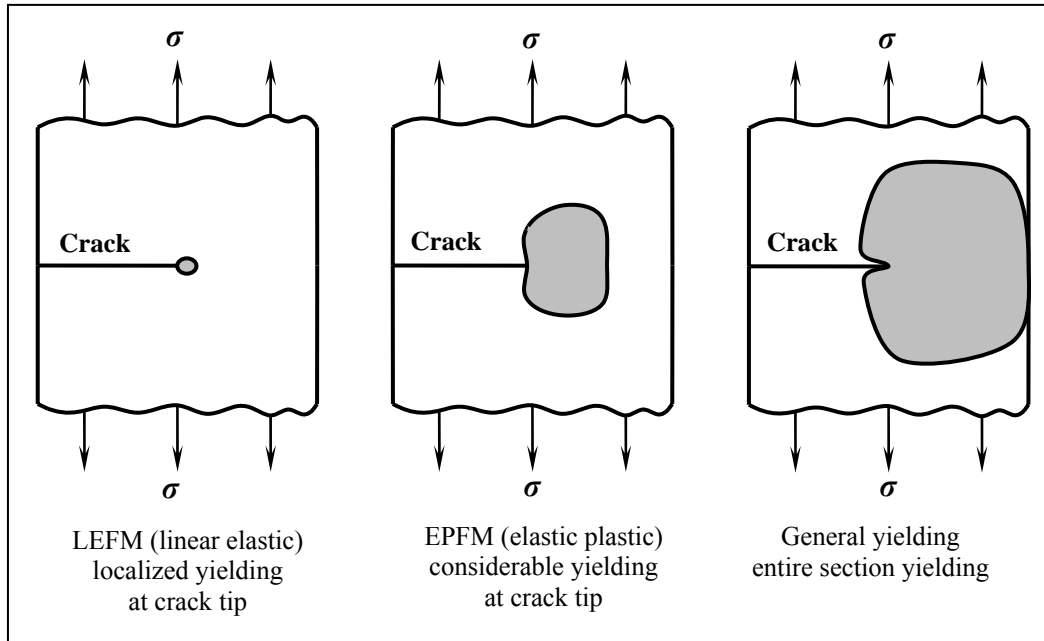
Fig 2.1 Regimes of fracture mechanics

In fracture mechanics, less attention has been paid towards the general yielding regime. The reason would be engineering materials with thinner sections are not considered as load bearing structural parts. Also, failure stress in this regime falls between yield strength and ultimate strength of the material, which is unlike LEFM and EPFM. Most of the fracture mechanics design concepts are applied to structural design where the failure stress is less than yield strength of material in presence of flaws. Fracture mechanics concepts can be explored for the situations where the working stress is above yield strength of the material e.g. forming operations (stretching, bending and drawing) of thin sheet metals. However different approach is being utilized to characterize the sheet materials which fall in the area of general yielding fracture mechanics (GYFM).

2.2 Present Characterization of Sheet Metals

The goal of every industry is to increase the performance of the manufactured product and reduce the manufacturing cost by reducing the wastage. Quality control of the sheet metals is presently dependent on formability characterization approach. Sheet metals used for such applications are subjected to various types of forming operations such as stamping, drawing, deep drawing, hydro-forming etc depending on the desirable shapes. In industry, the performance of such operations is assessed by formability characterization in terms of formability indices. The formability characterization tests can be broadly classified into two groups namely: simulated tests and intrinsic tests. The simulated tests are empirical in nature whereas the intrinsic tests are fundamental or semi empirical in nature. Steel, copper, aluminum and their alloys are most frequently used materials for formed parts. Low carbon steel (up to 1.5 % Carbon) is generally used for forming operations and being referred as deep drawn (DD) or extra deep drawn (EDD) steel sheets.

According to TATA steel, information about the formability of thin metal sheet is important to both, sheet manufacturers as well as industrial users. From the manufacturer's point of view, the most significant is the knowledge of the characteristics of the sheet metal correlated to its formability and fracture behaviour. From the industrial user's point of view, it is important to be able to select the semi-product that allows him to obtain finished products of definite size and shape without difficulties. Therefore, an understanding of the formability of sheet metals is essential for the production of quality components.

According to Singh *et al* (2010), Padmanabhan (2007), Fekete (1997), Hosford and Caddell (1993), sheet metal forming is a technique by which most body parts are produced in automobile industries. In sheet metal forming, a thin blank sheet is subjected to plastic deformation using forming tools to conform to a designed shape without failure, which is an important aspect of the sheet metal to produce complex sheet metal components. Many factors such as mechanical and metallurgical properties, die and punch geometry, lubrication, sheet thickness, sheet roughness, punch speed, etc. contribute to the success or failure of the stamping to varying degrees in an interdependent manner. The basic modes of forming a sheet metal are: stretching, drawing and bending. The primary difference between these forming modes originates from the nature of the strains imparted in the different directions in a sheet due to the

forming operation. Stretching implies a forming process in which the strains along the principal directions in the sheet plane are tensile; while in drawing, a sheet is subjected to compressive strain in the circumferential direction together with tensile strain in the radial direction. Bending, the most common amongst the three is associated with tensile stresses on the outer surface along with compressive stresses on the inner surface of the deformed sheet.

The term formability of sheet metal can be defined as the relative ease with which a sheet can be shaped through plastic deformation. Sheet metal formability is influenced by several process variables and material variables. The process variables determine the constraints of the forming process, while the material variables reflect the tendency of the material to deform easily. The process variables depend on the mode of forming whereas the material variables are of generalized nature for all the different modes. Different variables affecting the formability of sheet metals are discussed in the following sub section.

2.2.1 Variables Affecting Formability

2.2.1.1 Process variables

According to Padmanabhan (2007), Haung and Leu (1998), the prominent process variables are punch and die geometry, punch and die configuration, degree of lubrication, type of lubricants and clearances. During forming process, the blank sheet is likely to develop defects if the process parameters are not selected properly. Therefore, it is important to optimize the process parameters to avoid defects in the parts and to minimize production cost. Optimization of the process parameters such as die radius, blank holder force, friction coefficient, etc., can be accomplished based on their degree of importance on the sheet metal forming characteristics. Colgan and Monaghan (2003), Duan and Sheppard (2002), Lee (2002), Koa *et al* (1999), Koa *et al* (1998), Chen *et al* (1997), Park and Kim (1995) used a statistical approach based on Taguchi technique to determine the degree of importance of each of the process parameters on the thickness distribution of deep drawn circular cup. They have used three levels of process parameters to capture the non–linear effects in the experimental design.

Fracture and wrinkle are the two major modes of failure in sheet metal parts. Hence, using proper blank holder force is an essential criterion to restrict wrinkling tendency and avoid tearing of the blank sheet. Yoshihara (2005), Sheng(2004), Krishnan and Cao (2003),

Gunnarsson and Schedin (2001), Obermeyer and Majlessi (1998), Traversin and Kergen (1995) have reported that the blank holder force plays vital role as per as failure modes (i.e. Fracture and wrinkle) are concerned. They have suggested different blank holder force application scheme to eliminate these failure modes.

In addition to the blank holder force, the die radius and the friction coefficient control the metal flow into the die cavity in deep-drawing process. The flow of material into the die cavity reduces with small die radius while a large die radius lead to wastage in trimming excess material and induces springback characteristic [Verma and Chandra (2006), Duchêne and Habraken (2005), Leu (1999)]. An appropriate die radius allows smooth flow of materials on one hand and reduces springback and material wastage.

2.2.1.2 Material variables

The dependence of material formability on a particular mechanical property is a characteristic of the deformation mechanics of the forming process employed. For example hardening exponent is an indicator of stretchability, anisotropy is an indicator of drawability and percent reduction in area at tensile fracture is an indicator of spinnability in shear forming with some exceptions [Hussain *et al* (2009), Jackson and Allwood (2009), Fratini *et al* (2004), Hangan and Jeswiet (2003), Kegg (1961)]. The yield strength (S_y), modulus of elasticity (E), strain hardening exponent (n), strain rate sensitivity index (m), and normal anisotropy factor ($\bar{r}$) are the principal material variables that affect the formability of a sheet metal. Kumkum Banerjee (2007) performed textural and microstructural studies on cold–rolled batch annealed interstitial free-Ti (IF-Ti) stabilized steel and EDD steel. It has been found that both, IF-Ti steel and EDD steel contain α-fiber, which is not desirable for deep drawing applications. She has suggested that the deep drawability of both steels can be improved by modifying the rolling and annealing parameters. The good deep drawing qualities are specified in ASTM standard E8M-11 (2011) and E517-00 (2010). Based on these standards, following are the discussions on individual variables.

Yield strengths should be low enough so that it can be exceeded by the applied stresses in all localized regions during the forming process. Modulus of elasticity should be high enough to keep the elastic spring-back to a minimum. Elastic spring back is the elastic recovery, which

11

decides the final shape. Strain hardening exponent signifies the intrinsic ability of the material to harden with plastic deformation, which is of tremendous importance in sheet metal forming. Higher value of n ensures a region undergoing thinning can resist further deformation, and can spread the deformation to its neighboring region. This process promotes uniform thinning. The important requirement for good formability is not only a high value of n but also maintaining it up to a large strain. Strain rate sensitivity (SRS) index is defined as an increase in flow stress with increase in strain rate. The values of SRS index for most of the cold forming materials are small (≈ 0.05). However, the presence of even a small value of SRS index (e.g. 0.015 in low carbon steel) can be responsible for about 50% of the total elongation to failure. Anisotropy is difference in behaviour of material in different loading directions. Anisotropy is present not only in the plane of sheet, but also in its thickness direction. The former is called planar anisotropy and the latter is called as normal or plastic anisotropy. Anisotropy should be high enough for good formability.

2.2.2 Formability Tests

Different tests have been developed with time for evaluating sheet metal formability. Formability characterization of materials is done either by using intrinsic tests or by carrying out simulative tests. The intrinsic tests attempt to measure some basic mechanical properties, which can be related to the formability of the material. On the other hand, by using simulative tests, attempts are made to achieve some engineering information about a particular forming process mostly on an empirical basis. Following are the brief discussions on intrinsic and simulative tests.

2.2.2.1 Intrinsic tests

The most widely used test is, plotting forming limit curve (FLC), which represents the acceptable limits of strains (in a plot of the principal major (ϵ_1) and minor (ϵ_2) strains in a sheet metal) as per the ASTM E2218-02 (2008). The combination of principal major and minor strains leads to failure during forming. Keeler (1963, 1965) and Goodwin (1968) pioneered the construction of plotting FLC. The FLC is evaluated following Hecker's (1972) simplified technique. In this method, the experimental procedure mainly involves three stages: marking of grids in the sheet specimens, punch-stretching the grid-marked samples to failure or onset of

localized necking and measurement of strains. In this test, the goal is to measure fracture strain in thin sheets. It is well known that these experimental procedures are costly both in time and effort. Therefore theoretical methods were introduced to compensate for the experimental methods. The conventional theoretical methods used to predict localized necking are basically of two types: 1) M-K method, and 2) Linear Method. Both theoretical methods of prediction of FLC are found to be inefficient [Alsaati *et al* (2006)]. A series of modifications have been introduced on these methods in order to produce FLCs that are consistent with experimental curves. The FLD is very useful in FEM analysis, die design optimization, die tryout, and quality control during production [Stoughton and Zhu (2004)]. Wang and Lee (2006) reported ductile fracture criterion to predict the forming limits. Based on this criterion, the occurrence of ductile fracture is estimated using the macroscopic stress and strain that occurs during deformation. As mentioned by Djavanroodi and Derogar (2010), to predict the FLD requires complex calculations and this will limit their use in practical applications. Furthermore, a general model that can be applied for various sheet metals has not been proposed.

2.2.2.2 Simulative tests

According to Wu *et al*. (2000), the Erichsen and Olsen cup tests are the most popular simulative tests for formability characterization. In these tests, a specimen is stretched using a hardened steel ball and the height of the cup thus produced is measured. In these tests, the engineering criterion of interest is to determine the maximum load at which a crack initiates.

According to Haung and Leu (1998), the test results are significantly influenced by the size of the penetrator, degree of lubrication and rate of drawing, and hence, careful control of these parameters is a pre-requisite. Another simulative test is the hole-expansion test. In this test, a flat sheet specimen with a circular hole in the centre is clamped between two annular die plates and deformed by a punch, which expands and ultimately cracks the edge of the hole. Flat bottomed, hemispherical and conical punches have been used. The test is terminated when a visible crack is observed and the hole-expansion is expressed as the percentage increase in the hole diameter.

2.2.3 Limitations of Formability Characterization

From the extensive literature review, it is clear that the traditional industrial approach of characterizing steel sheets carries some limitations. As mentioned by Granzow and Armco (1990), the term formability is commonly used to describe the ability of steel to maintain its structural integrity while being plastically deformed into various shapes. However, not all shapes require the same forming characteristics, and steel that has excellent formability in one application may exhibit poor formability in another application. In practice, therefore, formability must be optimized by selecting a grade of steel that has the forming characteristics needed to make the required shape. Forming characteristics are normally estimated from an analysis of the mechanical properties of steel, which are determined by uniaxial tensile tests. According to Ozturk *et al* (2008), merely mechanical properties do not simulate any commercial forming operations. However, such properties have been universally used to evaluate formability.

The principle of the formability limit curves (FLC), as per the ASTM E2218-02 (2008), attempt to search for an engineering parameter, which indicates the mechanical environment for crack initiation and/or crack propagation under corresponding experimental conditions. The assessment of different parameters by this test primarily seeks to ascertain the safe limits up to which a sheet metal can be deformed without crack initiation or its subsequent propagation. However, according to Ravilson *et al* (2009), Park *et al* (2008), and Wu *et al*. (2000) construction of FLC is tedious and time consuming and consequently limited in engineering applications. Since the measurements involve some amount of subjective judgment in defining necking, a band of ± 2% in engineering strain values is drawn instead of a single line. As mentioned by Zhongqi *et al* (2007), due to the defect of low ductility of aluminium alloy sheets, fracture often occurs before necking instability. Therefore, the conventional forming limit curves based on the tensile instability which can predict the forming limit is not exact to evaluate the formability of aluminium alloy sheet. According to Isik *et al* (2011), despite their wide application in sheet metal forming analysis, Forming Limit Curves cannot supply reliable results and fracture criterion appears as a complimentary tool for the assessment of fracture limit.

According to Ravilson *et al* (2009) and Ravikumar (2002), while forming a sheet into a specific shape, material variables and process variables have greatest influence on the overall

formability and are usually assessed during die tryout. The material variables are: yield strength, ultimate tensile strength, modulus of elasticity, strain rate hardening exponent, strain rate sensitivity, plastic anisotropy factor, etc. The process variables are: punch and die geometry, degree of lubrication, clearances, etc. In addition to this, process variables depend on the mode of forming. However, due to the complex interaction of large number of variables, which affect formability of sheet metals, several factors are required to be considered to describe the forming characteristics of a material.

According to Rao and Mohan (2000), measure of cup depth and hole-expansion in simulative tests is an empirical basis because cup depth or hole-expansion brings out a relative engineering index for formability. However, these tests lack any fundamental scientific basis in such quantitative measurement. The use of Olsen or Erichsen cup tests in association with FLC constructions is an appropriate solution for characterising the quality of sheet metals. However, from the engineering applications point of view, it leads one for the search of alternative criterion for obtaining fracture limits of sheet metals.

As mentioned by Dorel (2008), with the application of new forming techniques (hydro-forming, incremental forming), it is necessary to improve the characterization of the formability of materials. A good understanding of fracture behaviour of the material during forming is necessary to industrial user as well as to manufacturer to use these techniques successfully for the successful production of quality products.

2.3   Fracture Behaviour in Thin Sheets

A few attempts have been made in the past to ascertain the fracture criterion and determine fracture toughness of thin sheets, but all these are in embryonic stage [Ray *et al* (2010)]. The feasibility of application of fracture mechanics in characterizing the quality of steel sheets through experimental analysis is explored by Ray *et al* (2010 & 1995), Kulkarni (2005) Amongst the past attempts, the one suggested by Cotterell (1977) and later refined by Pardoen *et al* (1999) is more widely used; the principle of this technique considers essential work of fracture (w_e) as the fracture criterion. Liu *et al* (1978) have proposed that thickness contraction ahead of a crack tip at the instance of crack initiation can be considered as a fracture toughness criterion for sheet metals. A few investigations [Pardoen (2004), Pardoen (1999), Mai (1986)] have

considered the use of *J*- integral technique to estimate fracture toughness of thin sheets. However few papers have been found related to fracture behaviour of thin sections as reported below.

According to Liu (1981), Liu and Kuo (1978), Liu and Ke (1976), the basic principle for obtaining fracture criteria of thin and tough sheets / plates is related to examinations of a strip necking zone which remains embedded inside the plastic zone ahead of a crack tip in a deformed specimen. These investigators have contended that such strip necking phenomenon is governed by the ratio of the plastic zone size and the plate thickness (*B*), and they concluded that a physical parameter $(K/S_Y)^2/B$ controls the occurrence of crack tip necking. The parameter henceforth will be referred to as the strip necking parameter. In addition, Liu and Kuo (1978) and Liu (1981), have observed that the crack tip opening displacement in the strip necking zone is equal to the thickness contraction at the crack tip as given by Eq. (2.1) for HY-80 steel.

$$CTOD = \delta_n = \varepsilon_z.B \qquad (2.1)$$

where, δ_n is thickness contraction at the crack tip and ε_z is strain in thickness direction. The *CTOD* in turn is related to the stress intensity factor. The estimation of the stress intensity factor for tough and thin plates by Liu (1981) has been carried out following the Dugdale model (1960), using the relationship (Eq 2.2):

$$\frac{K^2}{E} = S_y.CTOD = S_y.\delta_n \qquad (2.2)$$

The salient conclusions of Liu's reports (1981) indicate that the near tip strain or crack tip contraction can be used as a fracture criterion. The replica technique is used for the detection of crack tip necking and Moire fringe technique is used for the detection of crack tip opening displacement. However, these techniques could not become popular, as they are too elaborate in nature to employ them for quality control of sheet metals in terms of fracture mechanics based criteria. In addition, these investigations have not indicated any rationale for detecting the physical event of crack initiation.

Atkins and Mai (1987) have proposed a relationship between the specific work on fracture obtained from test pieces incorporating starter cracks and the work required locally to nucleate a crack in flawless thin sheet metals. According to him, the failure of thin sheets during

forming occurs first by localized necking, which is then followed by fracture inside the neck. Problems of the effect of necking preceding fracture are also studied by Atkins (1997, 1995 and 1993). Das *et al* (2011) investigated the fracture resistance of cryorolled Al 7075 alloy. They found a significant increase in yield strength and fracture toughness of the cryorolled Al alloy samples due to high density of dislocations and grain refinement. However, these investigations address towards the plane strain fracture toughness. Pardoen *et al* (2004), Pardoen *et al* (2002, 1999), Blyth and Atkins (2001) and Marchal and Delannay (1996) studied mode–I fracture under plane stress condition by using certain materials (e.g. stainless steel, mild steel, 6082-O and NS4 aluminium alloys, brass, bronze, lead, and zinc). They have reported that fracture toughness increases with size of the specimens (i.e for lower range of thicknesses) and then decreases gradually to the plane strain fracture toughness (i.e. for higher rage of thicknesses). This behaviour of an increasing toughness at small thicknesses is mentioned in most fracture mechanics textbooks (e.g. Anderson, 2005; Broek, 2002; Broberg, 1999; Atkins and Mai, 1985) but usually not explained.

Ray *et al* (2010) have confirmed the load drop point is a fracture criterion for industrially processed Ti-stabilized interstitial free (IF) steel sheets. They have studied IF steel sheets with thicknesses 1.6, 1.2 and 1.0 mm and found that the fracture toughness decreases with decreasing thickness in case of IF steel sheets. According to Ray *et al* (2010), this is expected variation of this criterion with specimen thickness in general yield regime.

2.4 Review on Test Methods

For a complete fracture study, fracture criterion, selection of suitable fracture parameters and selection of proper test methods to measure fracture parameters are essential. According to Anderson (2005), the *J*-integral and *CTOD* are the suitable parameters to describe crack tip conditions in elastic-plastic materials. However, the existing fracture criterion, test methods need to be reviewed and modified in order to understand the significant deformation ahead of crack tip. Following sub-sections discuss on available fracture criteria, ASTM standards, test methods and their applicability or limitations to the present problem.

2.4.1 Fracture Criterion

Present study deals with the fracture behaviour in general yield regime. In order to understand the fracture behaviour in the general yield regime, extra deep drawn (EDD) steel sheets are chosen as discussed earlier. In case of EDD steel sheet applications, it is very essential to predict accurate value of crack initiation toughness. Thus, these data could be used to design any critical components. The analyses of the load – load-line displacement curve are generally used to determine the load at crack initiation.

The most pertinent way to determine fracture toughness value at cracking initiation in ductile materials is metallographic observation of the crack tip after fracture test. Therefore, physical event of cracking initiation as well as an accurate definition of cracking initiation needs to be defined in case of EDD steel sheets. Recently Ray (2010) and Kulkarni (2005) investigated 'load drop technique' as a fracture criterion, after number of trials and errors. This is verified with the help of various metallographic tests.

2.4.2 *J*-integral Estimation Methods

Chen *et al* (2007), Chao and Sutton (1994) and Yang *et al* (1993) have shown, for mode-I loading, that two parameters, J and $A2$ (where J represents the level of loading and $A2$ quantifies the level of constraint), are needed to characterize the crack-tip fields at initiation of crack growth. Hutchinson (1968) and Rice and Rosengren (1968) independently showed that J-characterizes crack tip conditions in non-linear elastic material. The analysis, which leads to the HRR (Hutchinson, Rice and Rosengren) singularity neither consider the effect of the blunted crack tip on the stress fields, nor it take into account of large strains that are present near the crack tip. The standard, ASTM E1820-11 (2011), outlines a test method for estimating the critical J near initiation of ductile crack growth in elastic-plastic materials. This standard is described in detail in Chapter-3 and is proposed to validate the experimental results with FE analysis for the present study.

2.4.3 *CTOD* Estimation Methods

Experimental studies have shown that a critical Crack Opening Displacement (COD) has the potential to be a viable parameter for predicting the onset of crack growth in thin sheet 2024-

T3 aluminum [Sutton *et al* (2000) Amstutz *et al* (1997), Amstutz *et al* (1995) and Dawicke and Sutton (1994)]. According to Ray *et al* (2010), *J*- integral concept is valid only when *J* dominance is maintained. To overcome these limitations they examined the feasibility to estimate critical crack tip opening displacement (*CTOD*) based on some specified value of load drop during the fracture test.

There are a number of alternative definitions of *CTOD*. The displacement at the original crack tip is given by Wells (1961) and 90° intercept is given by Rice (1968). The former method requires a profile projector to superimpose the crack geometry before and after fracture test and find out the *CTOD* at original crack-tip. In 90° intercept method, two mutually perpendicular lines are drawn at blunt notch tip using an image of notch profile after the test. These lines intersect the crack flanks. The distance between two intersecting points at crack flanks is inferred as a plastic *CTOD*.

Standard methods for *CTOD* testing described in ASTM E1290-09 (2009) adopt a plastic hinge model (PHM) in which displacements are separated into elastic and plastic components. The PHM is based on determination of plastic rotational factor (PRF) r_{pl}, which allows the *CTOD* value to be extrapolated from load-line displacement data. According to ASTM E 1290-09 (2009), the PRF value for compact tension (CT) specimen is given by Eq. (2.3).

$$r_{pl} = 0.4 \left\{ 1 + 2 \left[\left(\frac{a_0}{b} \right)^2 + \frac{a_0}{b} + 0.5 \right]^{1/2} - 2 \left[\frac{a_0}{b} + 0.5 \right] \right\} \qquad (2.3)$$

The PRF value depends on initial crack length and unbroken ligament length as seen from Eq. (2.3). A large bank of PRF data is already published by Kumar and Bhattacharya (1995) and Bhattacharya and Kumar (1995a, 1995b). Results on plastic *CTOD*, based on PHM with PRF given by Merkle and Corten (1990). This is explained in Chapter 3. However, these reports lead to measure a PRF value, which does not account the thickness of specimen.

2.4.4   Finite Element Analysis

Finite element analysis (FEA) is one of the numerical methods widely used in fracture mechanics applications. The important aspects of FE analysis are selection of element to model

the crack region and modeling of the material behaviour. Two numerical models, namely the crack tip opening angle (CTOA) and a cohesive zone model (CZM) are widely used to characterize the fracture behaviour of the ductile materials.

The crack tip opening angle (CTOA), which has been introduced as driving force particularly for crack extension in metal sheets under quasi-static loading [O'Donoghue *et al* (1997), Dawicke *et al* (1995)], is used as the controlling parameter, and crack extension is realized by a node release technique. The advantage of this model is that it has only a single parameter, the critical CTOA, which can be determined by experiments [Heerens and Schodel (2003)]. Drawbacks of this model are that only initially flawed structures can be analyzed with this model and CTOA can be measured optically, but this is a costly procedure producing a large scatter of values [Scheider *et al* (2006)]. According to Scheider *et al* (2006) the results for the CTOA model are not as accurate as the cohesive model.

The Cohesive Zone Model (CZM) removes the crack tip singularity and represents physics of the fracture process at the atomic scale. CZM, formerly also called strip yield models, were first introduced by Dugdale (1960) and Barenblatt (1962). Later Needleman (1987) was the first to use them for the analysis of crack propagation in ductile materials. Recent reviews of the method are found in [Brocks and Cornec (2003), Brocks *et al* (2003) and Elices (2002),]. All cohesive zone models assume a process zone ahead of the crack tip. For mode–I loading the normal tensile stress is correlated with a relative displacement by a specific constitutive law designated as separation law. Each separation law is characterized by its specific shape and by two limiting parameters, a maximum tensile stress (σ_0) and a critical displacement (δ_f) after which no additional tensile stress is sustained. The area under the σ_0–δ_f curves is the separation energy Γ_0.

Nowadays cohesive zone models are usually implemented as interface elements, which transfer the cohesive stress between the continuum elements. The cohesive elements are one-dimensional for 2–D problem and two-dimensional for 3–D problem, i.e., they do not have a thickness dimension [Zerbst *et al* (2009)]. They are introduced at the boundaries of the continuum elements. Cohesive elements are inserted either along a pre-defined crack path or along all continuum elements boundaries within a distinct region. The latter option allows crack propagation in arbitrary directions [Scheider and Brocks (2003) and Xu and Needleman (1994)].

20

Fig 2.2 shows the applications of CZM to various materials and situations. Fig 2.3 shows modeling of fracture process zone with cohesive elements. Fig 2.4 shows cohesive elements (obeying traction separation law (TSL)) surrounded by continuum elements (elastic-plastic behaviour).
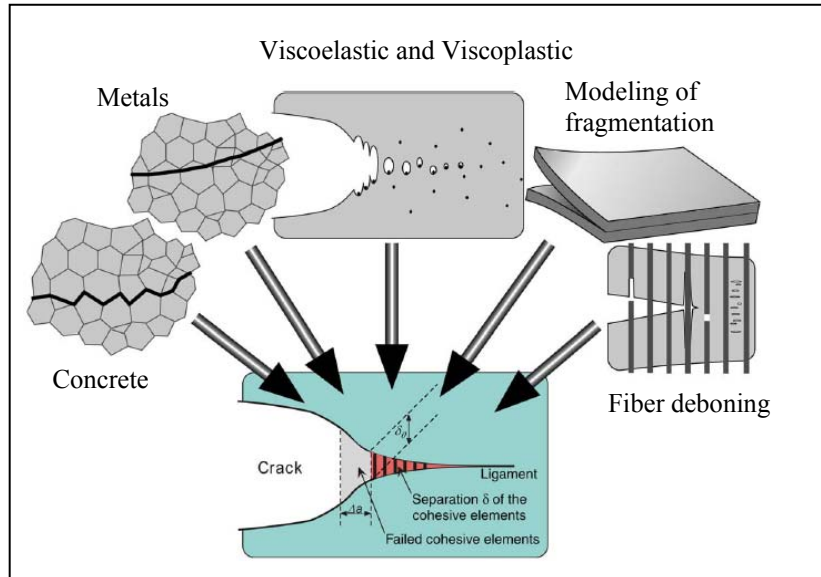
Fig 2.2 Schematic of cohesive model for various failure phenomena: damage is localized in a surface [Scheider (2006)]
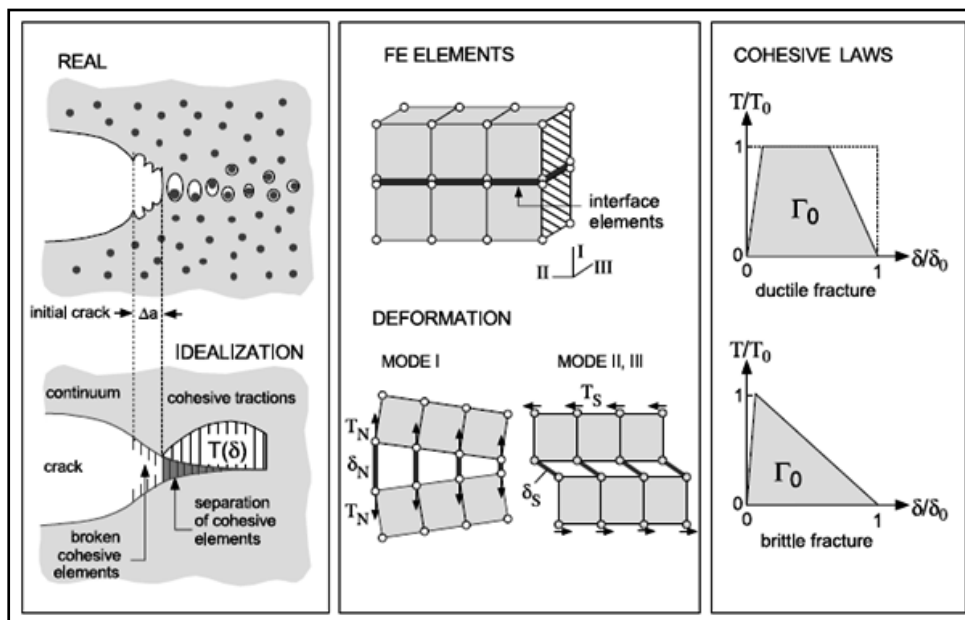
Fig 2.3 Representation of the ductile failure process by CZM [Cornec (2003)]
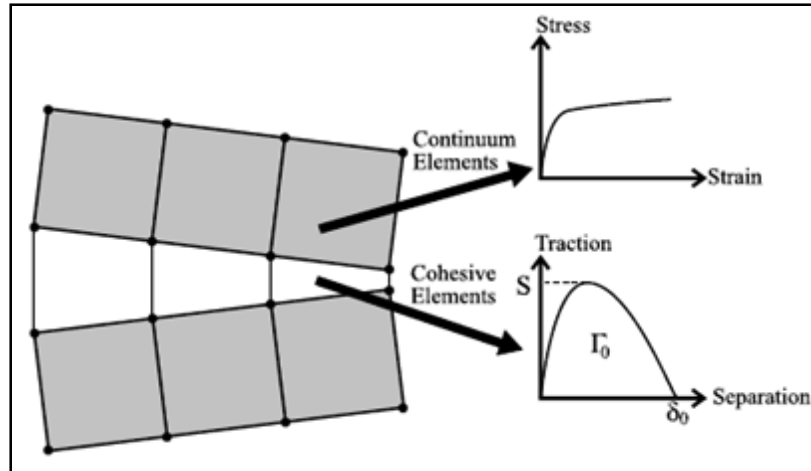
Fig 2.4 CZM obeying a TSL and the surrounding undamaged elastic–plastic material
[Anvari *et al* (2006)]

The cohesive parameters (σ_0, δ_f, and Γ_0) cannot be measured in a direct way for ductile materials but have to be identified by fitting finite element results to experimental data. These data comprise stress–strain curves of notched tensile specimens and R curves [Cornec *et al* (2003)]. Note that the cohesive parameters determined for different separation laws are also different; as a result they should not be regarded as model independent material parameters. Cornec *et al* (2003) proposed that the cohesive energy, Γ_0, as a first estimate can be taken identical to the *J*-integral at stable crack initiation, J_I. Starting with this as a default value fine-tuning of σ_0, δ_f and Γ_0 by finite elements is usually necessary.

Although thin-walled structures generally have plane stress characteristics, the application of plane shell elements in conjunction with the cohesive zone approach may not be straightforward [Negre *et al* (2005)]. Scheider (2009) give an example where the modeling of a stiffened structure by shell elements would cause unrealistic results due to undue deformation of the finite elements in the stiffener region. In order to cover the effect of necking Scheider and Brocks (2006) proposed the use of thickness-sensitive cohesive elements for shell structures. The thickness information is taken from the adjacent shell elements and transferred to the cohesive zone elements. The advantages of the cohesive model can be summarized in the following points [Scheider *et al* (2006)]:

1. The method leads to most accurate results for structures of different size and constraint conditions, needing two phenomenological, but nevertheless physically possible parameters, σ_0 and Γ_0, only.

2. The cohesive model can not only be used for 2D thin walled, but also for thick or complex three-dimensional structures.

3. The presence of an initial crack is not essential for the cohesive model, but it is suspected that the triaxiality in uncracked structures, which is very different from that at a crack tip, affects the cohesive model parameters significantly.

2.5   Analysis and Gaps in Existing Literature

Good amount of research is available to understand fracture behaviour in thin metal sheets, which fall into general yield regime. However, investigations on complete fracture behaviour in thin steel sheets, is not reported. Complete characterization of steel sheet material is important from formability and fracture mechanics point of view.   Good amount of research and improvements are observed in order to achieve better results on formability using experiments and simulations following formability techniques. These techniques, however, could not avoid wrinkles and cracks. In addition to this, maximum load at which crack initiates and critical forming rate beyond which formability is affected, are not being addressed by such techniques. Because of this, trial and error methods are adopted to reach to some thumb rules which leads to wastage of material. Even after trials and errors, invisible cracks cannot be avoided. The fracture resistance of DD/EDD steel sheets needs to be characterized using fracture mechanics approach as fracture mechanics approach is a comprehensive solution addressing material, geometry, rolling direction (anisotropy), and three modes of fracture which are observed in forming operations.

CHAPTER- 3

EXPERIMENTAL PROCEDURE

Introduction

This chapter discusses about experimental procedures adopted to characterize fracture behaviour of EDD steel sheets which fall in general yield regime. Subsequent topics focus on investigation of fracture parameters with existing standards, methods and proposed methods to determine fracture parameters and fulfill the planned objectives. The specimen specifications for various objectives are tabulated in details.

3.1 Methodology

The methods of accomplishing the experimental programme involve testing EDD steel sheets using compact tension (CT) type specimen. Four types of EDD sheets along with their chemical composition and mechanical properties are sponsored by TATA steel, Jamshedpur for the present work. They are designated as EDD 'A', EDD 'B' EDD 'C' and EDD 'D'. The study is conducted with respect to two approaches: 'formability approach' and 'fracture mechanics approach'. The formability approach is studied with the help of data obtained from TATA steel, Jamshedpur. In order to study fracture mechanics approach, fracture tests for crack initiation are conducted. Several image analysis techniques and measurement techniques are employed to determine fracture parameters. Various experimental techniques and ASTM standards are used to achieve the results. For comparative study, cohesive zone model is formulated by finite element method codes, ABAQUS 6.7. The details of experimental procedure, various tests, referred ASTM standards; experimental procedures are presented in subsequent sections.

3.2 Experimental Procedure

This section presents specimen preparation for fracture test and fabrication of grippers and anti–buckling plates. Various tests and ASTM standards, followed in the present investigations are also discussed.

3.2.1 Specimen Preparation

The geometry of CT specimen used in the current work is as per the recommended design in ASTM E1820-11 (2011). Specimens are fabricated by using wire electric discharge machine (WEDM) to maintain the exact relationship among all dimensions. During wire cutting operation, a bunch of ten to twelve specimens placed on a stack are cut together, which reduced cost as well as time. Instead of fatigue pre-cracking, a notch is cut with a 0.2 mm wire diameter. This operation creates a notch of 0.1 mm radius. Because of unavoidable heating during the notch cutting process, notch radii are not exactly 0.1 mm. The radii have gone up to about 0.13 mm. The configuration of the test specimen is shown in Fig 3.1. The photograph of notch profile is taken using a digital camera attached to optical microscope at a magnification of 100X. The notch radius is measured on the photograph, as shown in Appendix D.
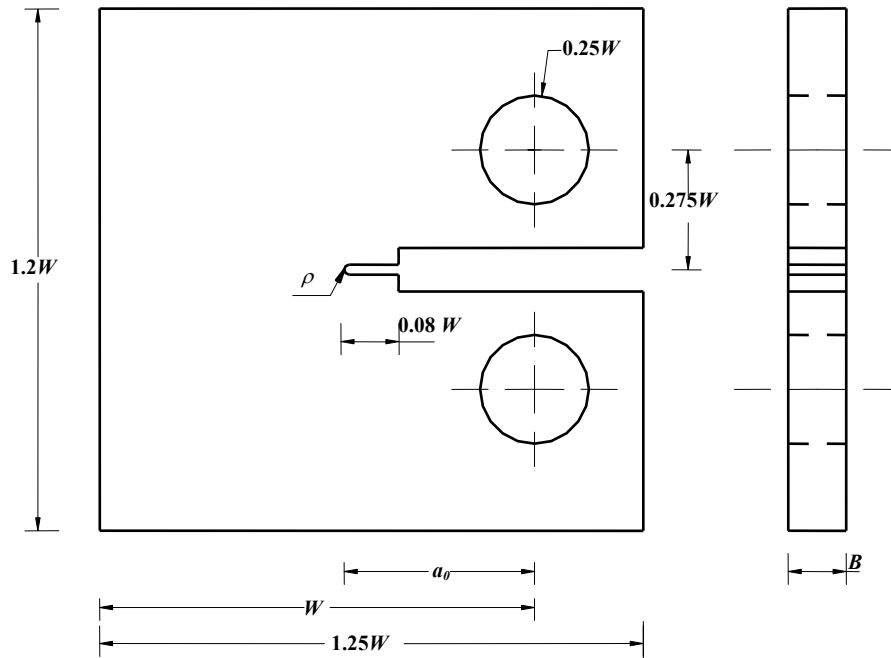
Fig 3.1 Dimensions of CT specimen as per ASTM standard E 1820-11 (2011)

The specimens are ground with emery papers following 1/0 (coarse), 2/0, 3/0 and 4/0 (fine). In order to have surface finish sufficient to distinguish between the elastic and plastic zone, these specimens are polished first using alundum and finally using 0.25 μm diamond pastes in polishing machine. The specifications of the CT specimens used for various objectives are given in section 3.5 (Table 3.1 to Table 3.4).

3.2.2 Fabrication of Grippers and Anti–Buckling Plates

Grippers are fabricated to hold the CT specimen in UTM. The grippers are prepared on shaper machine (Fig 3.2). A 5 mm slot is prepared in gripper with the help of EDM. A copper plate of dimensions 120 x 30 x 2.3 mm is used as electrode on EDM. Since the thickness of electrode is 2.3 mm in one pass it gives a slot of 2.5 mm.
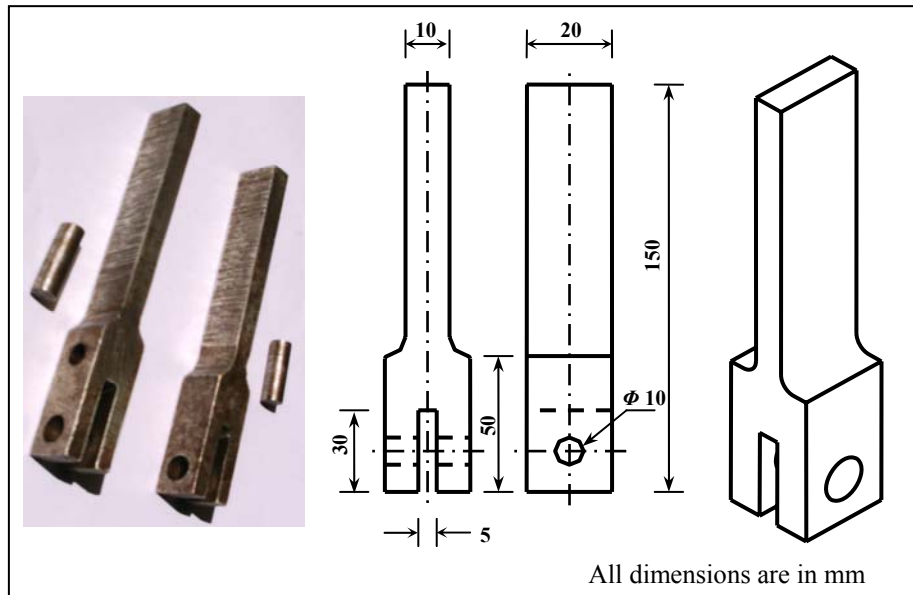
Fig 3.2 Grippers to hold the CT specimen

Anti–buckling plates are prepared to avoid out of plane buckling. A small window of 20 mm x 20 mm is prepared in the plates to observe region ahead the crack tip. Anti–buckling plates are prepared on shaper machine (Fig 3.3).
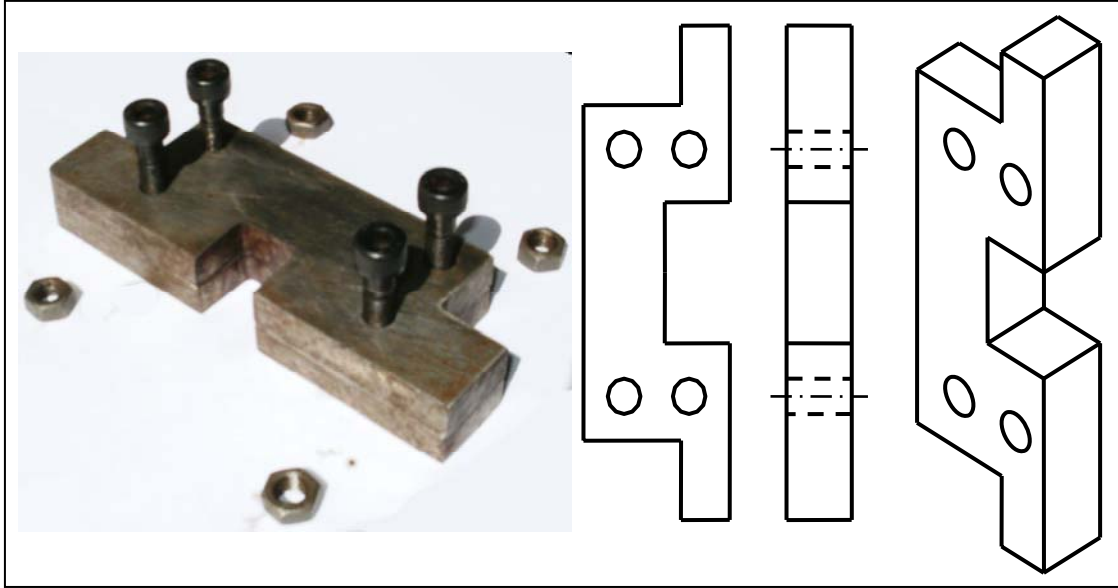
Fig 3.3 Anti–buckling plates for CT specimen

3.2.3 Chemical Analysis

The chemical composition of the materials (in wt. %) provided by TATA steel. It is analyzed by using a chemical analyzer, made by Worldwide Analytical System (WAS), model Foundry Master. The nitrogen content (in ppm) is estimated in the EDD steel samples using a LECO gas analyser. The information of model for these two equipments is given in Appendix E.

3.2.4 Grain Size Measurement

The grain size of EDD steel sheets is supplied by TATA steel, Jamshedpur. The two-dimensional grain size is measured using the average linear intercept method as described by Callister (2006). The average grain size is determined from individual grain intercept by viewing the two-phase microstructure at a magnification of 1000X. In this method, a graduated line grid is superimposed on the microstructure and the number of the smallest divisions of the grid intercepted by individual ferrite grain is counted. A total number of 300 random intercepts are considered for obtaining the average value of the grain size.

3.2.5 Mechanical Tests

Tensile test data is obtained from TATA steel, Jamshedpur. As per the literature and technical reports sent by them, tensile tests are carried out following ASTM standard E 8M-00

(2000) specifications. The specimens are tested along the three directions, with the tensile axis being parallel (0°), diagonal (45°), and perpendicular (90°) to the rolling direction of the sheet. The standard tensile properties namely, yield strength (YS), ultimate tensile strength (UTS), uniform elongation (e_u), total elongation (e_f) and strain hardening exponent (n) are determined from the load–elongation data obtained from these tests. Three samples are tested in each of the three directions and average values are taken to account for the scatter.

Strain rate sensitivity index, m, is calculated from the results of strain rate jump tests carried out on tensile specimens. The strain rate is suddenly increased during the uniform plastic deformation and in such a strain rate change test; m is defined according to Dieter (1988) as Eq. (3.1).

$$m = \frac{\ln(\sigma_2 / \sigma_1)}{\ln(\varepsilon_2 / \varepsilon_1)} = \frac{\ln(P_2 / P_1)}{\ln(V_2 / V_1)} \tag{3.1}$$

where, σ_1 and σ_2 are flow stress values at strain rates ε_1 and ε_2, respectively. P_1 and P_2 are loads corresponding to cross head speeds of V_1 and V_2, respectively.

3.2.6 Formability Parameters

The strain hardening exponent (n), normal anisotropy ($\bar{r}$), strain rate sensitivity index, yield strength and modulus of elasticity are the conventional indicators of formability of sheet metals. According to Murthy et al (2005) and Caddell (1980), the strain hardening exponent is taken as value of ultimate true strain (ε_u) from the true stress – true strain data. The normal anisotropy is calculated using the standard formula (Eq. 3.2) obtained from Hosford and Caddell (1993).

$$\bar{r} = \frac{1}{4}(r_o + 2r_{45} + r_{90}) \tag{3.2}$$

where, the r_0, r_{45}, and r_{90} are the strain ratios along 0, 45 and 90 degree to rolling direction, respectively given by Eq. (3.3).

$$strain\ ratio = \frac{true-width\ strain}{true-thickness\ strain} \tag{3.3}$$

The values of strain ratio are obtained from the supplier of EDD steel material. ASTM E8M-11 (2011) and E517-00 (2010) standards are used to access the deep drawing qualities.

3.2.7 Fracture Test

The fracture tests are carried out using a 100 kN Universal Testing Machine (FIE make). The specifications of this machine are given in Appendix F. The experimental set up is shown in Fig 3.4.
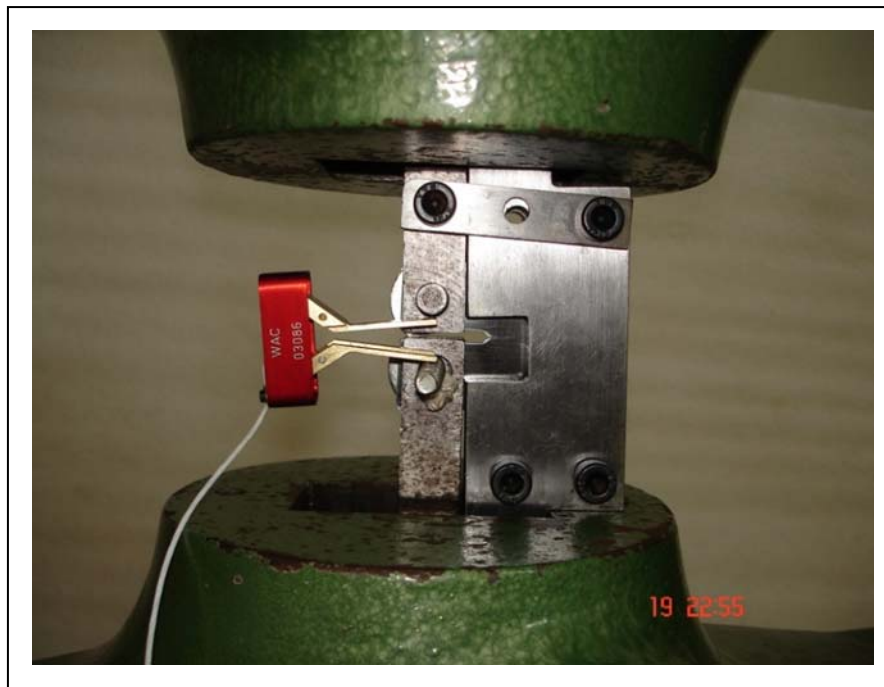
Fig 3.4 Test set-up for CT type specimen along with CMOD gauge and anti-buckling fixture

The load-line displacement is measured with the help of a crack mouth opening displacement (CMOD) gauge. The CMOD gauge model used is WAC 07.02.01 (WAZAU). The specifications of this gauge are given in Appendix E. As the specimen is small in size, measurement of CMOD is quite difficult. Instead of CMOD, the load-line displacement is measured by inserting the jaws of CMOD gauge in between two loading pins as shown Fig 3.4. The displacement rate is used corresponding to the constant cross head displacement of 0.2 mm/min at the room temperature of 28°C. During such tests, the magnitudes of load (P) and load-line displacement (V_{ll}) are recorded in computer, in graphical as well as in tabular form.

3.2.8　Fracture Criterion

The 'load drop technique', mentioned by Ray (2010), Kulkarni (2005) and Kulkarni *et al.* (2001 and 2003a), is used as a fracture criterion to measure fracture parameters. A typical load – load-line displacement curve is shown in Fig 3.5. It is observed that the load drops at a particular instant when surface crack is initiated. This load is considered as a critical load (P_c). At that instance of time, the loading of a specimen is discontinued and the specimen is taken out for subsequent measurement of fracture parameters i.e. *J*-integral and *CTOD*. Fig 3.5 also shows a photograph of a tested specimen and a micrograph (200X) showing the event of crack initiation in CT specimen.

It is observed from Fig 3.5 that, load is continuously increasing till a P_c value, however, the rate of increment in load just before the critical load is very low as compared with prior portion of the plot. The rate of increment in load continues to decrease and as soon as load drops, crack initiates. This observation is unlike other engineering materials, in which, crack initiates before the maximum load reaches. This is due to excessive plasticity possessed by the material before it fractures. Therefore, in case of EDD materials, the critical event of cracking initiation is defined as the load drop point, at which the process of plastic deformation at the original crack tip (i.e. the blunting process) is stopped.
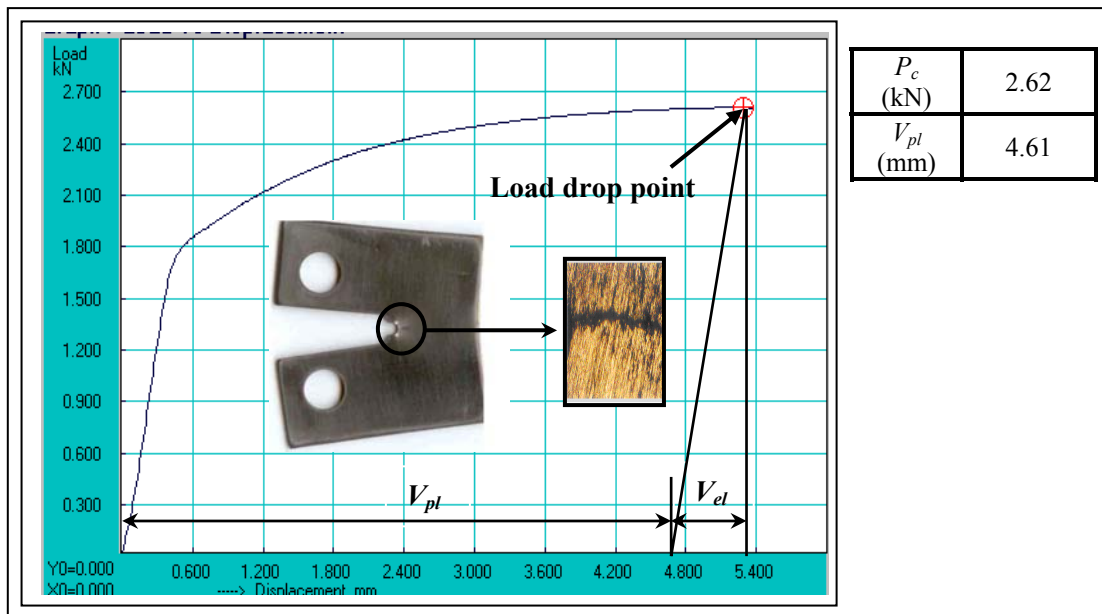
Fig 3.5 Typical test record at crack initiation point

3.2.9 Post Fracture Tests

The specimens are taken out at the event of crack initiation for subsequent measurement of *J*-integral and *CTOD*. Specimens are scanned using a flat bed scanner and a boundary lines are obtained using AutoCAD2002 software to measure the plastic *CTOD* by various techniques. The scale factor is taken with reference to the unreformed boundary of the specimen. In order to check, whether the crack initiates at the mid-thickness section, a few specimens are chosen before and at the load drop point. These are mounted in Bakelite and then ground successively layer by layer. The photographs are taken with a digital camera attached to optical microscope to study the damage ahead of a crack tip. This is to check the validity of fracture criterion with the help of a damage study ahead of crack tip. The thermal shock treatment is done using liquid nitrogen to break the specimens along the crack. The fracture surfaces of broken open up specimens are studied to check the validity of fracture criterion.

3.3 Estimation of *J*-Integral

To determine *J*-integral from the load–load-line displacement curve was proposed by Rice et al. (1973). The ASTM E1820-11 (2011) outlines a test method for estimating the value of *J*-integral for ductile materials. According to ASTM E1820-11 (2011) J-integral at crack initiation (J_C) is given by

$$J_c = J_{el} + J_{pl} \qquad (3.4)$$

where J_{el} is elastic part of *J*-integral and J_{pl} is plastic part of *J*-integral.

3.3.1 Calculation for the Elastic Part (J_{el})

The J_{el} is computed from the stress intensity based on critical load. For present study, predominant plane stress conditions are observed. J_{el} for plane stress conditions is given by Eq. (3.5).

$$J_{el} = \frac{K^2}{E} \qquad (3.5)$$

The linear stress intensity factor, K is calculated using Eq. (3.6) given by Murakami (1987),

$$K = \frac{P}{BW^{1/2}} f(\alpha) \tag{3.6}$$

The value of P is equal to P_c, load at crack initiation, B is the thickness of specimen, W is the width of the specimen, $\alpha = \frac{a_0}{W}$ (refer Fig 3.1) and

$$f(\alpha) = \frac{(2+\alpha)(0.886 + 4.64\alpha - 13.32\alpha^2 + 14.72\alpha^3 - 5.6\alpha^4)}{(1-\alpha)^{3/2}}$$

3.3.2 Calculation for the Plastic Part (J_{pl})

According to ASTM E1820-11 (2011), J_{pl} is determined from the plastic area (A_{pl}) under the load – load-line displacement curve (Fig 3.6). J_{pl} is defined in terms of the energy absorbed divided by the net cross sectional area (Thickness (B) x unbroken ligament length (b)) as shown in Eq. (3.7).

$$J_{pl} = \frac{\eta A_{pl}}{Bb} \tag{3.7}$$

where, A_{pl} is the area under load – plastic load-line displacement curve, the geometry factor $\eta = 2.0 + 0.522\left(\frac{b}{W}\right)$ and b is unbroken ligament length i.e. (W-a_0).
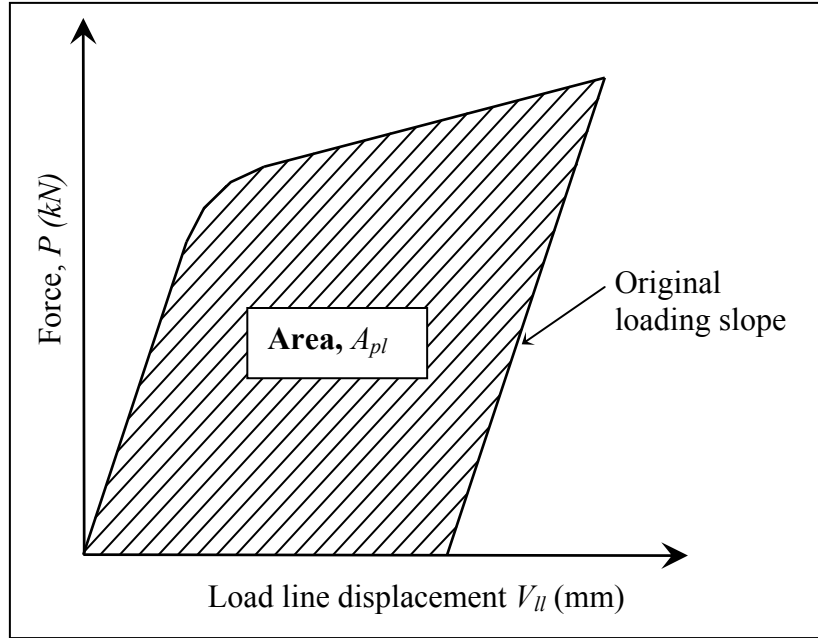
Fig 3.6 Definition of area for *J* calculation using the basic method

3.4 Estimation of Critical *CTOD*

According to the ASTM standard E1290-09 (2009), the critical crack tip opening displacement during the loading consists of elastic and plastic part, given by Eq. (3.8)

Critical *CTOD* = Elastic *CTOD* + Plastic *CTOD*

$$\delta_c = \delta_{el} + \delta_{pl} \tag{3.8}$$

3.4.1 Calculation for the Elastic Part (δ_{el})

The elastic part is calculated by using a standard Eq. (3.9) for plane stress condition,

$$\delta_{el} = \frac{K^2}{ES_y} \tag{3.9}$$

where, the elastic modulus (E), and yield strength (S_y) are the mechanical properties. The linear stress intensity factor K is calculated from Eq. (3.6).

3.4.2 Calculation for the Plastic Part (δ_{pl})

It seems reasonable to assume that the crack initiation of a ductile material is based solely on the plastic deformation behaviour near the crack tip. In the present investigation, the plastic *CTOD* is estimated by using two methods, existing plastic hinge model (PHM) specified in ASTM E1290-09 (2009) and proposed crack flank opening angle (CFOA) method. These methods are discussed in following sub-sections.

3.4.2.1 Plastic hinge model (PHM)

The plastic *CTOD* (δ_{pl}) is determined by assuming that the unbroken ligament works like a plastic hinge with its center (i.e. apparent axis of rotation) at a distance $r_{pl}b$ from the crack tip (*G*) as shown in Fig 3.7 (a). Referring to the Fig 3.7 (a) and (b): *O* is the apparent axis of rotation, *G* is crack tip, *AB* is plastic part of the *CTOD*, *CD* is plastic load-line displacement (V_{pl}), and *GH* is initial crack length (a_0). The *OG* is taken equal to $r_{pl}b$, where r_{pl} is a plastic rotational factor and b is the unbroken ligament length.
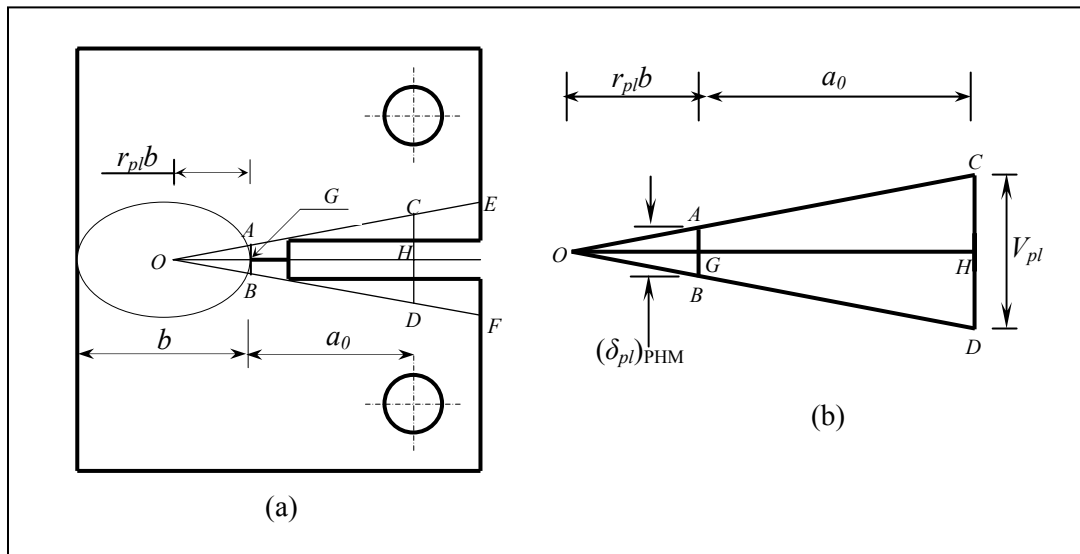
Fig 3.7 Plastic hinge model to determine plastic *CTOD*

From properties of the similarity of triangles given in Fig 3.7 (b),

$$\frac{AB}{CD} = \frac{OG}{OG+GH} \quad \text{or} \quad \frac{(\delta_{pl})_{PHM}}{V_{pl}} = \frac{r_{pl}b}{r_{pl}b+a_0}$$

34

$$(\delta_{pl})_{PHM} = \frac{r_{pl}b}{r_{pl}b + a_0}V_{pl} \qquad (3.10)$$

Eq. (3.10) gives a plastic *CTOD* based on a plastic hinge model. According to Merkle and Corten (1990), the value of PRF is given by Eq. (3.11).

$$PRF = r_{pl} = (1+\beta)/2 \qquad (3.11)$$

where, $\beta = \left[\left(\frac{2a_0}{b} \right)^2 + \frac{4a_0}{b} + 2 \right]^{1/2} - \left[\frac{2a_0}{b} + 1 \right]$. The value for V_{pl} is taken from Fig 3.5. With the help of equations (3.8), (3.9) and (3.10), the value of critical *CTOD* (δ_c) is calculated. This model assumes a linear relation between plastic load-line displacement (V_{pl}) and plastic *CTOD* (δ_{pl}). According to Wilson and Landes (1994), this model can be used for smaller plastic load line displacement. In case of EDD steel sheet, it is observed that there is a significant deformation ahead of crack tip resulting in higher value of plastic load line displacement. Moreover, in PHM, the determination of PRF is independent of thickness of the specimen.

3.4.2.2 Crack flank opening angle (CFOA) method

This is a modified plastic hinge model to account for the non-linearity between plastic *CTOD* and plastic load-line displacement. The image of a specimen is taken using flat bed scanner. The scanned image of specimen is imported in drafting software AutoCAD-2002 and a boundary lines are obtained as shown in Fig 3.8. Similar to PHM, the plastic portion (δ_{pl}) is determined by assuming that the unbroken ligament works like a plastic hinge with its center at a distance $O'G$ from the crack tip G as shown in Fig 3.8.
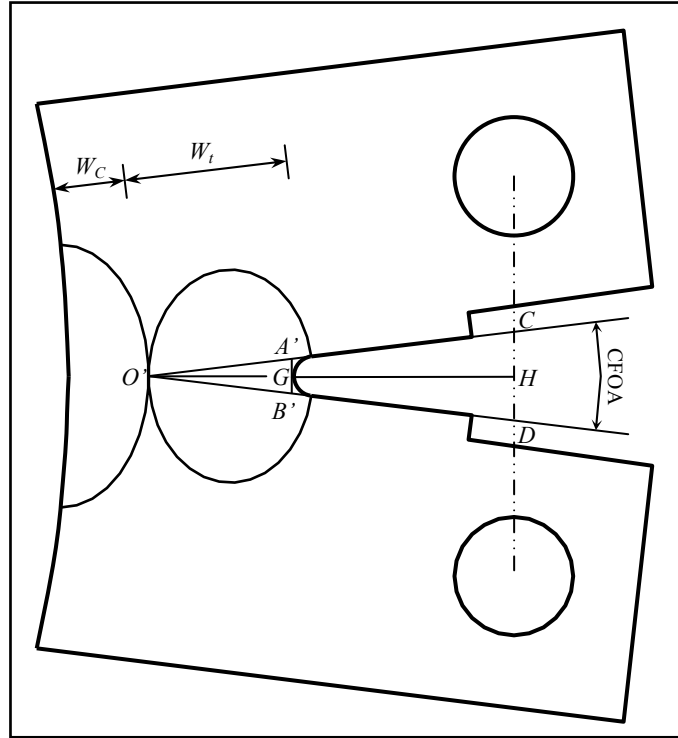
Fig 3.8 CFOA model to determine plastic *CTOD*

Referring to the Fig 3.8, *A'B'* is the plastic part of *CTOD* i.e. $(\delta_{pl})_{\text{CFOA}}$, *CD* is plastic load line displacement. In this model, the common point of tensile plastic and compressive plastic zone along the unbroken ligament length is taken as an apparent axis of rotation, as shown in Fig 3.8. Similar to a neutral axis in case of bending of a beam, there is a neutral line exists along thickness which falls into a point view *O'* on the specimen surface. The apparent axis of rotation, i.e. point *O'* is found with the help of hardness measurement across the elastic-plastic boundary of plastic zone. Hardness measurement across the elastic plastic boundary clearly shows the difference in hardness values. The deep point inside the plastic zone and ahead of crack tip is severely deformed showing highest hardness value. The apparent axis of rotation (*O'*), i.e. the common point of tensile and compressive plastic zone can be easily determined by measuring the hardness along the unbroken ligament length. The hardness value at *O'* point is equal to the hardness value in elastic field. The above findings are also confirmed by Cotterell *et al* (2002). It is observed that the location of point *O'* depends on crack flank opening angle (CFOA) which in turn depends on thickness of specimen. This location can be obtained as an intersection of lines coinciding with the crack flanks. The angle made by two crack flanks is measured at point *O'* as

36

CFOA. The width of compressive zone and tensile zone is shown as W_c and W_t, respectively in Fig 3.8. Fig 3.9 shows a comparison of geometry of triangles used in PHM and CFOA.
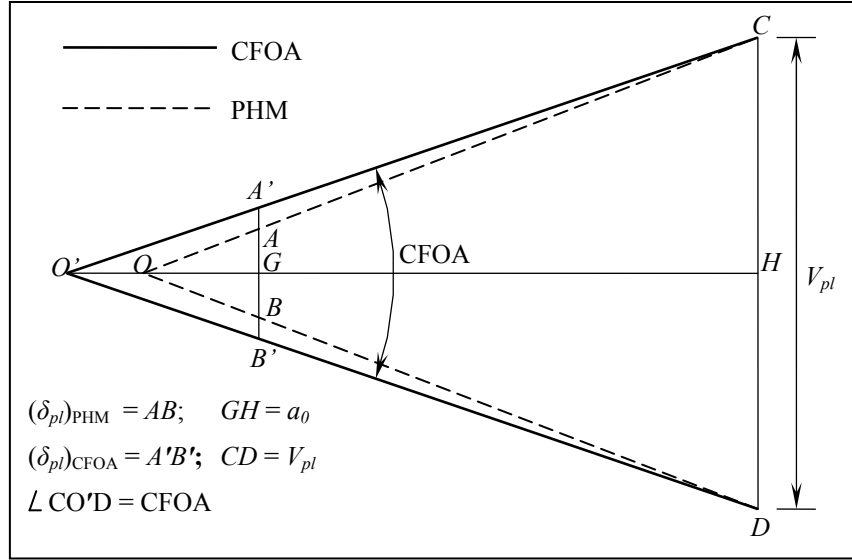
Fig 3.9 Comparison of PHM and CFOA model

From properties of the similarity of triangle with reference to Fig 3.8 and Fig 3.9,

$$\frac{A'B'}{CD} = \frac{O'G}{O'H}$$

$$\frac{(\delta_{pl})_{CFOA}}{V_{pl}} = \frac{O'G}{O'G + GH} \tag{3.12}$$

$$(\delta_{pl})_{CFOA} = \frac{O'G}{O'G + GH} V_{pl} \tag{3.13}$$

However, the location of point O' depends on crack flank opening angle *CFOA*, *O'H* can be expressed in terms of *CFOA* as give in Eq. (3.14).

$$O'H = O'C \cos\left(\frac{CFOA}{2}\right) \tag{3.14}$$

The $(\delta_{pl})_{CFOA}$ depends on O'G and V_{pl}, whereas $(\delta_{pl})_{PHM}$ depends only on V_{pl}, and is independent of thickness of specimen. In *CFOA* method, the position of apparent axis of rotation

37

i.e. point *O'* depends upon the crack flank opening angle, which in turn depends upon the thickness of specimen.

3.5   Specifications of Specimens

Four different objectives i.e. thickness effect, strain rate effect, notch radius effect, and a_0/W ratio effect have been considered to study the fracture behaviour of EDD steel sheets in general yield regime.

3.5.1   Thickness Effect Study

For this study, six specimens of different thicknesses of EDD 'A' have been considered. These specimens are coded as T1, T2,…, T6. All specimens are tested till crack initiation point. The specifications along with the specimen codes are given in Table 3.1.

Table 3.1 Geometry of CT specimens to study the effect of thickness in EDD 'A'

Sp-code	Thickness (B) mm	Crack length (a_0) mm	Width (W) mm	Notch radius (ρ) mm	Strain rate mm/min
T1	1.2	10.5	24	0.124	0.2
T2	1.3	10.5	24	0.117	0.2
T3	1.4	10.5	24	0.122	0.2
T4	1.5	10.5	24	0.115	0.2
T5	1.6	10.5	24	0.117	0.2
T6	1.7	10.5	24	0.121	0.2

3.5.2   Study of the Influence of Notch Radius

For notch radius effect, fifteen specimens of different notch radii of EDD 'B' have been considered. All specimens of same configuration and same thickness are prepared with various notch radii. These specimens are coded as N1, N2,…, N15. All specimens are tested till crack initiation point. The specifications along with the specimen codes are given in Table 3.2. In Table 3.2, the notch operation is mentioned as FC for fatigue pre-cracked specimens, WEDM for notched specimens using wire electric discharge machining process and saw blade for notched specimens using saw cut operation. It is observed that fatigue pre-cracking operation takes about

six to eight hours with low cycle fatigue. A few specimens are damaged when pre-cracking is done using high cycle fatigue.

Table 3.2 Geometry of CT specimens to study the effect of notch radius in EDD 'B'

Sp-code	Thickness (B) mm	Crack length (a_0) mm	Width (W) mm	Notch radius (ρ) mm	Stain rate mm/min.	Notch operation
N1	3.2	10.5	24	0.07	0.2	FC
N2	3.2	10.5	24	0.085	0.2	FC
N3	3.2	10.5	24	0.10	0.2	FC
N4	3.2	10.5	24	0.11	0.2	WEDM
N5	3.2	10.5	24	0.12	0.2	WEDM
N6	3.2	10.5	24	0.13	0.2	WEDM
N7	3.2	10.5	24	0.14	0.2	WEDM
N8	3.2	10.5	24	0.15	0.2	WEDM
N9	3.2	10.5	24	0.16	0.2	WEDM
N10	3.2	10.5	24	0.17	0.2	WEDM
N11	3.2	10.5	24	0.18	0.2	WEDM
N12	3.2	10.5	24	0.25	0.2	Saw-blade
N13	3.2	10.5	24	0.40	0.2	Saw-blade
N14	3.2	10.5	24	0.60	0.2	Saw-blade
N15	3.2	10.5	24	0.75	0.2	Saw-blade

3.5.3 Strain Rate Effect Study

For strain rate effect, eight specimens of EDD 'C' have been considered. These specimens are coded as S1, S2,…, S8. All specimens are tested till crack initiation point and tested at various strain rates. The specifications along with the specimen codes are given in Table 3.3.

Table 3.3 Geometry of CT specimens to study the effect of strain rate in EDD 'C'

Sp-code	Thickness (B) mm	Crack length (a_0) mm	Width (W) mm	Notch radius (ρ) mm	Stain rate mm/min.
S1	1.4	10.5	24	0.125	0.1
S2	1.4	10.5	24	0.116	0.2
S3	1.4	10.5	24	0.119	0.3
S4	1.4	10.5	24	0.124	0.4
S5	1.4	10.5	24	0.118	0.6
S6	1.4	10.5	24	0.122	1.0
S7	1.4	10.5	24	0.120	1.5
S8	1.4	10.5	24	0.123	2.5

3.5.4 Study of a_0/W Ratio

For a_0/W ratio effect, four specimens of different a_0/W ratios of EDD 'D' have been considered. These specimens are coded as A1, A2,…, A4. All specimens are tested till crack initiation point. The specifications along with the specimen codes are given in Table 3.4

Table 3.4 Geometry of CT specimens to study the effect of a_0/W ratio in EDD 'D'

Sp-code	Thickness (B) mm	Crack length (a_0) mm	Width (W) mm	a_0/W ratio	Notch radius (ρ) mm	Stain rate mm/min.
A1	2	20	40	0.5	0.117	0.2
A2	2	21	40	0.525	0.121	0.2
A3	2	22	40	0.55	0.125	0.2
A4	2	23	40	0.575	0.122	0.2

3.6 Validation of Experimental Procedures

In order to validate experimental findings such as fracture criterion and effect of various parameters (i.e. thickness effect, notch radius effect, strain rate effect and effect of a_0/W ratio) on fracture behaviour, cohesive zone model is proposed. The formulation and validation of CZM is discussed in chapter 4 and chapter 5 respectively.

CHAPTER- 4

COHESIVE ZONE MODEL

Introduction

This chapter presents the procedure adopted to perform the finite element analysis. Cohesive zone models are widely used to predict fracture behaviour in fracture mechanics applications. Suitable cohesive zone model (CZM) is developed to most accurately characterize the fracture behaviour of EDD steel sheets loaded in Mode–I and to establish the main finite element attributes (such as element size and type) to be used in general yield regime. CZM is formulated with the help of finite element analysis software ABAQUS 6.7 to verify experimental results. This software offers an advantage that the models can be easily used and customized by other users (i.e. researchers and engineers), which benefit the applicability of the proposed CZM for different boundary conditions, geometry, and material properties. ABAQUS also has the computational fracture mechanics features required for this work. It incorporates cohesive elements with customizable softening and a variety of nonlinear solvers such as Newton or modified Riks. The fracture model (CZM) for the compact tension (CT) specimen is used to study the effect of the type of softening (i.e. linear, exponential and constant traction) and cohesive parameters on the load versus load line displacement response in general yield regime.

4.1. Two-Dimensional CT Specimen Model

Two-dimensional finite element model is developed for CT type specimen geometry following the design standards, ASTM E1820-11 (2011). This model is used to compare experimental load versus load line displacement curves with the elastic–plastic softening response of EDD steel sheets. This model includes mesh, boundary conditions and special features such as the cohesive elements on the expected crack path and a nonlinear step definition to solve the nonlinear fracture problem. The necessary model parameters that define the model are presented in subsequent sections.

4.1.1   Model Formulation

As shown in Fig 4.1, the CT specimen model has a bulk section made with two dimensional plain stress elements (CPS4R) defined by its elastic–plastic properties. The crack path is modeled using cohesive elements (COH2D4) defined by a traction-separation law. The cohesive elements are placed along the crack path. Cohesive elements are taken to be square of side 0.1 mm. Plane stress elements around cohesive zone are taken to be squares of side 0.5 mm. Two more sizes, 0.3 mm and 1.0 mm, were also considered to examine the mesh sensitivity of the results. Since the size of cohesive elements is different from the surrounding elements, cohesive elements are placed along the crack line in the model using a tie constraint.
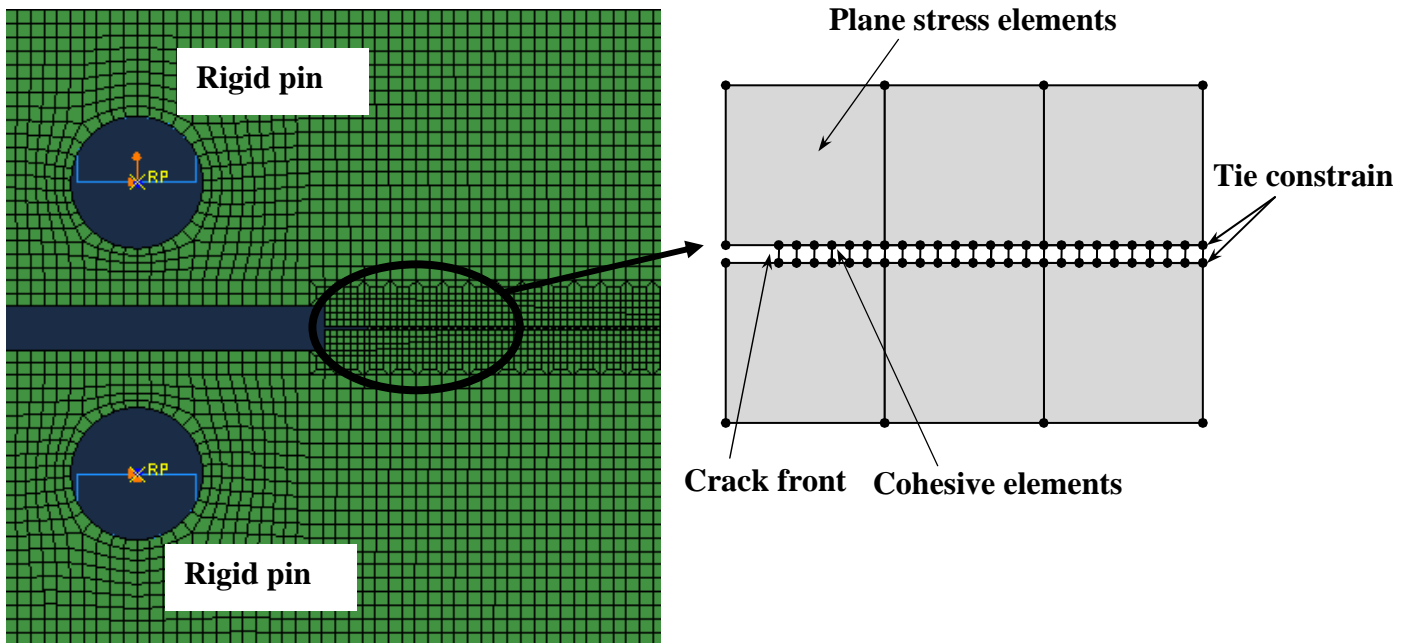
Fig 4.1 FE model, bulk elements and cohesive elements

4.1.2   Non-Linear Material Model

A true stress-strain curve up to breaking-strain point is used with multi-linear isotropic hardening to incorporate non-linear material properties. ABAQUS requires isotropic elastic–plastic material input in two stages; elastic input (i.e. Modulus of elastic and Poisson's ratio) and plastic data (i.e. true stress and logarithmic plastic strain). If nominal stress–strain data for a

uniaxial test of isotropic material having modulus of elasticity E, a simple conversion to true stress and logarithmic plastic strain is given by Eq. (4.1) and (4.2)

$$\sigma_{true} = \sigma_{nom}\left(1+\varepsilon_{nom}\right) \tag{4.1}$$

$$\varepsilon_{ln}{}^{pl} = \ln\left(1+\varepsilon_{nom}\right) - \frac{\sigma_{true}}{E} \tag{4.2}$$

The example demonstrated in Fig 4.2 indicates the input of material data for the classical metal plasticity model with isotropic hardening. Path OA shows elastic behaviour where path AD indicates plasticity. Plastic input is given in tabular form. For demonstration purpose four different points are considered on path AD (Point A, B, C and D). Point A is yield point and corresponding logarithmic plastic strain is zero. Similarly at point B, C and D the logarithmic plastic strains are $\varepsilon_1{}^{pl}$, $\varepsilon_2{}^{pl}$ and $\varepsilon_3{}^{pl}$ respectively as shown in Fig 4.2.
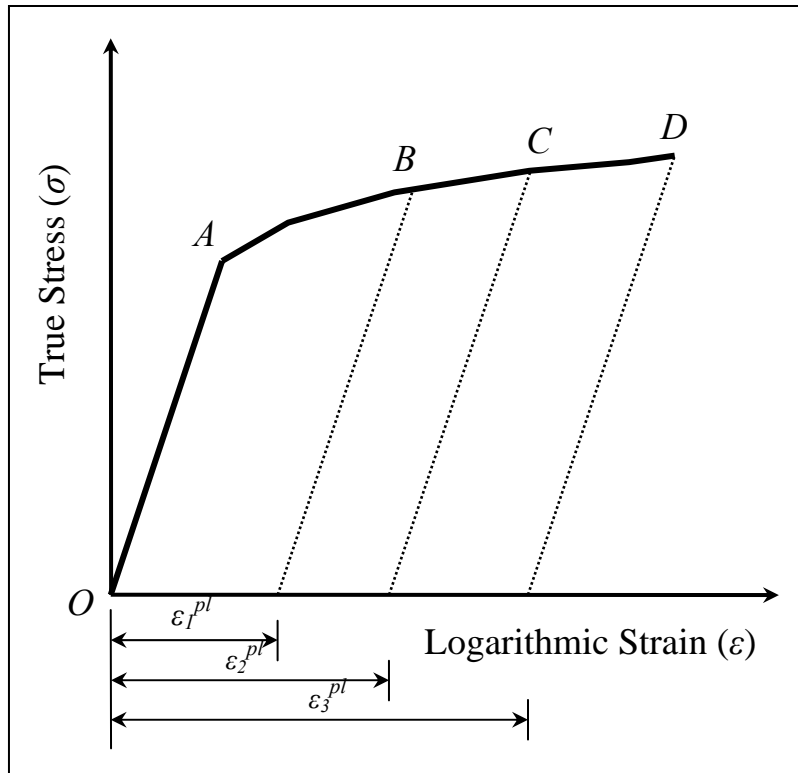
Fig 4.2 Input data for isotropic elastic – plastic material

The true stress–logarithmic plastic strain curves for EDD 'A', EDD 'B', EDD 'C' and EDD 'D' materials are shown in Fig 4.3, 4.4, 4.5 and 4.6 respectively. The elastic properties i.e.

modulus of elasticity and Poisson's ratio for four EDD steel sheets are 210 GPa and 0.33 respectively. The values of true stress – logarithmic plastic strain curve for EDD 'A', EDD 'B', EDD 'C' and EDD 'D' are tabulated in Appendix B.
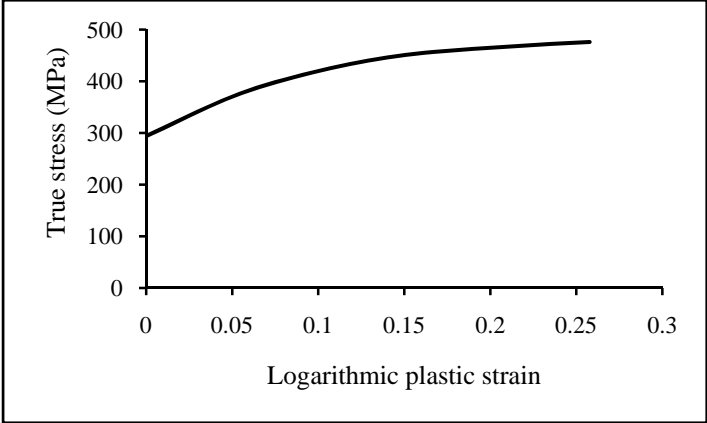
Fig 4.3 True stress–logarithmic plastic strain for EDD 'A' steel sheet
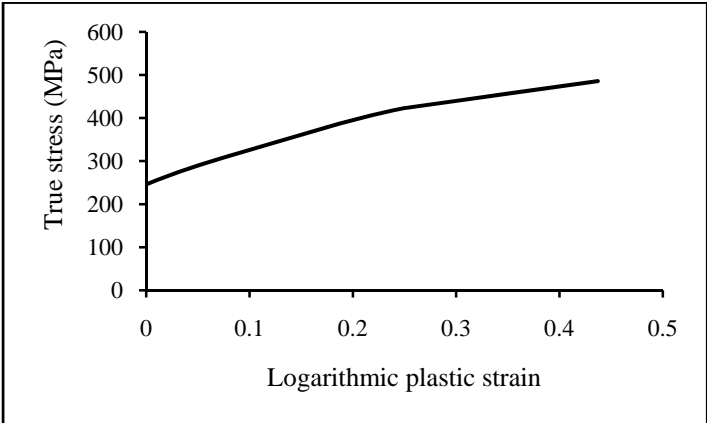
Fig 4.4 True stress–logarithmic plastic strain for EDD 'B' steel sheet
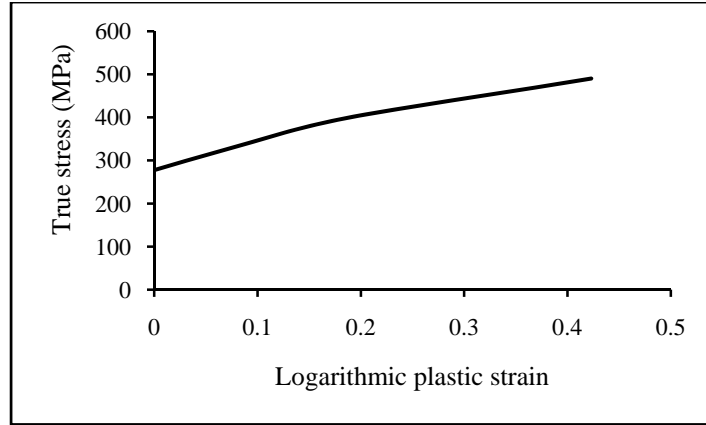
Fig 4.5 True stress–logarithmic plastic strain for EDD 'C' steel sheet
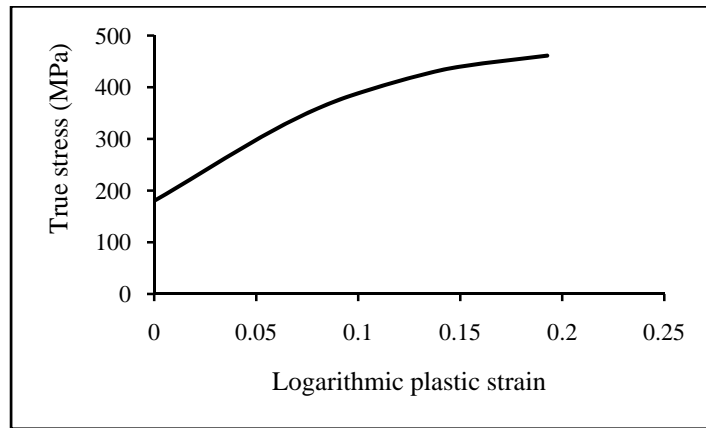
Fig 4.6 True stress–logarithmic plastic strain for EDD 'D' steel sheet

4.1.3   Loading and Boundary Conditions

The loading pins are modeled as rigid pins to avoid any severe local deformation at the contact points. The contact between loading pins and plane stress elements is considered smooth (friction less). The boundary conditions on the CT specimen model restrict the displacements along *x*–direction and *y*–direction and rotation about *z*–direction of the lower loading pin. The load is applied at upper loading pin using an incremental displacement step along *y*–direction where as its displacement along *x*–direction and rotation about *z*–direction is constrained. The load line displacement is calculated as the relative nodal displacements at the center of loading pins.

4.2   Non-Linear Analysis – Step Definition

Since the finite element model with cohesive fracture is a nonlinear problem, it must be solved in ABAQUS by defining the applied displacement as a function of time. The total time is divided into a user specified number of time increments (e.g., 500 increments are set for present study). The total number of time increments is set by the user; the size of each time increment (except the initial time increment) is defined by ABAQUS. Each increment involves solution of a nonlinear system which requires multiple iterations until convergence is achieved. If the convergence is accomplished quickly, the size of the subsequent increment will increase and vice versa. Each increment involves the solution of the complete FE problem for a given instant in the time step (i.e. one point on the load versus LLD curve is obtained). The present model has 500 increments and an initial time step size 0.01. The maximum time increment was set to 10. The Newton nonlinear solver is used for entire analysis.

4.3   Features of Cohesive Elements

Cohesive elements are used to model the behaviour of adhesive joints, interfaces in composites, and other situations where the integrity and strength of interfaces may be of interest [ABAQUS (2007)]. Cohesive zone model (CZM) provides insight into the fracture process of the materials. It is an ideal framework to model strength, stiffness and failure in an integrated manner. The cohesive elements for a two dimensional problem are 'one' dimensional because the cohesive elements can only open in one direction. Cohesive parameters (i.e. cohesive strength, initial stiffness and fracture energy or separation distance) are required to determine constitutive response of cohesive elements.

Since cohesive elements are incorporated in the model, the artificial elastic compliance of the system increases. While using cohesive elements a care should be taken that the overall compliance of the model is not overestimated, i.e. theoretically initial stiffness of cohesive elements should be infinite. Infinite value of initial cohesive stiffness makes the analysis numerically unstable. Numerically, finite value of initial stiffness for the cohesive element is to be chosen such that it will not interfere with the structure deformations. Traction separation law relates the traction and separation distance through cohesive stiffness as given by Eq. (4.3).

$$\delta_1 = \frac{t_0}{k_P} \qquad (4.3)$$

where δ_1 is the separation distance at damage initiation, $t_0 = \sigma_0$ i.e. cohesive strength and k_P is initial stiffness (penalty stiffness) of cohesive elements. The initial stiffness of the cohesive material is related to elastic modulus of cohesive interface and thickness of cohesive elements as given by Eq. (4.4)

$$k_P = \frac{E}{T_C} \qquad (4.4)$$

Where E is elastic modulus and T_C is thickness of cohesive elements. The above formulae provide a recipe for estimating the parameters required for modeling the traction-separation behaviour of an interface in terms of the material properties of the bulk adhesive material. Relatively very thin layer of cohesive elements needs to be placed along the expected crack path. As per as modeling aspect is concerned, the thickness of cohesive elements is close to zero [Diehl (2008), Xie and Waas (2006), Chen *et al* (2005), Pardoen *et al* (2005), and Tomar (2004)]. As the thickness of the cohesive elements tends to zero, Eq. (4.4) implies that the stiffness, k_P, tends to infinity. This stiffness is often chosen as a penalty parameter. Very large penalty stiffness may result in ill-conditioning of the element operator in ABAQUS [Jadhav and Maiti (2010) and de Borst Rene, (2003)].

4.3.1 Constitutive Response of Cohesive Elements

The traction-separation law represents the tractions (normal stress) on the cohesive elements for different levels of nodal separation. The complete curve, shown in Fig 4.7, has three main components: the initial linear-elastic behaviour (curve '*OA*'), the criterion for damage initiation (point '*A*'), and the damage evolution (curve '*AB*') [ABAQUS (2007)]. The area under the whole curve represents the total fracture energy (Γ_0). The traction separation law shown in Fig 4.7 is completely described by cohesive parameters, i.e. cohesive strength (σ_0), fracture energy (Γ_0) and initial cohesive stiffness often called as penalty stiffness (k_P). The cohesive parameters (k_P, σ_0, δ_f, and Γ_0) cannot be measured in a direct way for ductile materials but have to be identified by fitting finite element results to experimental data [Zerbst(2009)]. Calibration of cohesive parameters is discussed in details in Chapter 5.

The damage initiation criterion defines the conditions at which the material begins to show degradation or cracking. The damage criterion used for the cohesive elements is the quadratic nominal stress criterion (referred as QUADS in ABAQUS). According to this criterion, damage is assumed to initiate when quadratic interaction function involving the stress ratios (stress ratio: induced stress to tensile strength in any direction e.g. normal or tangential to the cohesive element) reaches a value one [ABAQUS (2007)].
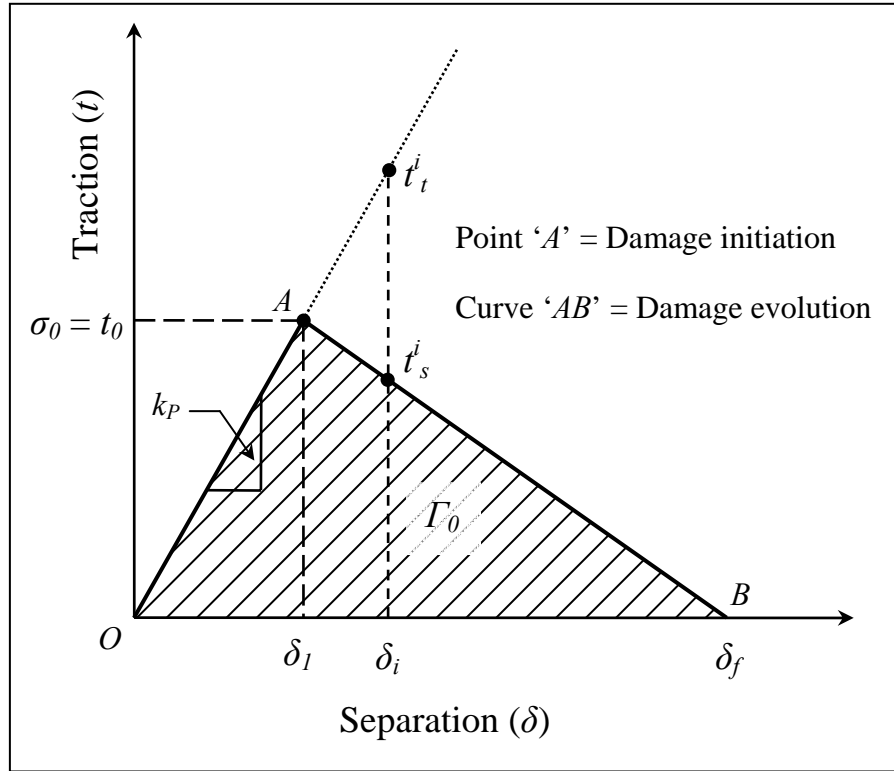
Fig 4.7 Constitutive response of cohesive element: Traction-separation law

The damage evolution (Curve 'AB'), also known as softening curve, is used to describe the rate at which the material stiffness degrades after the damage initiation criterion is reached. Softening curve can have different shapes (e.g., linear, bilinear, constant traction, exponential softening, etc.) depending on the fracture response of the material. ABAQUS allows the use of any softening curve shape by defining the overall material damage with the scalar damage variable, D. This damage variable has an initial value of 0.0 at damage initiation point (point 'A' in Fig 4.7) and evolves with separation to 1.0 when the material is fully degraded i.e. $\delta = \delta_f$ (point 'B' in Fig 4.7). The entire softening curve is defined as a tabular function in terms of the

48

damage variable versus the effective displacement at damage initiation [i.e. D_i versus $(\delta_i - \delta_1)$]. The stress components of the traction separation model are related to the damage variable by Eq. (4.5) [ABAQUS (2007)]:

$$D_i = \left(1 - \frac{t^i_s}{t^i_t}\right)$$

(4.5)

where t^i_s is the separation traction, D_i is the damage variable, and t^i_t is the stress component predicted by the elastic traction-separation behaviour for the current separation (δ_i) without damage. Therefore, the elastic traction t^i_t would be defined as Eq. (4.6)

$$t^i_t = k_P \times \delta_i$$

(4.6)

where k_P is the penalty stiffness and δ_i is the current element separation. Eq. (4.5) and (4.6) are only applicable to the tensile mode.

4.4   Calculation of Fracture Parameters

Xin et al (2011), Scheider *et al* (2006), Roy and Dodds (2001), Siegmund and Brocks (2000) reported that it is important to examine the CZM simulation prediction of the *CTOD* or *CTOA* value at the same distance away behind the current crack as in the experimental measurement of *CTOD* or *CTOA*. In the present work, the procedure to determine *J*-integral and critical *CTOD* is discussed in Chapter 3, section 3.3 and 3.4 respectively. The critical load and load versus LLD graph is obtained from CZM simulation and procedure discussed in Chapter 3, section 3.3 and 3.4 is followed to determine *J*-integral and critical *CTOD*. The experimental and CZM findings are compared and discussed in chapter 5 in order to arrive at conclusions

CHAPTER- 5

RESULTS & DISCUSSION

Introduction

This Chapter discusses determination of cohesive parameters and validation of cohesive zone model (CZM) with experimental observations. Subsequent topic focuses on the results obtained from the experiment and cohesive zone model (CZM) analysis. The results are summarized in tabular and graphical form. The discussion follows the results for various objectives. The results are discussed on formability indices and fracture behaviour. These results are discussed with reference to previously published journal papers, technical reports and conference proceedings.

5.1 Properties and Formability Parameters of EDD Steel Sheets

5.1.1 Chemical Composition

The chemical compositions of four EDD steel sheets are given in weight % in Table 5.1. The maximum percentage of carbon is observed in EDD 'A', amounting 0.06%. According to technical report published by TATA steel, this is an upper limit for EDD steel sheets, below which, the desired carbon level is good for formability. Higher carbon content leads to a decrease in the normal anisotropy ($\bar{r}$) [ASTM E517-00 (2010)]. This is attributed to an increase in the amount of cementite. High $\bar{r}$ values (>1.6) have been observed by Singh *et al* (2010a & 2010b) and Mizui and Okamoto (1990) in case of EDD steel sheets containing carbon less than 0.06%.

According to Ravi Kumar (2002), a sheet with a high $\bar{r}$ value generally possesses a high planar anisotropy value also. In the present work, since the difference in the carbon content among the four EDD steel sheets is significant, any variation in their formability can arise from carbon levels and grain size. Mizui and Okamoto (1991) studied the effect of Mn content (in the range 0.02–0.44%) on deep drawability of continuous annealed Al-killed steel sheets. They concluded that the $\bar{r}$ value in the rolling direction exhibited a maximum value at a medium Mn content. They attributed this to the changes in the distribution of MnS inclusions and the precipitations of

Al/N. Dasarathy and Hudd (1974) indicated that the presence of aluminum up to 0.08% have no adverse effect on the mechanical properties.

Table 5.1 Composition of the investigated EDD steel sheet in wt. %

No.	Material	C	Mn	S	P	Si	Al	N	Fe
1	EDD 'A'	0.06	0.38	0.03	0.017	0.05	0.040	0.0047	Balance
2	EDD 'B'	0.025	0.18	0.010	0.013	0.005	0.040	0.0040	Balance
3	EDD 'C'	0.015	0.16	0.010	0.010	0.005	0.041	0.0033	Balance
4	EDD 'D'	0.04	0.18	0.007	0.005	0.012	0.044	0.0034	Balance

5.1.2 Grain Size

The microstructure of the four EDD steel sheets in the as-received condition is studied using scanning electron microscopy. The values of average grain size determined by the linear intercept method are 7.2, 8.6, 10.3 and 16.7 μm, respectively for EDD 'A', EDD 'B', EDD 'C' and EDD 'D' steel. These values are accurate to within 2 μm. The investigations of Wilson and Acselrad (1984) on the effect of grain size showed that the favourable grain size for good formability is in the range of 7–18 μm. They have concluded that, strain hardening exponent, n and normal anisotropy, $\bar{r}$ increase with increase in grain size.

5.1.3 Strain Hardening Exponent

The formability of sheet metals is strongly influenced by the strain hardening exponent (n). The n values of four EDD steel sheets, determined by two methods are listed in Table 5.2.

By method-I, the value of n is taken equal to value of ultimate strain ε_u in true stress-strain curve, following Murthy (2005) and Caddell (1980). In the method-II, the value of n is calculated by using an empirical relationship given by Ravi Kumar (2002) and Schedin and Melander (1987). This empirical relation i.e. Eq. (5.1) is given below.

$$\varepsilon_u = 0.28 - 0.2[C] - 0.25[Mn] - 0.44[Si] - 0.39[S] - 1.2\,[N] \tag{5.1}$$

However, factors like grain size, heat treatment on which n greatly depends, are not taken into account in this relation. This empirical equation (i.e. Eq. 5.1) has very limited applicability. In the present work, only the value obtained from the true stress-strain curve is used. The material EDD 'A' possesses a lower n value (0.145) indicating its inferior formability. Other three materials have n values in the range of 0.185 – 0.234 and hence greater formability.

Table 5.2 Strain hardening exponent (n) of EDD steel sheets

EDD-STEEL	Method-I $n = \varepsilon_u$	Method-II by Eq. (5.1)
EDD 'A'	0.145	0.134
EDD 'B'	0.234	0.219
EDD 'C'	0.234	0.227
EDD 'D'	0.185	0.215

5.1.4 Mechanical Properties

The mechanical properties of the EDD steel sheets for three different rolling directions (RD), obtained from TATA steel, Jamshedpur are summarised below, in Table 5.3. From Table 5.3, it is observed that, except EDD 'A', in all cases the YS and UTS values are higher at 45° to the rolling direction than in the direction parallel or perpendicular to the rolling direction. The elongation to fracture is greater along the rolling direction than along directions perpendicular or diagonal to the same. The results obtained from the tension tests in all three directions are qualitatively same. The average values of strength are closest to the values of strength in rolling direction. Therefore, the results are described by means of values obtained from the tests in the rolling direction only. The tensile test data along rolling direction is tabulated in Appendix A.

The strain rate sensitivity index (m), is found to be very similar for all the three directions, i.e. 0°, 45°, and 90° to the rolling direction (RD). The m values are also reported in Table 5.3, which are seen to be moderate. This is consistent with the fact that most of the common metals like low carbon steel have low sensitivity to the strain rate at room temperature. This is also observed by Tejedor *et al* (2008), Itabashi and Kawata (2000) and Swaminathan and Padmanabhan (1991).

Table 5.3 Mechanical properties of EDD steel obtained from TATA steel, Jamshedpur

EDD steel	Orientation w.r.t RD (^{o})	YS (MPa)	UTS (MPa)	Uniform elongation (%)	Total elongation (%)	SRS index, *m*
EDD 'A'	0	293.59	387.12	15.6	29.69	
	45	291.52	391.88	15.31	25.23	0.017
	90	289.95	386.65	14.46	23.87	
Average		291.64	389.38	15.17	26.01	
EDD 'B'	0	276.97	342.04	26.4	53	
	45	279.22	348.45	24.89	44.93	0.012
	90	274.32	339.04	22.29	40.55	
Average		277.43	344.50	24.62	45.85	
EDD 'C'	0	245.41	330.043	26.4	55.19	
	45	246.55	334.143	24.89	45.72	0.01
	90	241.70	329.393	22.29	39.52	
Average		245.05	331.93	24.62	46.54	
EDD 'D'	0	180.74	381.93	20.23	29.5	
	45	181.88	386.03	18.37	20.03	0.01
	90	177.03	380.98	14.9	13.83	
Average		180.38	383.74	17.97	20.85	
Average, $X = (X_0 + 2X_{45} + X_{90})/4$						

5.1.5 Normal Anisotropy ($\bar{r}$)

As given in Table 5.4, the product $n\bar{r}$, which is indicative of overall press performance factor, is high for EDD 'B', EDD 'C' and EDD 'D'. As expected, EDD 'A' has relatively low value. However, according to Cada (1996) and Mellor (1981), this factor has little physical significance, as it is only a numerical index used for a rough assessment of formability.

Following ASTM E8M-11 (2011) and E517-00 (2010) standards, EDD 'B', EDD 'C' and EDD 'D' steel sheet has relatively high formability than EDD 'A' steel sheet. However, from the above study, it is very clear that the formability test is influenced by number of material

variables. Apart from these material variables, the process variables also affect the forming test. These include punch and die configuration/assembly, clearances, and lubrications. According to Ravilson *et al* (2009), Hussain *et al* (2009), Jackson and Allwood (2009) and Ravi Kumar (2002), any minor discrepancy in the relative overall formability could be due to the complex interaction of large number of (process and/or material) variables. Hence several parameters are considered to completely explain the formability limits.

Table 5.4 Press performance factor of three EDD steel materials

EDD-STEEL	n	r_0	r_{45}	r_{90}	$\bar{r}$	$n\bar{r}$
EDD 'A'	0.145	0.97	0.82	1.21	0.96	0.14
EDD 'B'	0.234	1.37	1.04	1.58	1.26	0.29
EDD 'C'	0.234	1.47	1.21	1.83	1.43	0.33
EDD 'D'	0.185	1.57	1.29	1.99	1.54	0.28
$\bar{r} = (r_0 + 2r_{45} + r_{90})/4$						

Fracture mechanics may not be able to remove all variables of the conventional forming tests. However, the fracture test data could be utilised to find out critical load at which crack initiates, amount of necking and fracture stress/strain with least number of variables. The test facilities also need not to be changed as it is done in case of forming tests discussed by Ravilson *et al* (2009), Yoshihara (2005) and Ravi Kumar (2002).

5.2   Fracture Criterion

As discussed by Pardoen and Delannay (2000), the detection of cracking initiation is a remnant problem in fracture tests performed on ductile materials. From the application point of view, the present study investigates precise load and fracture parameter calculations at crack initiation. The criterion should ascertain that either the crack has already moved by a small amount or it is definite to move if load is increased by a small amount.

The 'load drop technique', mentioned by Ray (2010), Kulkarni (2005) and Kulkarni *et al.* (2002, 2003a) is used as a fracture criterion to measure the fracture parameters. As soon as the load drops the crack is initiated on the surface in the necking zone. However, to check the

possibility of crack initiation inside the neck, a few specimens are chosen before and at the load drop point. Fig 5.1 shows a crack profile at mid-thickness section for a specimen unloaded just before load drop point. The blunt profile does not show any crack. From this observation, it is concluded that the crack is not initiated at mid-thickness section before it reaches the load drop point.

Fig 5.2 (a) and (b) shows a small crack initiated, respectively on the surface and at mid-thickness section of a specimen unloaded at the load drop point. Both the cracks show same length, only the damage in front of crack tip at surface level is not clearly visible. This observation supports that the crack is initiated only at load drop point. Therefore, it is concluded that, the crack initiates at the center of necking zone and reaches the surface without any significant travel.
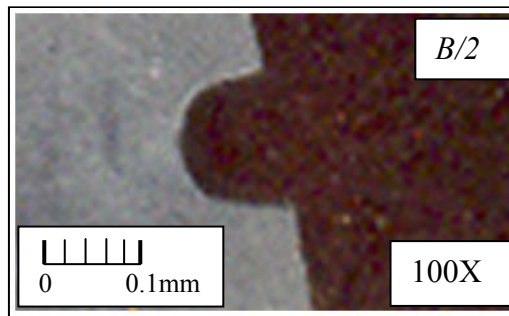
Fig 5.1 Crack profile at mid-thickness section of a specimen unloaded before load drop point
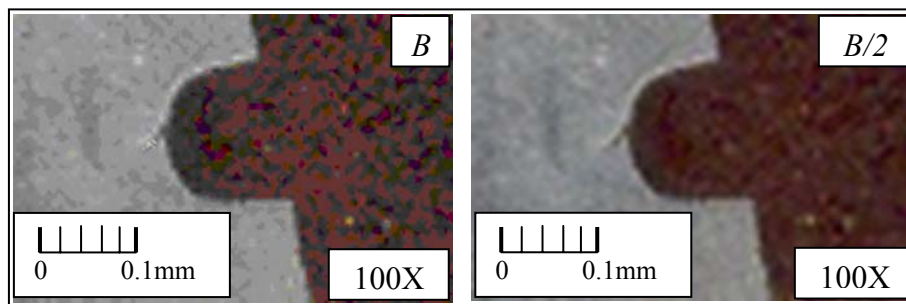
(a)   (b)

Fig 5.2 (a) Crack on surface of a specimen unloaded at the load drop point. **(b)** Crack at the mid-thickness section of specimen at the load drop point.

From this observation, it is found that cracking initiation corresponds to the nucleation of a micro-crack in front of a blunt notch. This is the result of linking of the blunted crack tip with the closet damage site (a void or a micro-crack). Therefore, more accurate definition of cracking initiation is proposed that 'the critical event of cracking initiation is the point at which the process of plastic deformation at the original crack tip (i.e. the blunting process) is stopped'. Thereafter, the load is carried mainly by the new crack tip.

Fig 5.3 (a) and (b) shows fracture surface of broken open up specimen before load drop point and at load drop point, respectively. The fracture surface before load drop point in Fig 5.3 (a) is complete shiny, right from the notch tip with an indication of complete brittle fracture and no crack initiation or ductile tearing. Whereas, the fracture surface at the load drop point in Fig 5.3 (b) consists of two parts. The smaller part is with minute ductile tearing in the necking zone with an indication of crack initiation and a large shiny zone with an indication of brittle fracture. The brittle fracture is due to the thermal shock treatment.

(a)   (b)
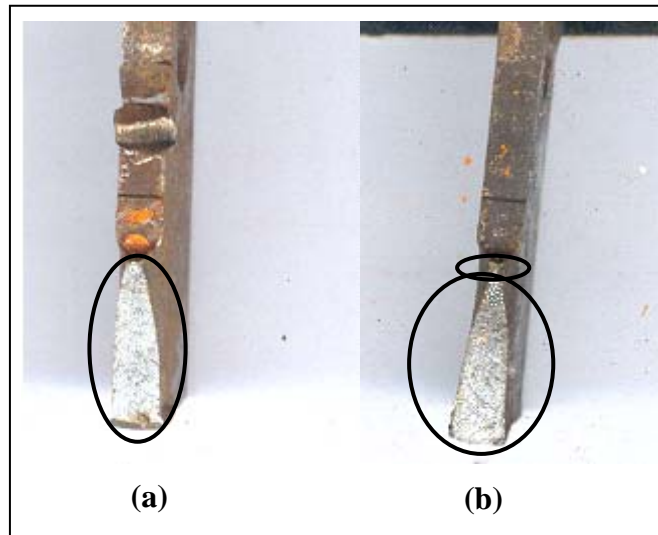
Fig 5.3 Fracture surface: **(a)** at the load drop point **(b)** before the load drop point

From these observations i.e. Fig 5.1, 5.2 and 5.3, it is clear that in case of EDD steel sheets, the crack initiation occurs when load drops. The fracture surface observations present the advantage of giving insight into the macro-mechanisms of damage ahead of crack tip.

5.3 Validation of Cohesive Zone Model (CZM)

Specimen T1 was first analyzed. There are 2916 nodes and 2704 four nodded quadrilateral continuum elements. The cohesive zone is modeled separately. It contains 272 nodes and 135 cohesive elements. The cohesive elements placed along the crack path with tie constrained. Cohesive elements are taken to be square of side 0.1 mm. The continuum elements around cohesive zone are taken to be squares of side 0.5 mm. Two more sizes, 0.3 mm and 1.0 mm, were also considered to examine the mesh sensitivity of the results. The loading pins were modeled as rigid pins to avoid any severe local deformation at the contact points. The analysis was done under displacement control; the displacement was applied at the center of the pin as shown in Fig 5.4.
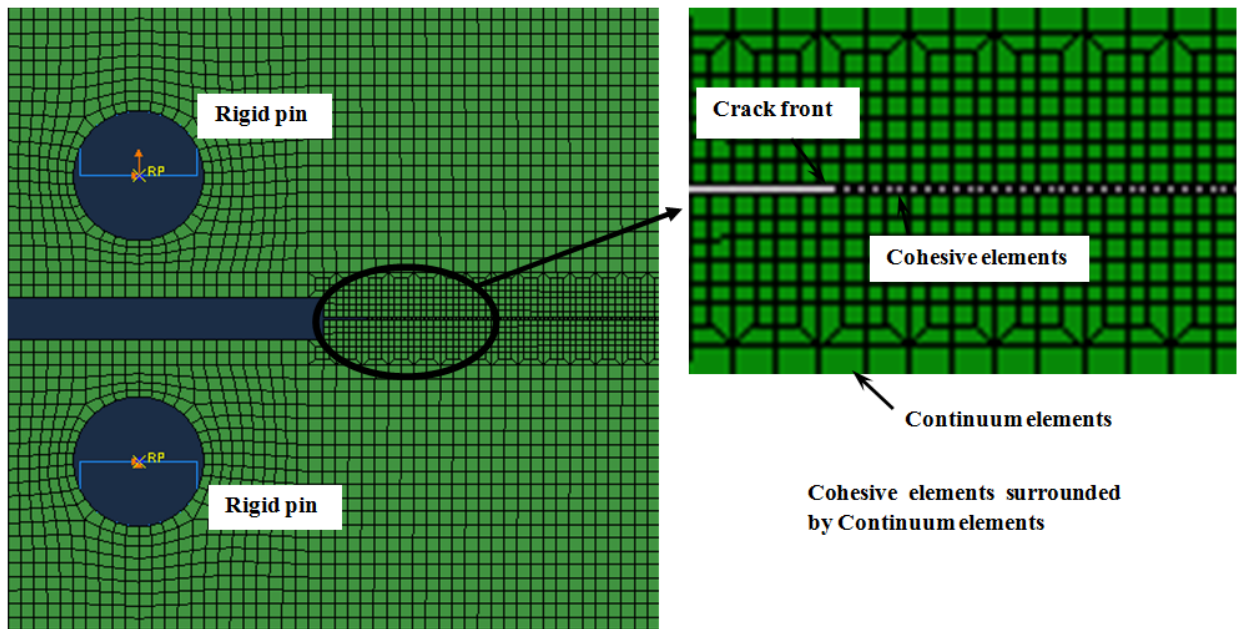
Fig 5.4 Finite element model with cohesive layer for CT specimen

5.3.1 Traction–Separation Law and Cohesive Parameters

There are basically two potential approaches to develop a cohesive law: by experimental measurements or by a phenomenological way with predefined functional assumption and estimated parameters. Since there is no effective experimental method available to directly measure the traction–separation relation, few researchers attempted experiments related to the determination of cohesive laws [Tan 2005]. The commonly adopted approach assumes certain

law of the traction–separation relation for the cohesive zone and the cohesive parameters are treated as modeling constants which are determined by fitting the CZM simulation results to a set of experimental data. The key features of a cohesive zone model include the shape of the traction-separation curve and the value of the cohesive parameters.

5.3.1.1 Shape of traction-separation curve

Many variations of cohesive zone models have been proposed in literature and successfully applied to predict fracture behaviours. The applications of the CZM mostly fall in the range of exponential [Xu and Needleman 1994, Ortiz and Pandolfi 1999, Roy and Dodds 2001, Scheider and Brocks 2003, etc.], linear/bilinear [Qiu et.al 2001, Blackman etal 2003 a b& c, Turon 2006, Ortiz and Suresh 1993, etc.], and trapezoidal [Tvergaard and Hutchinson 1992, etc.] forms of traction-separation laws. Fig 5.5 shows the representative cohesive law shapes.

The key cohesive parameters describing the CZM consist of the cohesive strength (σ_0), defined by the peak value of the traction-separation curve; the cohesive energy (Γ_0), represented by the area under the traction-separation curve, and maximum separation distance (δ_f). Calibration of theses parameters is discussed in subsequent topic (i.e. section 5.3.1.2). Among the various forms of cohesive laws, there is one common feature, i.e. the magnitude of the cohesive traction usually increases with accrued separation between the cohesive surfaces, and after a critical peak value is reached, the traction drops towards zero with further separation.For the ductile materials literature suggests (e.g., Jadhav and Maiti, 2010, Scheider and Brocks, 2006, Scheider and Brocks, 2003a) use of exponential or constant variation of normal traction with the relative normal displacement. Scheider and Brocks, 2003a, used constant traction separation law with $\delta_1 = 0.01\delta_f$ and $\delta_2 = 0.7\delta_f$.
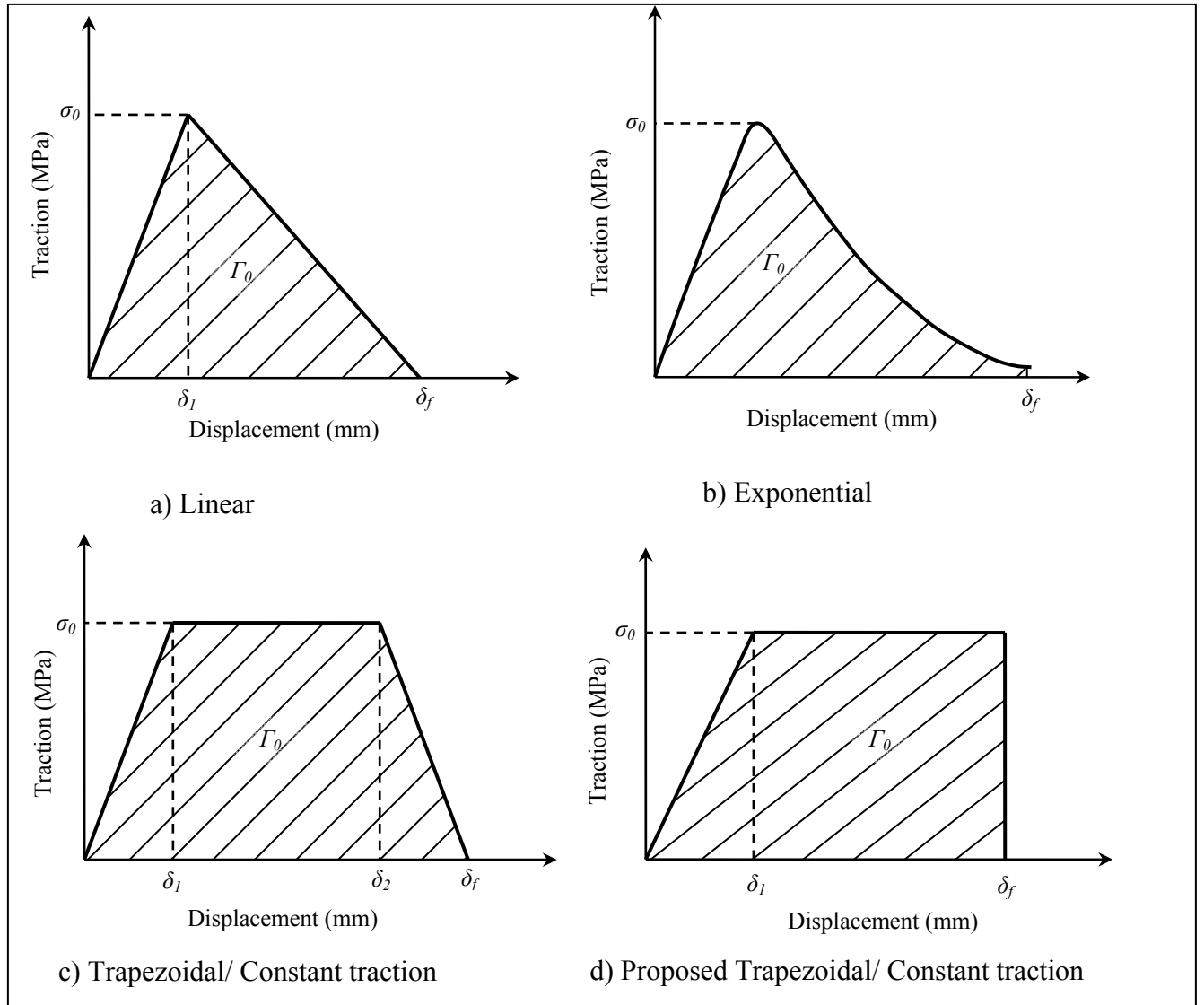
Fig 5.5 Different forms of the traction separation law

In the present case, the material used is high ductile material with load maxima is fracture criteria. The constant traction law is chosen with $\delta_2 = \delta_f$ (Fig 5.5d) and δ_1 is related to cohesive strength and cohesive stiffness (discussed in section 5.3.1.2). The analysis is done using linear, exponential and proposed constant traction law and results are compared with the experimental load vs. load line displacement curve (Fig 5.6). For simulation of this problem, load line displacement is given as input. From Fig 5.6 it is observed that linear traction separation law (Fig 5.5 (a)) underestimates the maximum load and literature says that [Turon (2006) and Blackman *et al* 2003 a b& c] it is used for brittle material/ linear elastic analysis. Exponential law (Fig 5.5 (b)) is used for ductile materials but in present case it underestimates load line

displacement. For example experimentally the maximum load observed at 1.58 mm load line displacement where as exponential law gives maximum load at 1.22 mm. The results from proposed constant traction separation law with $\delta_2 = \delta_f$ are found to be close to the experimental observations; the maximum load is over–estimated only by 1.44% and corresponding J value at crack initiation i.e. J_i, based on load vs LLD is 2.14% more than experimental value. Thus the proposed constant traction- separation law is considered for the further study.
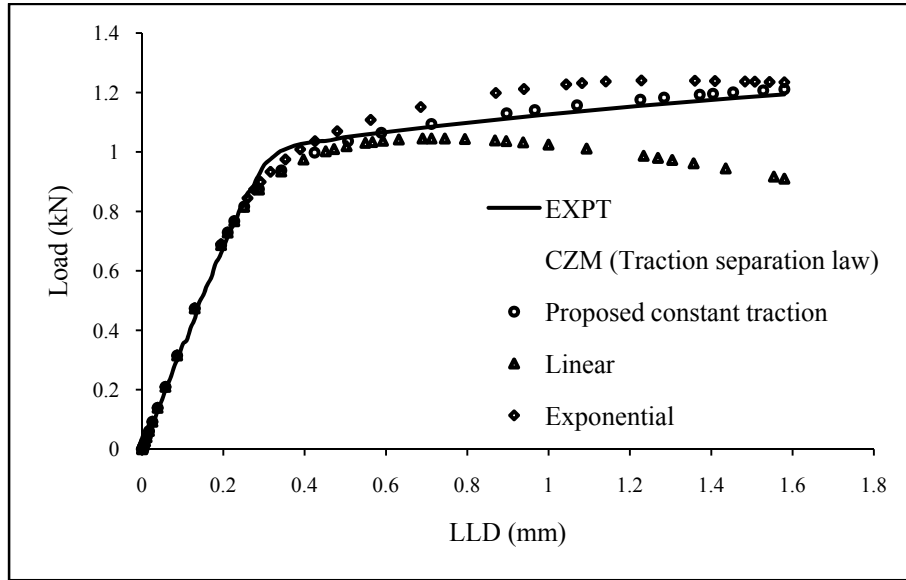
Fig 5.6 Comparison of load–LLD curves based on three cohesive laws with experimental data

5.3.1.2 Calibration of cohesive parameters

To describe the proposed constant traction–separation law, the cohesive parameters i.e. cohesive strength (σ_0), fracture energy (Γ_0) and critical separation distance (δ_f) are required. Out of these three parameters only two parameters are sufficient to describe the tration- separation curve and third parameter can be evaluated from traction–separation curve. Additional parameter i.e. δ_1 is relted to cohesive stiffness and cohesive strength (Fig 5.7). Subsequent paragraphs discuss about fracture enegry, cohesive stiffness and cohesive strength.

A procedure for the determination of the cohesive parameters for normal fracture in ductile materials has been proposed by Cornec *et al* 2003. According to this procedure, J_i is taken as a first approximation of the cohesive energy, Γ_0. For present study, J_i is determined from the fracture test of CT specimen (based on experimental load vs LLD curve) and using ASTM

standard E1820-11 (2011) described earlier. Following this procedure, first approximation of fracture energy is taken as J_i calculated from experimental load vs LLD data, which is found to be 204.38 N/mm. Few trials have been conducted to fit the CZM results to experimental observations. The calculated value of fracture energy from proposed constant traction- separation law is found to be 224.35 N/mm (Fig 5.7). The percentage difference of calculated J_i from load vs LLD curve based on CZM over J_i based on experimental load vs LLD data is found to be 2.14%, and is acceptable.

The graph shows the equations:
$$k_P = \frac{\sigma_0}{\delta_1} \quad \text{and} \quad \Gamma_0 = \sigma_0 \times \delta_f - \frac{1}{2}\sigma_0 \times \delta_1$$

with Traction (MPa) on the vertical axis and Displacement (mm) on the horizontal axis, showing σ_0, k_P, Γ_0, δ_1, and δ_f.
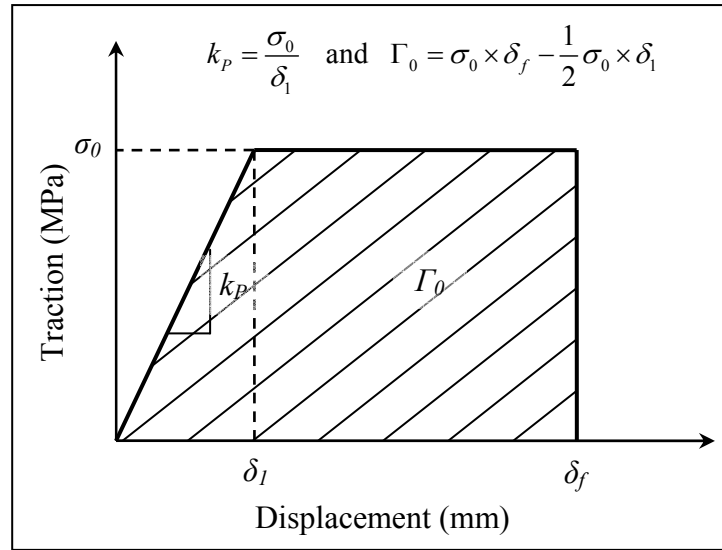
Fig 5.7 Proposed constant traction- separation curve

As discussed earlier, the thickness of cohesive elements is close to zero, its stiffness becomes infinite. Often this stiffness for the cohesive element is chosen as a penalty parameter. It is reported [de Borst Rene, 2003] that a very high penalty stiffness sometimes creates numerical error. Jadhav and Maiti (2010) used initial cohesive element stiffness same as the continuum material stiffness. The small ratio of continuum material stiffness to initial cohesive stiffness leads computational process unstable [Bonifaz, 2011]. In literature [Turon *et al* (2007), Camanho *et al* (2003), Zou *et al* (2002), Falk *et al* (2001), Ruiz *et al* (2001), Camacho and Ortiz (1996), Daudeville *et al* (1995), Rice and Beltz (1994), Rice (1992)] different guidelines are proposed to define initial stiffness of cohesive materials. A more versatile cohesive law was proposed by Schneider (2003) which fulfils the requirement that the initial stiffness of the cohesive elements can be varied. An initial penalty stiffness is required for the intrinsic cohesive

element formulation, i.e., where the cohesive elements are in the expected crack path. The penalty stiffness has to be steep to generate an accurate pre-peak load versus CMOD response. The penalty stiffness can only be increased to a certain limit since an excessively large value may be detrimental to the convergence of the solution. While low penalty stiffness can reduce the initial stiffness of the specimen's load versus LLD curves. Therefore, as this quantity has no direct relation with material properties such as the modulus of elasticity used on bulk elements in the model, it should be determined by successive trials to obtain the highest penalty stiffness that does not significantly compromise the convergence of the FE model.

For the present study, number of trials has been performed by choosing different values of penalty stiffness and the results are compared with the experimental observations. For demonstration purpose three different values of penalty stiffness 1) k_P = 210e4 N/mm^3 (i.e. k_P is equal to continuum material stiffness), 2) k_P = 9000 N/mm^3, 3) k_P = 5000 N/mm^3 are considered (Fig 5.8). It is observed that high initial stiffness over estimates the load at all values of load line displacement. Lower value of initial stiffness increases compliance between the cohesive and continuum element interface. Since the system compliance is increased, the load values in elastic part are underestimated. The moderate initial stiffness gives the load value close to experimental results. For present case the initial stiffness for CZM is taken as 9000 N/mm^3.
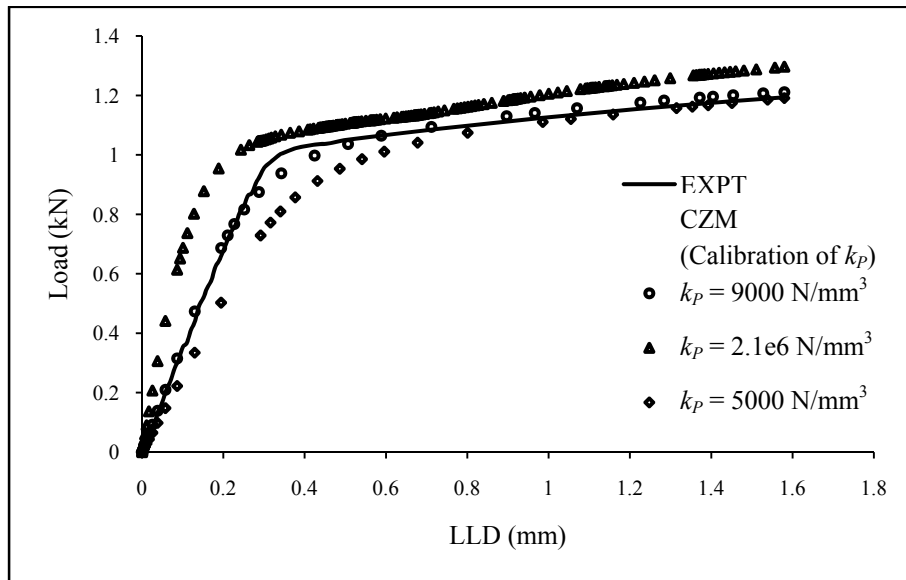
Fig 5.8 Effect of penalty stiffness on load–LLD curve

In present case, an isotropic hardening material with Young's modulus (E) = 210 GPa and yield strength (σ_y) = 293 MPa is used. The material separation process is characteristic of atomistic separation and cleavage processes. Consequently, the cohesive strength is related to Young's modulus. i.e. $\sigma_0 = E/20$ [Brinckmann and Siegmund, 2008]. The cohesive strength is equal to 10.5 GPa. The ratio between cohesive strength and yield strength is σ_0/σ_y = 35.8. For such conditions no crack propagation would occur even under monotonic loading conditions in a framework of conventional plasticity. In most of the practical applications of CZM, the cohesive strength is either related to yield strength or fracture strength.

According to Cornec *et al* 2003, the cohesive strength, σ_0, can be taken as the maximum stress at fracture in a round notched tensile bar. Since round notched bars cannot be machined from sheet metal and the respective failure mode (normal fracture) would be different from that in the thin C(T) specimen (slant fracture). The cohesive strength is the maximum resistance to fracture and is usually related to the yield stress of the material [Scheider and Brocks 2006, Chen and Kolednik 2005, Chen and Kolednik 2003, etc.].

In order to determine cohesive stress, Chen *et al* (2002) reported two methods, 1) Necking stress method: the cohesive stress equals to the necking stress and 2) Equal-Area Method: the cohesive stress is selected to give the same area below the stress-strain curve. They suggested that necking stress method is suitable for small scale yielding (SSY) whereas equal-area method is used for large scale yielding (LSY). According to equal- area method, it is realized that cohesive strength falls in between yield strength and ultimate strength.

Initially equal–area method is used to determine cohesive strength. The cohesive strength is found to be equal to 425 MPa with the ratio of cohesive strength to yield strength is σ_0/σ_y = 1.45. It is observed that the results obtained by CZM with σ_0 = 425 MPa overestimates the experimental load values. As mentioned by Anvari *et al* (2006), Tvergaard (2001) and Siegmund and Brocks (2000), the cohesive strength is directly related to stress triaxiality. Low stress triaxiality lowers the cohesive stress value and vice versa. However in the present study, predominating plane stress conditions and significant crack necking is observed which further reduces the stress triaxiality ahead of the crack tip. Therefore the cohesive strength, σ_0 = 425 MPa overestimates the experimental load values is because of significant crack necking and less stress triaxiality ahead of crack tip.

Therefore different strategy i.e. procedure by fitting simulation results to experimental records is followed to determine cohesive strength [Zerbst *et al* (2009)]. Based on experimental stress-strain data and the corresponding true stress-strain values, the true stresses corresponding to yield point and fracture point are determined (Fig 5.9).
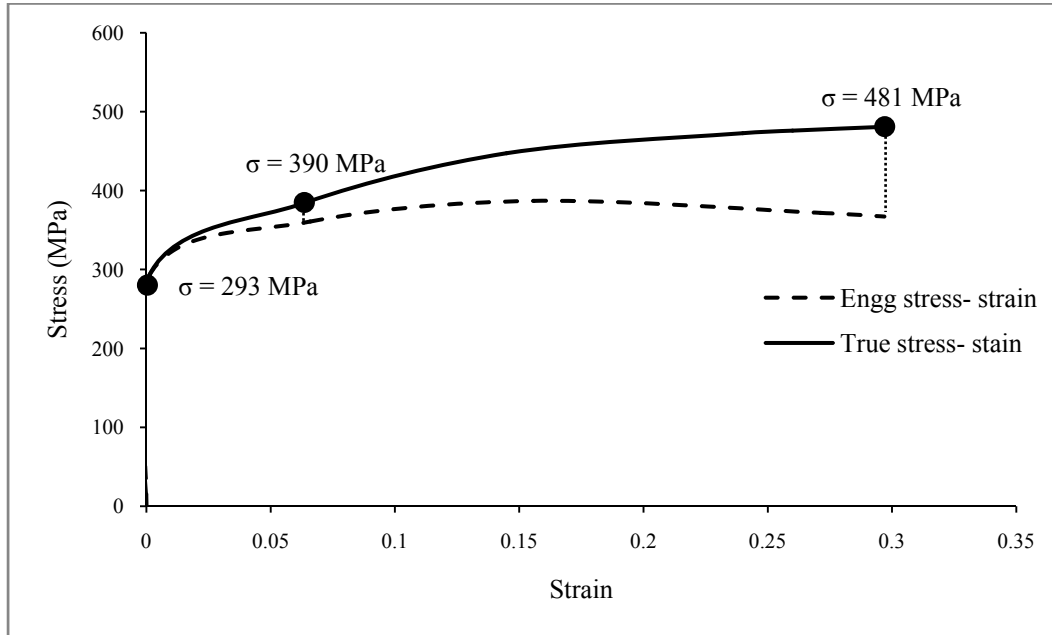
Fig 5.9 Cohesive strength determination

For the present study number of trials has been performed by choosing different values of cohesive strength and the results are compared with the experimental observations. For demonstration purpose three different values of cohesive strength 1) $\sigma_0 = \sigma_y = 293$ MPa (i.e. $\sigma_0/\sigma_y = 1$), 2) $\sigma_0 = 1.33\sigma_y = 390$ MPa (i.e. $\sigma_0/\sigma_y = 1.33$) and 3) $\sigma_0 = 1.64\sigma_y = 481$ MPa (i.e. $\sigma_0/\sigma_y = 1.64$) are considered (Fig 5.10). It is observed that higher value of cohesive strength over estimates the load where as lower value of cohesive strength, underestimates the load. The moderate value of cohesive strength gives the load values close to experimental results. For the present case, the cohesive strength for CZM is taken as 390 MPa.

In order to decide on a suitable element size around cohesive elements, results based on three sizes (0.3 mm, 0.5 mm and 1.0 mm) are compared in Fig 5.11. The element size, 0.3 mm and 0.5 mm give better results. Overall both the sizes (0.3 mm and 0.5 mm) were found to be equally acceptable. Finally, element size of 0.5 mm was selected for further computations to take

advantage of the fact that this leads to lower number of steps, hence less computational time for an analysis.
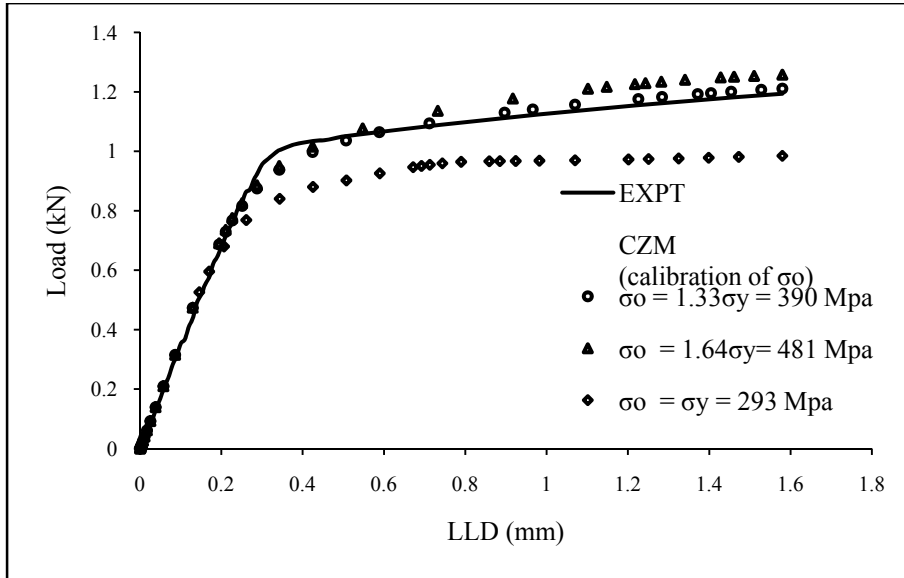
Fig 5.10 Effect of cohesive strength (σ_0) on load–LLD curve
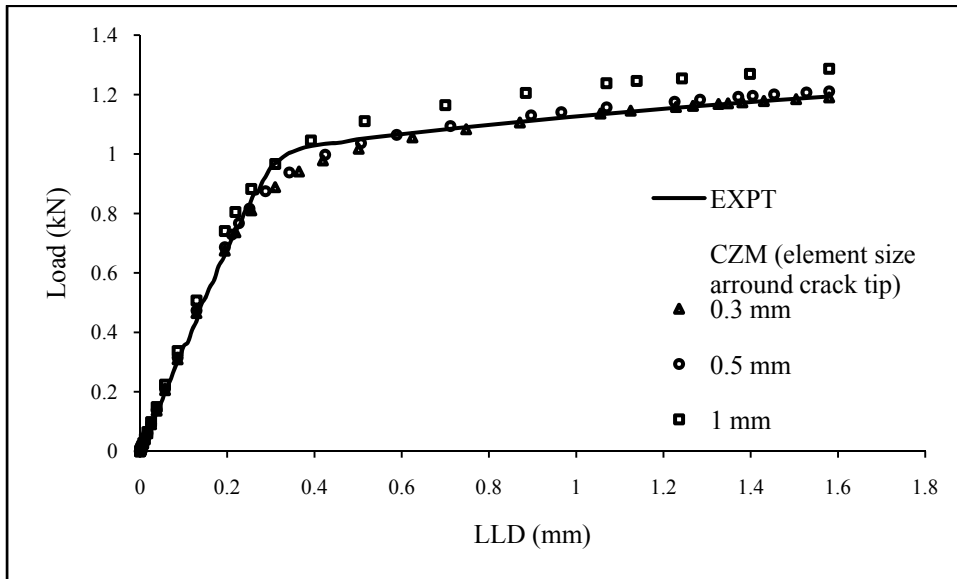
Fig 5.11 Effect of element size on load–LLD curve

5.3.2   Validation of the Other Cases

The traction- separation for fracture simulation using CZM is characterized by cohesive parameters i.e. fracture energy, initial stiffness and cohesive strength. All three parameters are

material constants, only fracture energy can be measured experimentally. The other two parameters are difficult to determine and may be treated as penalty or fitting parameters. It can be seen from the preceding sections that there is no hard-and-fast guideline for determining the parameters of the traction- separation relationship – it is dependent on the problem under consideration.

The remaining specimens i.e. T2 – T6 , N1 – N15, S1 – S8 and A1 – A4 were studied using proposed constant traction separation law and 0.5 mm element size. The cohesive parameters for each case are determined by using the calibration procedure as discussed in preceding section. The comparisons of predicted load–LLD with the experimental results for two cases are only shown in Fig 5.12. There is a good agreement in all the cases (Appendix C; Fig C1 – Fig C33).
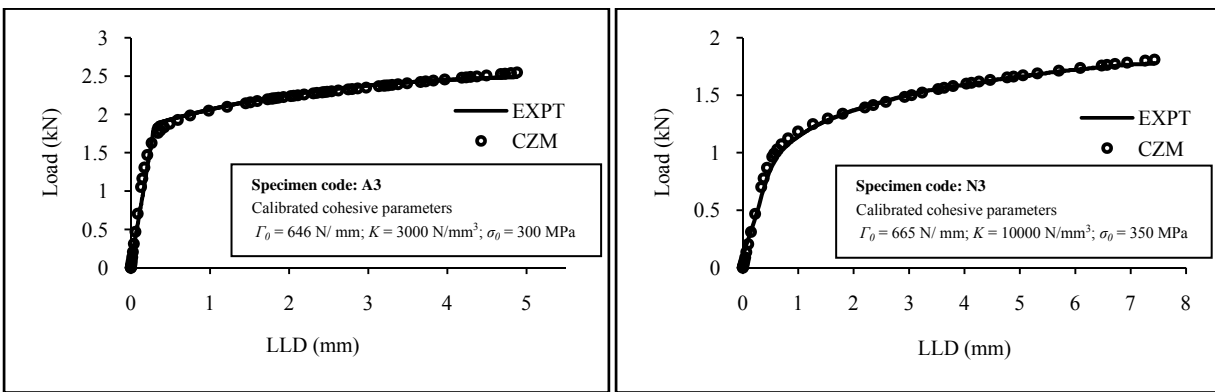
Fig 5.12 Validation of CZM: Comparison of load–LLD curves with experimental data for two cases

Table 5.5 to 5.8 shows the peak load values obtained from CZM and experimental observations for thickness effect (specimen T2 – T6), Notch radius effect (specimen N1 – N15), strain rate effect (specimen S1 – S8) and a_0/W ration effect (specimen A1 – A4) respectively. The percentage difference between peak load from experimental data and peak load calculated from CZM is found to be within 4%, thus the values of peak loads calculated from CZM are acceptable.

Table 5.5 Comparison of peak load values (Specimen T2 – T6)

Specimen code	Thickness (mm)	Peak load, kN (Expt)	Peak load, kN (CZM)	% difference
T1	1.2	1.19	1.21	1.44
T2	1.3	1.31	1.34	2.14
T3	1.4	1.43	1.45	1.38
T4	1.5	1.57	1.58	0.57
T5	1.6	1.71	1.72	0.11
T6	1.7	1.78	1.81	1.49

Table 5.6 Comparison of peak load values (Specimen N1 – N15)

Specimen code	Notch radius (mm)	Peak load, kN (Expt)	Peak load, kN (CZM)	% difference
N1	0.07	2.49	2.55	2.58
N2	0.085	2.49	2.49	0.06
N3	0.1	2.49	2.55	2.43
N4	0.11	2.61	2.67	2.31
N5	0.12	2.54	2.54	0.06
N6	0.13	2.49	2.52	1.45
N7	0.14	2.48	2.56	2.85
N8	0.15	2.58	2.60	0.61
N9	0.16	2.59	2.66	2.69
N10	0.17	2.62	2.69	2.48
N11	0.18	2.61	2.69	3.00
N12	0.25	2.71	2.72	0.32
N13	0.4	2.75	2.79	1.20
N14	0.6	2.85	2.86	0.17
N15	0.75	2.91	2.92	0.33

Table 5.7 Comparison of peak load values (Specimen S1 – S8)

Specimen code	Strain rate (mm/min.)	Peak load, kN (Expt)	Peak load, kN (CZM)	% difference
S1	0.1	0.972	0.998	2.66
S2	0.2	0.972	0.997	2.64
S3	0.3	0.972	0.997	2.60
S4	0.4	0.968	0.997	3.03
S5	0.6	0.960	0.990	3.17
S6	1	0.855	0.869	1.65
S7	1.5	0.821	0.849	3.49
S8	2.5	0.781	0.804	2.96

Table 5.8 Comparison of peak load values (Specimen A1 – A4)

Specimen code	a_0/w ratio	Peak load, kN (Expt)	Peak load, kN (CZM)	% difference
A1	0.5	2.07	2.12	2.30
A2	0.525	1.98	2.02	2.17
A3	0.55	1.78	1.84	3.18
A4	0.575	1.62	1.64	1.28

Table 5.9 to 5.12 shows the J_i values based on load vs LLD data obtained from CZM and experimental observations for thickness effect (specimen T2 – T6), Notch radius effect (specimen N1 – N 15), strain rate effect (specimen S1 – S8) and a_0/W ratio effect (specimen A1 – A4) respectively.

Table 5.9 Comparison of J_i values (Specimen T2 – T6)

Specimen code	Thickness (mm)	J- integral, N/mm	J- integral, N/mm	% difference
T1	1.2	204.38	208.75	2.14
T2	1.3	205.94	222.68	8.13
T3	1.4	224.26	233.31	4.03
T4	1.5	226.48	247.98	9.49
T5	1.6	250.85	261.12	4.10
T6	1.7	248.45	268.44	8.04

Table 5.10 Comparison of J_i values (Specimen N1 – N15)

Specimen code	Notch radius (mm)	J- integral, N/mm	J- integral, N/mm	% difference
N1	0.07	583.4743	584.0521	0.10
N2	0.085	532.1311	534.1619	0.38
N3	0.1	551.6413	556.0022	0.79
N4	0.11	525.4401	523.32	0.40
N5	0.12	539.8656	545.2823	1.00
N6	0.13	514.3757	520.3975	1.17
N7	0.14	558.381	565.8601	1.34
N8	0.15	541.1943	564.3308	4.28
N9	0.16	577.2952	571.0877	1.08
N10	0.17	597.8835	583.8503	2.35
N11	0.18	598.6687	586.6515	2.01
N12	0.25	644.7871	658.2333	2.09
N13	0.4	666.6713	683.4738	2.52
N14	0.6	696.1426	725.7879	4.26
N15	0.75	729.0518	770.0279	5.62

Table 5.11 Comparison of J_i values (Specimen S1 – S8)

Specimen code	Strain rate (mm/min.)	J- integral, N/mm	J- integral, N/mm	% difference
S1	0.1	355.51	369.21	3.85
S2	0.2	354.33	368.01	3.86
S3	0.3	353.15	366.81	3.87
S4	0.4	353.16	367.06	3.94
S5	0.6	325.58	342.19	5.10
S6	1	279.41	282.78	1.21
S7	1.5	268.80	270.73	0.72
S8	2.5	229.19	230.76	0.69

Table 5.12 Comparison of J_i values (Specimen A1 – A4)

Specimen code	a_0/w ratio	J integral, N/mm	J integral, N/mm	% difference
A1	0.5	661.8276	674.0268	1.84
A2	0.525	652.0813	669.0236	2.60
A3	0.55	623.2651	643.8313	3.30
A4	0.575	613.2286	616.7742	0.58

The percentage difference between J_i from experimental data and J_i calculated from CZM for specimens T2, T4 and T6 is found to be 8.13%, 9.49 % and 8.04% respectively which is slightly higher. The reason would be there is a small slippage found during experiment (for specimen T4) as well as more tuning of cohesive parameters (penalty stiffness and cohesive strength) is required for specimen T2, T4 and T6 (Fig C2, Fig C4 and Fig C6). The percentage difference between J_i from experimental data and J_i calculated from CZM for all other cases is found to be within 5%, thus the values of J_i calculated from CZM are acceptable.

5.4   Crack Frank Opening Angle (CFOA) Method

As discussed in methodology, CFOA method was used to determine plastic *CTOD*. Fig 5.13 shows a superimposition of geometry of triangles used in PHM and CFOA. The plastic *CTOD* using CFOA method $(\delta_{pl})_{CFOA}$ depends on O'G and plastic load line displacement (V_{pl}), whereas plastic *CTOD* using PHM (plastic hinge model) $(\delta_{pl})_{PHM}$ depends on OG and V_{pl}. Eq. (3.10) and (3.13) can be rewritten as Eq. (5.2) and (5.3), respectively.

$$(\delta_{pl})_{PHM} = \frac{r_{pl}b}{r_{pl}b + a_0} V_{pl} = (C) V_{pl} \tag{5.2}$$

$$(\delta_{pl})_{CFOA} = \frac{O'G}{O'G + GH} V_{pl} = (X) V_{pl} \tag{5.3}$$

In Eq. (5.2), C is dependent upon plastic rotational factor (r_{pl}), initial crack length (a_0) and unbroken ligament length (b) and is found to be constant having value 0.4313 for the given geometry of CT specimen (except specimen A1 to A4). Therefore, there is a linear relation between (δ_{pl}) and V_{pl} in PHM. In Eq. (5.3), X is variable because of variation in CFOA which is due to change in V_{pl}. Therefore there is a non-linear relation between (δ_{pl}) and V_{pl} in CFOA.
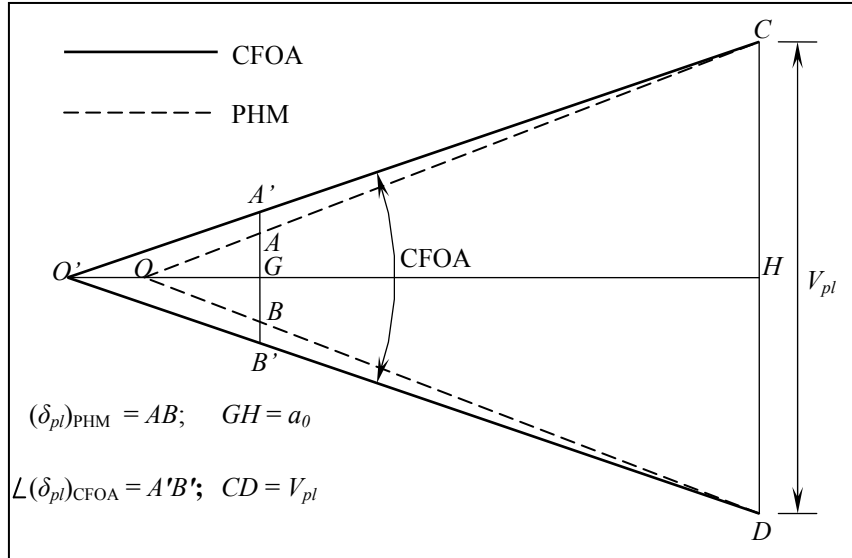
Fig 5.13 Comparison of PHM and CFOA method.

In comparison, the PHM results on plastic *CTOD* are on lower side because of linear relation between *CTOD* and plastic load-line displacement (V_{pl}) as given by Eq. (5.2), which may be applicable to a higher range of thickness, falling in LEFM and EPFM regime. According to Toda *et al* (2008) and Wilson and Landes (1994), this model can be used for low deformation ahead of crack tip. In case of EDD steel sheet, it is observed that there is a significant deformation ahead of crack tip resulting in higher value of plastic load line displacement also degree of blunting at the crack-tip is very high and fracture behaviour fall in general yield regime. The linear relation in between load-line displacement and *CTOD* cannot account for the high degree of blunting. The suggested CFOA method accounts for the nonlinearity in between load line displacement and *CTOD*. The CFOA method results are good in agreement with CZM results. The CZM results are found slightly on higher side compared to CFOA method as FE model is based on ideal assumptions.

For thickness effect the percentage difference in *CTOD*s determined from CFOA and CZM is found to be within 3–7%. Whereas, the percent difference in between PHM and CZM is found to be within 13–21% (Table 5.13). For notch radius effect the percentage difference in *CTOD*s determined from CFOA and CZM is found to be within 1–3%. Whereas, the percent difference in between PHM and CZM is found to be within 6–8% (Table 5.14). For strain rate effect the percentage difference in *CTOD*s determined from CFOA and CZM is found to be

within 3–5%. Whereas, the percent difference in between PHM and CZM is found to be within 6–10% (Table 5.15). For a_0/W ratio effect the percentage difference in $CTOD$s determined from CFOA and CZM is found to be within 0.25–3%. Whereas, the percent difference in between PHM and CZM is found to be within 13–25% (Table 5.16). The reason behind this is the underestimation of plastic rotational factor considered in PHM for the general yield regime. Thus, the CFOA method is found to be suitable for significant deformation ahead of crack tip in case of EDD steel sheets in general yield situation.

Table 5.13 Thickness effect: % difference in critical $CTOD$ values.

Thickness (mm)	$(\delta_C)_{PHM}$ (mm)	$(\delta_C)_{CFOA}$ (mm)	$(\delta_C)_{CZM}$ (mm)	% difference (PHM vs CZM)	% difference (CFOA vs CZM)
1.2	0.574	0.649	0.678	18.132	4.485
1.3	0.590	0.671	0.713	20.911	6.356
1.4	0.619	0.686	0.740	19.527	7.853
1.5	0.650	0.725	0.768	18.159	5.941
1.6	0.683	0.757	0.790	15.715	4.400
1.7	0.715	0.790	0.815	13.941	3.124

Table 5.14 Notch radius effect: % difference in critical $CTOD$ values.

Notch radius (mm)	$(\delta_C)_{PHM}$ (mm)	$(\delta_C)_{CFOA}$ (mm)	$(\delta_C)_{CZM}$ (mm)	% difference (PHM vs CZM)	% difference (CFOA vs CZM)
0.070	2.056	2.160	2.209	7.431	2.258
0.085	2.056	2.160	2.214	7.707	2.521
0.100	2.057	2.165	2.196	6.763	1.437
0.110	2.058	2.165	2.219	7.859	2.503
0.120	2.059	2.170	2.218	7.763	2.226
0.130	2.059	2.173	2.220	7.830	2.149
0.140	2.059	2.175	2.218	7.727	1.957
0.150	2.059	2.180	2.214	7.552	1.558
0.160	2.091	2.183	2.247	7.443	2.938
0.170	2.104	2.200	2.257	7.277	2.596
0.180	2.116	2.222	2.267	7.126	2.016
0.250	2.186	2.290	2.348	7.389	2.512
0.400	2.300	2.430	2.464	7.137	1.426
0.600	2.486	2.580	2.647	6.460	2.581
0.750	2.590	2.720	2.773	7.072	1.954

Table 5.15 Strain rate effect: % difference in critical *CTOD* values

Strain rate (mm/min.)	$(\delta_C)_{PHM}$ (mm)	$(\delta_C)_{CFOA}$ (mm)	$(\delta_C)_{CZM}$ (mm)	% difference (PHM vs CZM)	% difference (CFOA vs CZM)
0.1	1.408	1.437	1.499	6.410	4.295
0.2	1.408	1.437	1.499	6.394	4.316
0.3	1.408	1.436	1.499	6.400	4.344
0.4	1.408	1.436	1.499	6.420	4.387
0.6	1.330	1.391	1.455	9.369	4.572
1	1.264	1.306	1.351	6.835	3.430
1.5	1.220	1.242	1.288	5.565	3.708
2.5	1.104	1.153	1.191	7.881	3.279

Table 5.16 a_0/W ratio: % difference in critical *CTOD* values

a_0/w ratio	$(\delta_C)_{PHM}$ (mm)	$(\delta_C)_{CFOA}$ (mm)	$(\delta_C)_{CZM}$ (mm)	% difference (PHM vs CZM)	% difference (CFOA vs CZM)
0.5	2.479	2.732	2.824	13.905	3.374
0.525	2.202	2.591	2.654	20.521	2.456
0.55	2.076	2.518	2.591	24.775	2.897
0.575	1.996	2.494	2.500	25.258	0.253

5.5   Effect of Various Parameters on Fracture Toughness

Four different objectives i.e. thickness effect, notch radius effect, strain rate effect and a_0/W ratio effect have been considered to study and summarize the fracture behaviour of EDD steel sheets in general yield regime. Critical *CTOD* is taken as fracture toughness parameter for all the cases. Critical *CTOD* is evaluated using plastic hinge model (PHM), proposed CFOA method and by using cohesive zone model (CZM). The results obtained are discussed in details in subsequent topics.

5.5.1 Effect of Thickness on Fracture Behaviour

Specimens with different thicknesses are considered to predict the thickness effect on fracture toughness. Table 5.17 shows elastic part of *CTOD* and plastic part of *CTOD* predicted from experimental results (measured by using PHM and CFOA method). Table 5.17 also shows elastic and plastic part of *CTOD* determined from CZM.

Table 5.17 Thickness effect: Critical *CTOD* values evaluated from experiments (using PHM and CFOA method) and CZM

Thickness (mm)	$(\delta_{el})_{Expt}$ (mm)	$(\delta_{pl})_{PHM}$ (mm)	$(\delta_C)_{PHM}$ (mm)	$(\delta_{pl})_{CFOA}$ (mm)	$(\delta_C)_{CFOA}$ (mm)	$(\delta_{el})_{CZM}$ (mm)	$(\delta_{pl})_{CZM}$ (mm)	$(\delta_C)_{CZM}$ (mm)
1.2	0.043	0.531	0.574	0.606	0.649	0.045	0.633	0.678
1.3	0.045	0.545	0.590	0.626	0.671	0.047	0.667	0.713
1.4	0.046	0.573	0.619	0.640	0.686	0.047	0.693	0.740
1.5	0.048	0.602	0.650	0.677	0.725	0.049	0.719	0.768
1.6	0.050	0.633	0.683	0.707	0.757	0.051	0.740	0.790
1.7	0.049	0.666	0.715	0.741	0.790	0.050	0.765	0.815

Fig 5.14 shows the variation of critical *CTOD* with thickness. The graph shows that as thickness increases, the critical *CTOD* also increases. This fracture behaviour is unlike that for thick plates, wherein the fracture toughness decreases as thickness increases as reported by Heydari *et al* (2011), Kang (2005), Mahmoud and Lease (2003), Pandey *et al*. (1997) and Srawely and Brown (1975). The reason behind the increase in fracture toughness with increase in thickness is explained below.
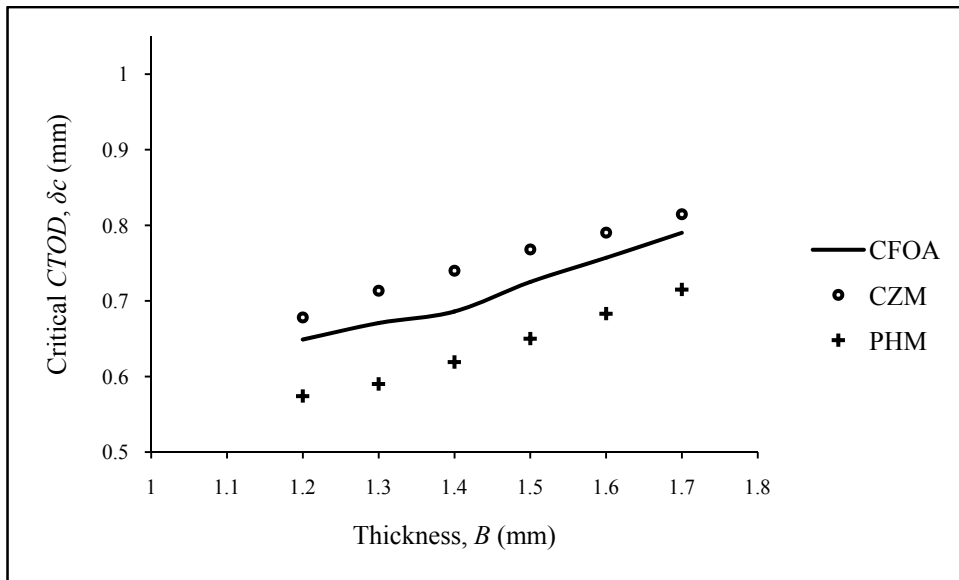
Fig 5.14 Variation of critical *CTOD* with thickness.

Castrodeza *et al*. (2004) have reported that, close to the free surfaces, material deforms in plane stress condition and in the interior, plane strain condition exist. In some cases, degree of

plane strain is higher than the degree of plane stress, whereas in other cases it is other way round, depending on material as well as size. For EDD steel sheets, as mentioned by Kulkarni (2005) that for the thickness range (1 – 3.2 mm), there exist a predominantly plane stress conditions in the vicinity of crack tip.

Fracture toughness of thin sheets is mainly associated with the amount of energy required to reduce the initial cracked specimen thickness (i.e. necking) which is frequently higher than the energy needed for crack growth [Shahani *et al* (2010) and Pardoen *et al* (2004 & 2002)]. The former depends on the initial specimen thickness [Broek (2002)]. As mentioned by Shukla (2005), in thin sheets, the work of fracture and the degree of thickness necking can be very high, so that the material is able to absorb energy and resist fracture. In the other words, fracture resistance of thin metallic sheets is significantly dependent on the energy dissipated in crack tip necking. It has already been proved by Wang *et al* (2008) that in the regime of general yield amount of necking increased with the thickness. Also it is reported that in the vicinity of crack, the state of stress is close to plane stress, the energy which causes thickness reduction and thus, the fracture toughness is higher for thicker specimens in general yield regime.

In case of thick plates (EPFM regime) as mentioned by Shukla (2005) as the thickness increases, the state of stress in crack tip field gradually changes to plane strain and less amount of necking is observed. Stress triaxiality tends to increase at the crack tip for the thicker specimen leading to higher rate of void growth and lower fracture strain and degree of crack tip necking. It causes the fracture toughness to decrease. While according to Shahani *et al* (2010) in thicker specimens, as the thickness increases, the input energy is dominantly spent on forming new surfaces, and so growing the crack. Therefore, the crack growth occurs earlier than the thinner specimens for which the major proportion of the input energy causes plastic zone formation.

In the present work, crack surface from the broken ligament of specimens (T1 – T6), it is found that the shear lips which can be considered as the indication of the predominating plane stress state prevail on the total surface of specimens. Also a significant amount of crack tip necking is observed in specimens (T1 – T6). Therefore the increase in fracture toughness with increase in thickness is attributed to predominating plane stress conditions, localized necking, and large plastic zone ahead of the crack tip in the regime of general yield.

5.5.2 Influence of Notch Radius on Fracture Behaviour

Different notch root radii have been considered to predict the notch radius effect on fracture toughness. Table 5.18 shows elastic part of *CTOD* and plastic part of *CTOD* predicted from experimental results (measured by using PHM and CFOA method). Table 5.18 also shows elastic and plastic part of *CTOD* determined from CZM.

Table 5.18 Notch radius effect: Critical *CTOD* values evaluated from experiments (using PHM and CFOA method) and CZM

Notch radius (mm)	$(\delta_{el})_{Expt}$ (mm)	$(\delta_{pl})_{PHM}$ (mm)	$(\delta_C)_{PHM}$ (mm)	$(\delta_{pl})_{CFOA}$ (mm)	$(\delta_C)_{CFOA}$ (mm)	$(\delta_{el})_{CZM}$ (mm)	$(\delta_{pl})_{CZM}$ (mm)	$(\delta_C)_{CZM}$ (mm)
0.070	0.032	2.024	2.056	2.128	2.160	0.033	2.175	2.209
0.085	0.032	2.024	2.056	2.128	2.160	0.032	2.183	2.214
0.100	0.032	2.025	2.057	2.133	2.165	0.033	2.163	2.196
0.110	0.035	2.023	2.058	2.130	2.165	0.037	2.183	2.219
0.120	0.033	2.025	2.059	2.137	2.170	0.033	2.185	2.218
0.130	0.032	2.027	2.059	2.141	2.173	0.033	2.187	2.220
0.140	0.032	2.027	2.059	2.143	2.175	0.034	2.184	2.218
0.150	0.034	2.024	2.059	2.146	2.180	0.035	2.179	2.214
0.160	0.034	2.057	2.091	2.148	2.183	0.036	2.210	2.247
0.170	0.035	2.069	2.104	2.165	2.200	0.037	2.220	2.257
0.180	0.035	2.081	2.116	2.187	2.222	0.037	2.230	2.267
0.250	0.038	2.148	2.186	2.252	2.290	0.038	2.310	2.348
0.400	0.039	2.261	2.300	2.391	2.430	0.040	2.424	2.464
0.600	0.042	2.444	2.486	2.538	2.580	0.042	2.605	2.647
0.750	0.044	2.546	2.590	2.676	2.720	0.044	2.729	2.773

The results on critical *CTOD* for different notch radii are presented in Fig 5.15. It shows the variation of critical *CTOD* with notch radius (ρ = 0.07- 0.75). From Fig 5.15 it is observed that there is an increase of 0.93% in fracture toughness in the notch radius range 0.07 mm to 0.15 mm. From practical point of view, this change in fracture toughness is negligible. Furthermore, it is observed that there is a sharp increase in fracture toughness in the notch radius range 0.15 mm to 0.75 mm.
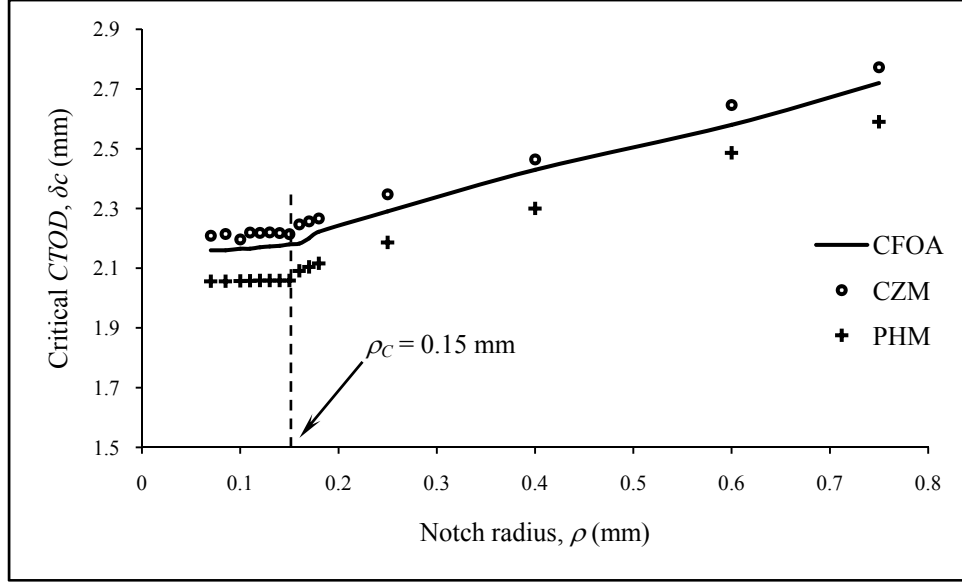
Fig 5.15 Variation of critical *CTOD* with notch radius.

Therefore, the notch radius of 0.15 mm is considered to be a critical notch radius value, below which, fracture toughness remains almost independent of notch radius. According to Mourad *et al* (2012 & 2005), Vratnica (2010), Srinivas and Kamat (1992) and Schindler (1991) the fracture toughness beyond the critical notch radius is referred as apparent fracture toughness. Available literature [Mourad and Aly (2011), Mourad (2008), Akourri *etal* (2000), Srinivas *etal* (1994), Srinivas & Kamat (1992), Schindler (1991), Faucher *etal* (1990), Yoda (1987), Firrao & Roberti (1982), Landes & Begley (1979)] shows a linear relationship between apparent fracture toughness and notch radius. They have used *J- integral* as a fracture toughness parameter. In the present work, *CTOD* is used as a fracture toughness parameter and current results are in agreement with the literature. The linear increase of apparent fracture toughness can be approximately expressed by Eq. (5.4) for CFOA method.

$$CTOD_{c,\text{App}} = 0.94 \, \rho' + CTOD_c \qquad (5.4)$$

where, $\rho' = (\rho - \rho_c)$. Eq. (5.4) is valid for notch radius (ρ), greater than or equal to critical notch radius (ρ_c). The approximate slope of line is 0.94 in this case. The value of critical *CTOD* ($CTOD_c$) is equal to 2.18 mm. Therefore, the relation given by Eq. (5.4) becomes

$$CTOD_{c,\text{App}} = 0.94 \, (\rho - 0.15) + 2.18 \qquad (5.5)$$

77

Mourad and Aly (2011), Vratnica (2010), Srinivas and Kamat (1992) have given the explanation for the increase in apparent fracture toughness with increase in notch radii. According to them, the fracture toughness is proportional to the work done for fracture per unit of ligament area. It is asserted that the existence of a finite notch root radius causes an increase in the value of toughness, because an additional energy is used for plastic deformation in order to increase the stress concentration at the notch root to an equivalent level at the crack tip. There is a critical notch radius below which there is no significant effect of notch radius on fracture toughness.

Kulkarni (2005) has studied stress triaxiality with notch radius for EDD steel sheets. He found that peak values of stresses (σ_x, σ_y and σ_z) are located in the vicinity of notch radius for smaller notch radii. However, in case of higher value of notch radii, peak value of stresses shift away from notch radius.

In the present work the z- direction stress (i.e. along the thickness) is small indicating a predominantly plane stress condition along unbroken ligament length. Stress in x–direction assists the notch–tip to grow in x–direction (i.e. along unbroken ligament length). The stress in y–direction assists the notch-tip to grow along y–direction for crack tip opening displacement. For lower notch radii, the peak stress level is found to be in the vicinity (within 0.50 mm) of notch-tip. It is also observed that there is a minor variation in the intensity of peak stress level with increase in notch radius. However, with increase in notch radius it is observed that the location of peak stress level is shifting away from the notch tip along the unbroken ligament length.

From these observations, it is predicted that the stresses are localized in the vicinity of crack tip for lower value of notch radii (0.05, 0.10, 0.12 and 0.15 mm). Therefore, crack initiation occurs at lower critical load, due to high stress concentration in the vicinity of crack tip.

It is also observed that with increase in notch radii, there is increase in the plastic zone size. The plastic zone is increasing gradually with notch radii and assists the degree of blunting. There is hardly increase in plastic zone size up to 0.15 mm notch radius. Beyond 0.15 mm notch radius, there is continuous increase in plastic zone size.

In extra deep drawn steel sheet, it is observed that the critical *CTOD* is larger than the notch radius. The reason may be high formability, smaller size of sheets, almost 100 % degree of shear-lip and large plastic zone size. Fig 5.16 shows the degree of shear lip during complete tearing of the specimen. Plastic zone has two parts: tensile and compressive. As observed from Fig 5.17, the plastic zone touches the boundary of ligament. These features of EDD steel sheet help to increase the deformation ahead of notch tip. Based upon these observations, it is suggested that using notch is convenient instead of using fatigue crack for pre-cracking in case of EDD steel sheets.
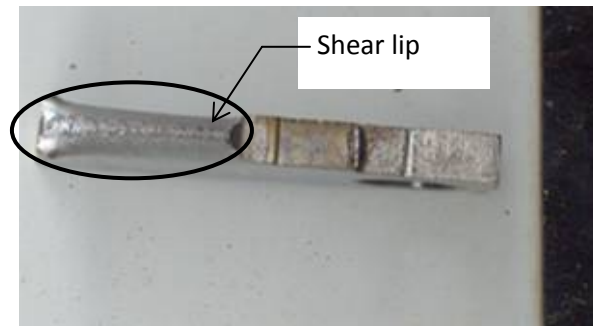
Fig 5.16 General features of fracture surfaces produced during stable and complete tearing.
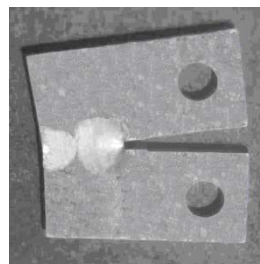
Fig 5.17 Plastic zone ahead of notch tip for specimen code N10 at crack initiation load i.e. 2.62 kN in this case.

In the present work, 0.2 mm wire diameter is used to create a notch having 0.1 mm notch radius. However, because of unavoidable heating during WEDM process, the maximum average notch radius has gone up to 0.13 mm. This value is sufficiently below the critical value (0.15 mm) for the validity of the present fracture study. Otherwise it is a time consuming and costly procedure for preparation of fatigue pre-cracked specimens.

5.5.3 Effect of Strain Rate on Fracture Behaviour

The fracture behaviour of EDD steel sheets is studied for various strain rates, in order to observe the effect of strain rate on fracture toughness if any. Table 5.19 shows elastic part of *CTOD* and plastic part of *CTOD* predicted from experimental results (measured by using PHM and CFOA method). Table 5.19 also shows elastic and plastic part of *CTOD* determined from CZM.

Table 5.19 Strain rate effect: Critical *CTOD* values evaluated from experiments (using PHM and CFOA method) and CZM

Strain rate (mm/min.)	$(\delta_{el})_{Expt}$ (mm)	$(\delta_{pl})_{PHM}$ (mm)	$(\delta_C)_{PHM}$ (mm)	$(\delta_{pl})_{CFOA}$ (mm)	$(\delta_C)_{CFOA}$ (mm)	$(\delta_{el})_{CZM}$ (mm)	$(\delta_{pl})_{CZM}$ (mm)	$(\delta_C)_{CZM}$ (mm)
0.1	0.022	1.386	1.408	1.415	1.437	0.024	1.475	1.499
0.2	0.022	1.386	1.408	1.414	1.437	0.024	1.475	1.499
0.3	0.022	1.386	1.408	1.414	1.436	0.024	1.475	1.499
0.4	0.022	1.386	1.408	1.414	1.436	0.024	1.475	1.499
0.6	0.022	1.308	1.330	1.369	1.391	0.023	1.432	1.455
1	0.017	1.247	1.264	1.289	1.306	0.018	1.333	1.351
1.5	0.016	1.204	1.220	1.226	1.242	0.017	1.271	1.288
2.5	0.014	1.090	1.104	1.139	1.153	0.015	1.176	1.191

The results on critical *CTOD* for different strain rates are presented in Fig 5.18. It shows the variation of critical *CTOD* with strain rate (0.1- 2.5 mm/ min.). From Fig 5.18 it is observed that the fracture toughness is almost constant up to the strain rate 0.4 mm/ min. Furthermore it is observed that there is a sharp decrease in fracture toughness with increase in strain rate beyond 0.4 mm/min. Therefore, the strain rate 0.4 mm/min. is considered to be a critical strain rate value, below which, fracture toughness remains almost independent of strain rate.
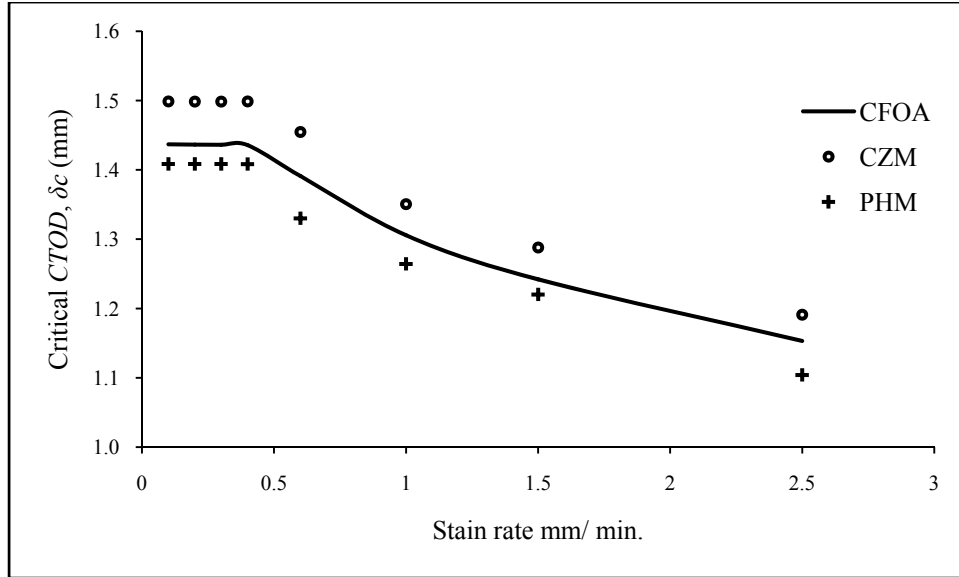
Fig 5.18 Variation of critical *CTOD* with strain rate.

In the present work, only the general macroscopic behaviour involving strain rate is considered. The effect of strain rate on fracture parameters shows very small difference in results up to about 0.4 mm/min. However, beyond this strain rate level, it is found that EDD sheet has considerable sensitivity at high strain rate even at room temperature.

The reason may be same as in case of strain rate effects on strength and ductility. According to He *et al* (2012), Verleysen *et al* (2011), Jie *et al* (2009), Bayraktar *et al* (2007), Qiu *et al* (2005), Smith *et al* (2008) and Callister (2006), as strain rate increases, the tensile strength of steel and other alloys increases, however, the ductility values tend to diminish. With high strain rate, plastic deformation becomes a difficult process, as dislocation motion is restricted. Dislocation movements through crystal lattice involve atomic diffusion and displacements under the applied stress. When the strain rate increases, the atomic diffusion vis-à-vis the dislocations motion becomes difficult because of short duration. In other words, process of deformation becomes limited resulting in reduced plasticity and toughness. Elastic contribution towards *J* or *CTOD* values is small indicating that the plasticity is the source of toughness. Therefore, it is concluded that for higher formability, the forming of the EDD steel sheet should be done at lower strain rates. The strain rate 0.4 mm/min is found to be critical strain rate in case of EDD steel sheet. Beyond the critical strain rate, the results found are not good for the forming operations.

5.5.4 Effect of a_0/W Ratio on Fracture Behaviour

In practice, steel components are too large in dimensions and too expensive to be tested in their operating conditions for the characterization of fracture toughness. Therefore fracture toughness is evaluated by using standard laboratory test procedures recommended by ASTM. The advantage of following standard test procedures is the cost associated with the specimens that can be tested in laboratories is less as well as low load capacity machines can be used for the testing. However the fracture toughness data obtained from standard test procedures is corresponding to plan strain fracture toughness (lower shelf fracture toughness) [Sun *et al* (2011), Wang *et al* (2010)]. As per as design aspect is concern, the lower shelf fracture toughness data is more conservative. Under large scale yielding the specimen boundaries affect the crack tip stress field by relaxing the triaxial stress state. In such situations, fracture toughness is strongly dependent on specimen size and crack depth. The fracture toughness values for shallow cracks are higher than those determined from standard deep cracked test specimens. This fact is referred as the constraint effect [Holtam *et al* (2010), Chen *et al* (2007)]. Therefore, there is a strong incentive to reduce excess conservatism in order to provide more realistic estimate of remaining life of the components (Budden and Dean, 2007). For this purpose, the experimental and numerical investigations are required to characterize the constraint quantitatively [Wang *et al* (2010)].

For the present work, to investigate effect of a_0/W ratio on fracture toughness, various values of a_0/W ratio have considered. *CTOD* is considered as a fracture parameter as discussed earlier. It is observed from table 5.8, the critical load decreases with increasing values of a_0/W ratio. It is expected also because as a_0/W ratio increases means length of unbroken ligament reduces. For such case stiffness of plate reduced which further reduces the critical load.

Table 5.20 shows elastic part of *CTOD* and plastic part of *CTOD* predicted from experimental results (measured by using PHM and CFOA method). Table 5.20 also shows elastic and plastic part of *CTOD* determined from CZM.

Table 5.20 a_0/W ratio: Critical *CTOD* values evaluated from experiments (using PHM and CFOA method) and CZM

a_0/W ratio	$(\delta_{el})_{\text{Expt}}$ (mm)	$(\delta_{pl})_{\text{PHM}}$ (mm)	$(\delta_C)_{\text{PHM}}$ (mm)	$(\delta_{pl})_{\text{CFOA}}$ (mm)	$(\delta_C)_{\text{CFOA}}$ (mm)	$(\delta_{el})_{\text{CZM}}$ (mm)	$(\delta_{pl})_{\text{CZM}}$ (mm)	$(\delta_C)_{\text{CZM}}$ (mm)
0.5	0.066	2.413	2.479	2.666	2.732	0.068	2.756	2.824
0.525	0.071	2.132	2.202	2.520	2.591	0.072	2.582	2.654
0.55	0.068	2.009	2.076	2.450	2.518	0.070	2.521	2.591
0.575	0.066	1.930	1.996	2.428	2.494	0.066	2.435	2.500

The results on critical *CTOD* for different a_0/W ratios are presented in Fig 5.19. It shows the variation of critical *CTOD* with a_0/W ratio (0.5 – 0.575). From Fig 5.19 it is observed that the fracture toughness decreases with a_0/W ratio.

Li *etal* (2005), Sorem (1991), Shen (1978), Lewis *etal* (1975) have studied the effect of a_0/W ratio on fracture toughness for LEFM. They have found that fracture toughness increases with decrease in a_0/W ratio. Their experimental observations show that the fracture toughness parameters for the short crack specimens *(a/W -- 0.15 to 0.20)* are 2-3 times greater than the deep crack specimens *(a/W = 0.50)*. They have reported that for shallow cracks, the hydrostatic stress is lower than the deeply cracked specimens which develops a high level of crack tip constraint, provides a lower bound estimate of toughness.
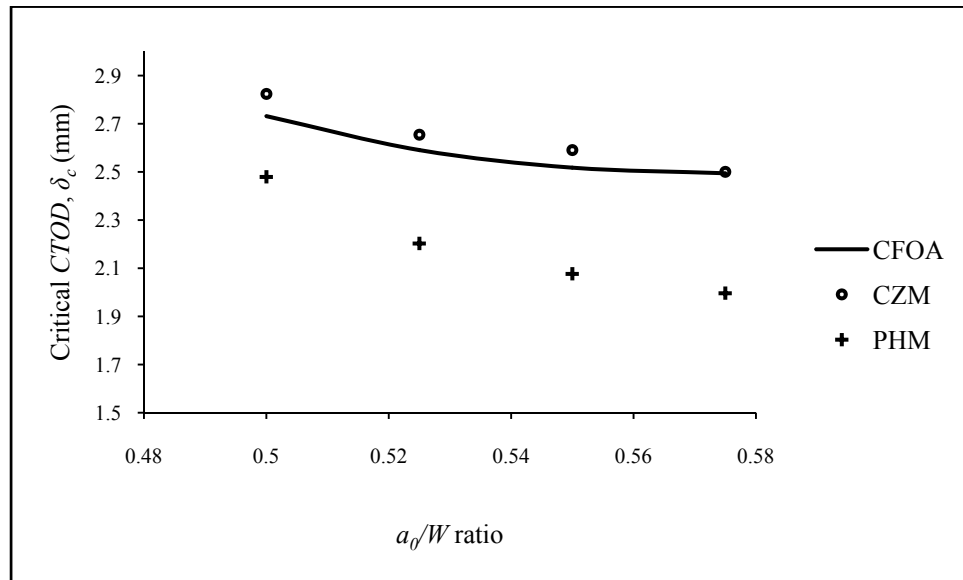
Fig 5.19 Variation of critical *CTOD* with a_0/W ratio.

Li *etal* (2005), Li (2003), Li *etal* (2002), Sorem (1991), Li & Shi (1991), Huang (1987), Lin (1987), Li & Zhou (1986), Li & Zhou (1986), Cotferel *etal* (1985), Li (1985), Chipperefied (1978) have shown that shallow cracks have greater COD and J-integral values at initiation than deeply cracked specimens in EPFM regimes. Furthermore it has been reported that there is considerably crack-tip blunting and larger plastic zones in the vicinity of crack tip present in the short crack specimens than in the deep crack specimens. It has also been reported that for the short crack specimens, the plastic zone (tension) extends to the free surface. They have found the critical *CTOD* for the short crack specimens $(a/W = 0.15)$ are aproximately 2.5 times larger than critical *CTOD* for the deep crack specimens $(a/W = 0.50)$.

The study of effect of *a/W* ratio revealed significant differences in fracture toughness for small and large *a/W* ratios, the ASTM standard for *CTOD* testing restricts *a/W* ratios to 0.45-0.55 for plane strain fracture toughness test. For the present work four different a_0/W ratios (0.5, 0.525, 0.55 & 0.575) have been considered. Although the chosen a_0/W ratios do not indicate any shallow crack $(a_0/W \cong 0.15\text{-}0.3)$, qualitatively comments on shallow cracks are demonstrated here. As plastic zone forms at the vicinity of crack tip in general yielding, plastic hinge often develops prior to failure. As a_0/W ratio increases the location of plastic hinge shifts towards the crack tip (table 5.21). As hinge points shifts towards crack tip, the size of tensile plastic zone is reduced which decreases fracture toughness on increasing values of a_0/W ratio (Fig 5.19).

Table 5.21 Variation of location of plastic hinge with a_0/W ratio.

a_0/W ratio	Plastic hinge from crack tip (mm)
0.5	11.62278
0.525	10.94527
0.55	10.28002
0.575	9.626676

For lower values of a_0/w ratio, the drop in fracture toughness is sharp but at higher values of a_0/w ratio the drop in fracture toughness gradually reduced (Fig 5.19). The decrease in fracture toughness for a_0/w ratio values, 0.5 to 0.525 is more than 5%; however the drop in fracture toughness for a_0/w ratio values, 0.55 to 0.575 is just 0.95%. Further if we increase the a_0/W

ratio, fracture toughness would become independent of a_0/W ratio however this is qualitative comment. From present observations of effect of a_0/W ratios on fracture toughness following qualitative comments are derived.

If $(W - a_0)$ is not sufficiently large, the plastic zone size for determination of fracture toughness is significantly affected by the close presence of a free surface (the back face of the specimen).That is, the material is more resistant to crack growth when the crack is shallow. Also it would be expected that if the notch was deep enough to prevent plastic work reaching the surface, then the critical *CTOD* would be independent of the notch depth. For shallower notches the plastic constraint would be less and the maximum stress attainable would be smaller than that in a more deeply notched specimen strained to the same crack opening displacement. Consequently the critical *CTOD* will be greater for shallow crack. However theoretical study on constraint correction and the effect of a_0/W on fracture toughness is necessary to find an appropriate parameter(s) to characterize the crack tip stress–strain fields, so that fracture toughness results can be transferred from one test geometry to another. Summary of results and discussion is presented in chapter 6.

CHAPTER- 6

CONCLUSIONS

6.1   Summary

The research work presented in this thesis is aimed to understand the fracture behaviour of EDD steel sheets in general yield regime. EDD steel sheets are widely used among the most important sheet metals in industrialized countries. From engineering and economic viewpoint, a thorough understanding of fracture behaviour of EDD steel sheets and their products is essential to steel manufacturers as well as industrial users (like automotive component manufacturer). Four types EDD steel sheets are received from TATA Steel, which are named as EDD 'A', EDD 'B', EDD 'C' and EDD 'D' for the reference. The mechanical properties of EDD steel sheets are obtained from TATA Steel. Presently the EDD steel sheets are characterized using a formability approach. In the present work, formability point of view, the EDD steel sheets are studied based on their mechanical properties. Fracture test are conducted using CT specimens. Cohesive zone model is formulated to validate the experimental results. Suitable traction separation law is implemented and procedure to calibrate cohesive parameters is presented. In order to characterize the fracture behaviour, critical *CTOD* is considered as a fracture parameter. The critical *CTOD* from experimental observations is calculated using PHM and proposed CFOA method. The calculated values of critical *CTOD* using PHM and CFOA method are compared with the critical *CTOD* values, calculated from CZM. Finally, the effect of various parameters i.e. thickness effect, notch radius effect, strain rate effect and effect of a_0/W ratio on fracture toughness are studied to characterize the fracture behaviour of EDD steel sheets in general yielding regime.

6.2   Critical Findings

The major outcomes of the present research work are:

The formability and fracture mechanics are the two approaches to understand the fracture behaviour in EDD steel sheets. Using formability approach, intrinsic and simulative tests give relative engineering index of formability. Because of complex interactions of material and process variables, many factors are required to be considered for the crack initiation phenomena.

However from literature, it is found that prevention of failure in EDD steel material during forming operation currently requires fracture mechanics based design parameters. In order to characterize fracture behaviour of EDD steel sheets in general yield regime, fracture criterion (critical load at which crack initiates) and critical *CTOD* (as fracture toughness parameter) are used. Analysis of formability parameters is important to understand the forming qualities of EDD steel sheets. According to ASTM E8M-11 (2011) and E 517-00 (2010), the study of formability shows that EDD 'B', EDD 'C' and EDD 'D' steel sheets have relatively high formability than EDD 'A' steel sheet, based on normal anisotropy, stain hardening exponent and % elongation.

The precise determination of crack initiation event necessitates successive experimental attempts. A 'load drop technique' or 'load maxima' is experimentally confirmed as fracture criterion for EDD steel sheets, which assists in detecting the physical event of crack initiation. Using load drop technique, precise determination of critical load is possible without any change in experimental set up.

Cohesive zone models are suitable tool for the characterization of fracture behaviour in the materials of interest. CZM concepts have been applied in order to study mode–I fracture in pre-cracked CT specimens and verify experimental findings (like fracture criterion and critical *CTOD*s).

First, linear and exponential traction laws are used for simulation. It is observed that linear traction separation law underestimates the maximum load approximately by 23% and it is most suitable for LEFM regime i.e. brittle materials and linear elastic solids. Exponential law is being used for ductile materials however in the present case it underestimates load line displacement approximately by 22% and perhaps it is most suitable for EPFM regime. Therefore, an alternative constant traction separation law is proposed to account for maximum load and large load line displacements. The results from proposed constant traction separation law are found to be close with the experimental findings. By using proposed traction separation law, the maximum load is over- estimated only by 1.44% and corresponding J_i based on load vs LLD is 2.14% more than experimental value. The proposed constant traction separation law is found suitable for EDD steel sheets in general yield regime.

This study clearly shows that there are no hard-and-fast guidelines for determining the cohesive parameters of the traction-separation relationship. It is dependent on the problem under consideration. It is recommended that the cohesive parameters estimated with the guidelines presented in this thesis be assessed by first conducting simple benchmark simulations (for which analytical and/or experimental results are available) before using them in actual models. Furthermore, as some of the parameters estimated from one problem may not be valid for other problems.

The CFOA model is proposed to find the plastic *CTOD* in addition to the existing Plastic hinge model (PHM). The PHM results on plastic *CTOD* are found to be conservative because the value of plastic rotational factor (PRF) in PHM depends only on initial crack length and unbroken ligament length and the model does not account for non-linearity between plastic load– line displacement and plastic *CTOD*. The suggested CFOA model accounts for this non-linearity. In this model, the value of apparent axis of rotation depends upon the crack flank opening angle, which in turn depends upon the thickness of specimen. CFOA model is found to be consistent and well agreed with cohesive zone model. The suggested CFOA model can be easily applicable to predict the effect of various edge–notched specimen geometry and loading configuration in the general yield regime.

The effect of various parameters on fracture toughness of EDD steel sheets in general yielding is studied. Few key features, which do not observe in LEFM and EPFM regime, are found during experiment: large plastic zone size ahead of crack tip, high degree of shear lips, pre–dominant plane stress condition, high degree of crack blunting and significant amount of crack tip necking. The plastic zone in general yielding regime touches ligament boundary of specimen and also increases with increase in specimen thickness. In addition to these observations, effect of various parameters i.e. thickness effect, strain rate effect, notch radius effect, and effect of a_0/W ratio on fracture toughness are studied and discussed below.

The critical *CTOD* values are found to increase with increase in thickness, this observation is found to be unlike that of thick plates (LEFM and EPFM regime). The reason is, in lower range of thickness, the material is free to move in the plane of sheet because of predominantly plane stress condition. Fracture toughness of thin sheets is associated with the amount of energy required to reduce the initial cracked specimen thickness (i.e. necking) and

energy needed for crack growth fracture resistance of thin metallic sheets is significantly dependent on the energy dissipated in crack tip necking. In the regime of general yield, amount of necking is observed to increase with increase in thickness. Therefore in case of the EDD steel sheets, increase in fracture toughness with increase in thickness is attributed as predominating plane stress conditions, localized necking and large plastic zone ahead of crack tip.

Experimental findings as well as CZM shows that the strain rate has no significant effect on fracture toughness till the strain rate is 0.4 mm/min at room temperature; however, there is a sharp decrease in fracture toughness beyond 0.4 mm/min. This may be because of the dislocation motion restricted with high strain rate. Therefore, in order to have high formability, the forming of the EDD steel sheets should be done at lower strain rates.

Influence of notch radius on fracture toughness has been studied with a wide range of notch radii. The apparent fracture toughness is observed to increase linearly with increase in notch radius. This observation is in agreement with the results available in literature. The critical notch radius is found to be 0.15 mm. This study is essential to verify the validity of results of notched specimens having notch radii in the range of 0.11-0.13 mm. The critical observation of increase in apparent fracture toughness with increase in notch radius is attributed to the stress triaxiallity which is low for high notch radius. With this study, it is recommended that fatigue pre-cracking, which is a time consuming job, in case of EDD steel sheets is not essential. The wire electric discharge machining (WEDM) process can be successively used for pre-cracking.

The effect of a_0/W ratio on fracture toughness of EDD steel sheets is studied. Similar to EPFM, in general yielding, plastic zone forms at the vicinity of crack tip and plastic hinge often develops prior to failure. It has been observed that as a_0/W ratio increases the location of plastic hinge shifts towards the crack tip (i.e. size of tensile plastic zone reduces), which reduces fracture toughness. That is, the material is less resistant to crack growth when the crack is deeper. For shallow notches the plastic constraint would be less and the maximum stress attainable would be smaller than that in a more deeply notched specimen strained to the same crack opening displacement. Consequently the critical *CTOD* will be greater for shallow crack. However theoretical study on constraint correction and the effect of a_0/W on fracture toughness is necessary to find an appropriate parameter(s) to characterize the crack tip stress–strain fields, so that fracture toughness results can be transferred from one test geometry to another.

6.3 Specific Contribution

1. To simulate the fracture behaviour of EDD steel sheets with CZM, constant traction law is proposed to verify fracture criterion and fracture toughness.

2. To formulate CZM for EDD steel sheets, calibration procedure is formulated to select the cohesive parameters.

3. To measure the fracture toughness of EDD steel sheets in general yield regime, CFOA method is suggested.

6.4 Recommendations

Formability study is important to know the forming characteristics of sheet material. However, in order to understand the fracture behaviour in thin EDD steel sheet which fall into a general yield regime, following recommendations are made.

1. Load drop technique can be used as a fracture criterion.

2. Higher formability can be achieved using lower forming rates.

3. Selection of EDD steel sheet with sufficiently high thickness may be used, if there are no other design constraints as it will have more fracture toughness.

4. CZM with proposed traction separation law can be easily implemented and used to simulate the fracture problem.

5. CFOA method is suitable and can be effectively used to determine fracture toughness parameters.

6. To avoid dependency of a_0/W ratio on the fracture toughness, higher values of a_0/W (0.5 ~ 0.6) ratio should be chosen.

7. Wire electric machining (WEDM) can be competently used instead of fatigue pre-cracking to induce crack in the fracture test specimens.

6.5 Utilization of Research Outcome

The present research outcome will help steel manufacturers to design fracture test set up and fracture simulation with the help of which they will be able to give fracture data apart from the forming indices and mechanical properties. In turn, it will help the industrial customers (e.g. automotive component manufacturer) to determine critical load and critical strain rate. There by

industrial customers will be able to avoid trial and error methods and hence wastage of materials. This research will also help academicians to understand fracture behaviour more in detail in the developing regime of fracture mechanics.

6.6   Future Scope for Work

1. Present study is carried out at atmospheric temperature, however, low temperature and high temperature effect on fracture toughness can be studied for specific applications.

2. As mode–I loading is a worse loading condition, in the present work, specimens were loaded in mode–I and the crack direction was predefined. In practice, due to complex loading mode and geometry, crack initiation and propagation usually does not follow a predefined path. So it is required to develop mixed mode loading test setup to study the fracture behaviour of thin sheets. Also CZM is required to develop for mixed mode loading.

3. This study can be extended to light metal alloy sheets used for aerospace applications which fall in general yield regime.

REFERENCES

1   ABAQUS 6.7 User's Manual, by Karlsson Hibbit, Sorensen, 2007.

2   Akourri O, Louah M, Kifani A, Gilgert G, Pluvinage G. The effect of notch radius on fracture toughness J_{Ic}. Engineering Fracture Mechanics 2000;65:491–505.

3   Alsaati A, Ali WJ, Alkaissy FM. Friction technique for determining forming limit curves. Al-Rafidain Engineering 2006;14(4):11–23.

4   Amstutz BE, Sutton MA, Dawicke DS, Boone ML. Effects of mixed mode I/II loading and grain orientation on crack initiation and stable tearing in 2024-T3 aluminum. ASTM STP 1296 on Fatigue and Fracture Mechanics 1997;27:105–126.

5   Amstutz BE, Sutton MA, Dawicke DS, Newman Jr JC. An experimental study of COD for mode I/II stable crack growth in thin 2024-T3 aluminum specimens. ASTM STP 1256 on Fracture Mechanics 1995;26:256–271.

6   Anderson TL. Fracture Mechanics: Fundamentals and Applications. 3rd edition, CRC Press, Boca Raton 2005.

7   Anvari M, Scheider I, Thaulow C. Simulation of dynamic ductile crack growth using strain-rate and triaxiality-dependent cohesive elements. Engineering Fracture Mechanics 2006;73:2210–2228

8   ASTM E1290-09: Standard test method for crack-tip opening displacement (CTOD) Fracture toughness measurement. American Society of Testing and Materials, Philadelphia; 2009.

9   ASTM E1820-11: Standard test method for measurement of fracture toughness. American Society of Testing and Materials, Philadelphia; 2011.

10   ASTM E2218-02: Standard test method for determining forming limit curves. American Society of Testing and Materials, Philadelphia; 2008.

11   ASTM E517-00: Sandard test method for plastic strain ratio r for sheet metal. American Society of Testing and Materials, Philadelphia; 2010.

12   ASTM E8M-11: Standard test methods for tension testing of metallic materials. American Society of Testing and Materials, Philadelphia; 2011.

13   Atkins AG, Mai YW. Fracture Strains in Sheet Metal Forming and Specific Essential Work on Fracture. Engineering Fracture Mechanics 1987;27:291–297.

14   Atkins AG. Deformability versus Fracture Limit Diagrams in Material Processing Defects. In: S.K. Ghosh & M. Predeleanu editors. Material Processing Defects. Elsevier Studies in Applied Mechanics Vol. 43 1995 pp. 235–250.

15   Atkins AG. Fracture in Forming. Proc. Int. Conf. On Advances in Materials and Processing Technologies, (Ed. Hashmi). Dublin: City University 1993 pp. 234–245.

16   Atkins AG. Mai YW. Elastic and Plastic Fracture—metals, polymers, ceramics, composites, biological materials. Ellis Horwood Limited. Wiley, Chichester 1985.

17   Atkins AG. Strange Multiplier Crack Paths in Ductile Fracture. Proc. 9th Int. Conf. On Fracture, Sydney, 1997 pp. 2391–2402.

18   Barenblatt GI. The mathematical theory of equilibrium of cracks in brittle fracture. Advanced Applied Mechanics 1962;7:55–129.

19   Bayraktar E, Grumbach M, Kaplan D. Effect of forming rate on the impact tensile properties of the steels under crash test Journal of of Achievements in Materials and Manufacturing Engineering 2007; 20(1-2):55–60

20   Bhattacharya S, and Kumar AN. A New Approach for CTOD Evaluation in Slow Crack Growth Situations. Engineering Fracture Mechanics 1991;40 (6):1089–1103

21   Bhattacharya S, and Kumar AN. Modeling of Rotational Factor in Notched Bend Specimen under General and Local Yield Situation. Theoretical and Applied Fracture Mechanics 1995b;24:33–46.

22   Bhattacharya S, and Kumar AN. Rotational Factor using Bending Moment Approach under Elasto-Plastic Situation – I Notch 3PB geometry. Engineering Fracture Mechanics 1995a;50(4): 493–505.

23   Blackman B, Dear JP, Kinloch AJ. The calculation of adhesive fracture energies from double-cantilever beam test specimens. Journal of Materials Science Letters 1991;10(5):253–256.

24   Blackman B, Hadavinia H, Kinloch AJ. The calculation of adhesive fracture energies in mode I: revisiting the tapered double cantilever beam (TDCB) test. Engineering Fracture Mechanics 2003b;70(2):233–248.

25   Blackman B, Hadavinia H, Kinloch AJ. The use of a cohesive zone model to study the fracture of fibre composites and adhesively-bonded joints. International Journal of Fracture 2003c;119(1):25–46.

26   Blackman B, Kinloch AJ, Paraschi M. Teo WS. Measuring Mode I Adhesive Fracture Energy, G_{IC}, of Structural Adhesive Joints: The Results of an International Round-Robin. International Journal of Adhesion & Adhesives 2003a;23:293–305.

27   Blyth PH, Atkins AG. Stabbing of metal sheets by a triangular knife. An archeological investigation. International Journal of Impact Engineering 2001;27:459–473.

28   Bonifaz EA. Cohesive zone modeling to predict failure processes. Canadian Journal on Mechanical Sciences and Engineering 2011;2(3):42–54.

29   Brighton IJ, Christopherb T. Developments in Elastic-Plastic Fracture Mechanics and Analysis using R- Curve. European Journal of Scientific Research 2012;75(3):346–360.

30   Brinckmann S, Siegmund TA. Cohesive zone model based on the micromechanics of dislocations. Modelling and Simulation in Materials Science and Engineering 2008;16:1–19.

31   Broberg BK. Cracks and Fracture. 1st edition, Academic Press, New York 1999.

32   Brocks W, Cornec A, Scheider I. Computational aspects of nonlinear fracture mechanics. In: de Borst R, Mang HA, editors. Comprehensive structural integrity. Numerical and computational methods, vol. 3. Elsevier Ltd.; 2003. pp. 127–209.

33   Brocks W, Cornec A. Special issue on cohesive models. Engineering Fracture Mechanics 2003;70(14):1741–1987.

34   Broek, D. Elementary Fracture Mechanics, 4th edition, Nijhof, The Hague 2002.

35   Budden PJ, Dean DW. Constraint effects on creep crack growth. In: Proc. Eighth Int. Conf. Creep and Fatigue at Elevated Temperatures, July 22–26, 2007, San Antonio, Texas (article number: CREEP2007-26104).

36   Cada R. Comparison of formability of steel strips, which are used for deep drawing of stampings. Journal of Materials Processing Technology 1996;60:283–290.

37   Caddell RM. Deformation and Fracture of Solids. 1st edition, Prentice-Hall, INC. Englewood Cliffs, New Jersey USA, 1980.

38   Callister Jr WD. Materials Science and Engineering An Introduction. 6th Edition. Published by John Wiley and Sons, Inc. 2006.

39   Camacho GT, Ortiz M. Computational modelling of impact damage in brittle materials. International Journal of Solids and Structures 1996;33:2899–2938.

40   Camanho PP, Da´vila CG, de Moura MF. Numerical simulation of mixed-mode progressive delamination in composite materials. Journal of Composite Materials 2003;37(16):1415–1438.

41   Castrodeza EM, Ipina J EP, Bastian FL. Fracture Toughness Evaluation of Unidirectional Fibre Metal Laminates using Traditional CTOD (δ) and Schwalbe (δ_5) Methodologies. Engineering Fracture Mechanics 2004;71:1127–1138.

42   Chao YJ, Sutton MA. On the fracture of solids characterized by one or two parameters: theory and practice. Journal of the Mechanics and Physics of Solids 1994;42(4):629–647.

43   Chen CR, Kolednik O, Heerens J, Fischer FD. Three-dimensional modeling of ductile crack growth: Cohesive zone parameters and crack tip triaxiality. Engineering Fracture Mechanics 2005;72:2072–2094.

44   Chen CR, Kolednik O. Comparison of Cohesive Zone Parameters and Crack Tip Stress States between Two Different Specimen Types. International Journal of Fracture 2005;132:135–152.

45   Chen CR, Kolednik O. On the Determination of the Cohesive Zone Parameters for the Modeling of Micro-Ductile Crack Growth in Thick Specimens. International Journal of Fracture 2003;120:517–536.

46   Chen GX, Wang CH, Rose LR F. A Strain-based Cohesive Zone Model for a Crack in a Power-Law Material under Grossly Plastic Conditions. DSTO Aeronautical and Maritime Research Laboratory 506 Lorimer St Fishermans Bend, Victoria 3207 Australia 2002: 1–18

47   Chen RS, Lee HH, Yu CY. Application of Taguchi's method on the optimal process design of an injection molded PC/PBT automobile bumper. Composite Structures 1997;39 (3–4):209–214.

48   Chen ZA, Zeng Z, Chao YJ. Effect of crack depth on the shift of the ductile–brittle transition curve of steels. Engineering Fracture Mechanics 2007;74:2437–2448

49   Chipperfied CG. Some observation on ductile crack initiation and propagation in fracture toughness specimens. Proceedings of specialist meeting on elasto-plastic fracture mechanics. OECP Nuclear Energy Agency, Daresbury, 1978;2:15–19.

50   Colgan M, Monaghan J. Deep drawing process: analysis and experiment. Journal of Materials Processing Technology 2003;132:35–41.

51   Cornec A, Scheider I, Schwalbe KH. On the practical application of the cohesive model. Engineering Fracture Mechanics 2003;70:1963–1987.

52   Cotferel B, LI Q F. On the effect of plastic constraint on ductile tearing in a structural steel. Engineering Fracture Mechanics 1985;21:239–244.

53   Cotterell B, Reddell JK. The essential work of plane stress ductile fracture. International Journal of Fracture 1977;13:267–277.

54   Cotterell B. The Past, Present, and Future of Fracture Mechanics. Engineering Fracture Mechanics 2002;69:533–553.

55   Cotterell M, Schambergerova J, Ziegelheim J, Janovec J. Dependence of micro-hardness on deformation of deep-drawing steel sheets. Journal of Materials Processing Technology 2002;124:293–296.

56   Das P, Jayaganthan R, Chowdhury T, Singh IV. Improvement of Fracture toughness (K_{Ic}) of 7075 Al alloy by Cryorolling process. Materials Science Forum, 2011;683:81–94.

57   Das P, Jayaganthan R, Chowdhury T, Singh IV. Fatigue behaviour and Crack   Growth rate of Cryorolled Al 7075 alloy. Material Science and Engineering: A, 2011;528 (24):7124–7132.

58   Dasarathy C, Hudd RC. Effect of Al Content on the Deep Drawing Properties of Continuous Annealed Al-killed Sheet Steels. Technical Report No. 632/A/1974, B.S.C., Strip Mill Division, Port Talbot Works 1974.

59   Daudeville L, Allix O, Ladeve`ze P. Delamination analysis by damage mechanics. Some applications. Composites Engineering 1995;5(1):17–24.

60   Dawicke DS, Sutton MA, Newman JC Jr, Bigelow CA. Measurement and analysis of critical CTOA for aluminum alloy sheet. Fracture Mechanics ASTM STP 1995;1220:358–379.

61   Dawicke DS, Sutton MA. CTOA and crack-tunneling measurements in thin sheet 2024-T3 aluminum alloy. Experimental Mechanics 1994;34(4):357–368 .

62   de Borst Rene. Numerical aspects of cohesive-zone models. Engineering Fracture Mechanics 2003;70:1743–1757.

63   Diehl T. On using a penalty-based cohesive-zone finite element approach, Part I: Elastic solution benchmarks. International Journal of Adhesion & Adhesives 2008;28:237–255.

64   Dieter GE. Mechanical Metallurgy. Published by McGraw-Hill, London 1988.

65   Djavanroodi F, Derogar A. Experimental and numerical evaluation of forming limit diagram for Ti6Al4V titanium and Al6061-T6 aluminum alloys sheets Materials and Design 2010;31:4866–4875

66   Dorel B. The European Scientific Association for material Forming. ESAFORM Bulletin 2008;8(1):2–10.

67   Duan X, Sheppard T. Influence of forming parameters on the final subgrain size during hot rolling of aluminium alloys. Journal of Materials Processing Technology 2002;130:245–249.

68   Duchêne L, Habraken AM. Analysis of the sensitivity of FEM predictions to numerical parameters in deep drawing simulations. European Journal of Mechanics - A/Solids 2005;24:614–629.

69   Dugdale DS. Yielding in Steel Sheets Containing Slits. Journal of Mechanics and Physics of Solids. 1960;8:100–108.

70   Elices GV, Guinea J, Gomez J, Planas J. The cohesive zone model: advantages, limitations and challenges. Engineering Fracture Mechanics 2002;69:137–163.

71   Falk ML, Needleman A, Rice JR. A critical evaluation of cohesive zone models of dynamic fracture. Journal de Physique IV 2001:543–550.

72   Faucher B, Tyson WR, Hong Y, Boutin J. Dependence of Ductile Fracture Toughness of a Weld Metal on Notch Root Radius and Inclusion Content. International Journal of Fracture 1990;46:173–184.

73   Fekete JR. Overview of sheet metal for stamping. Society of Automotive Engineers 1997;106:699–710.

74   Firrao R, Roberti R. A model for plane strain ductile fracture toughness. In: Proceedings of ICSMA6, Melbourn 1982;2:947–952.

75   Fratini L, Ambrogio G, Lorenzo RD, Filice L, Micari F. Influence of mechanical properties of the sheet material on formability in single point incremental forming. CIRP Annals - Manufacturing Technology 2004;53:207–210.

76   Goodwin GM. Application of Strain Analysis to Sheet Metal Forming Problems in the Press Shop. Society of Automotive Engineers. SAE Technical paper No. 680093, 1968.

77   Granzow WG, Armco Inc. Sheet Formability of Steels. ASM Handbook Vol. 1, Properties and Selection: Irons, Steels, and High-Performance Alloys, 1990.

78   Gunnarsson L, Schedin E. Improving the properties of exterior body panels in automobiles using variable blank holder force. Journal of Materials Processing Technology 2001;114:168–173.

79   Hangan E, Jeswiet J. A review of conventional and modern single point sheet metal forming methods. Proceedings of the Institution of Mechanical Engineers, Part B: Journal of Engineering Manufacture 2003;217:213–225.

80   Haung YM, Leu DK. Effect of Process Variables on V-Die Bending Process of Steel Sheet. International Journal of Mechanical Sciences 1998;40:631–650.

81   He Z, He Y, Ling Y, Wu Q, Gao Y, Li L. Effect of strain rate on deformation behavior of TRIP steels. Journal of Materials Processing Technology 2012;212:2141–2147.

82   Hecker SS. Simple technique for determining forming limit curves. Sheet Metal Industries 1972;52:671–675.

83   Heerens J, Schodel M. On the determination of crack tip opening angle, CTOA, using light microscopy and δ5 measurement technique. Engineering Fracture Mechanics 2003;70:417–426.

84   Heydari MH, Choupani N. Effects of thickness on fracture toughness of carbon/polyester composite. Key Engineering Materials, 2011;471:886–891.

85   Holtam CM, Baxter DP, Ashcroft IA, Thomson RC. Effect of crack depth on fatigue crack growth rates for a C–Mn pipeline steel in a sour environment. International Journal of Fatigue 2010;32:288–296.

86   Hosford WF, Caddell RM. Metal forming-mechanics and metallurgy. Published by Prentice Hall, USA, 1993.

87   Huang XD. A study about elastic-plastic fracture with deep and shallow crack. Harbin: Harbin shipbuilding Engineering Institute, 1987.

88   Hussain G, Gao L, Hayat N, Ziran Xu. A new formability indicator in single point incremental forming. Journal of Materials Processing Technology 2009;209:4237–4242.

89   Hutchinson JW. Singular behaviour at the end of a tensile crack tip in a hardening material. Journal of Mechanics and Physics of Solids 1968;16:13–31.

90   Isik K, Soyarslan C, Richter H, Tekkaya AE. Analysis of formability of advanced high strength steel sheets with phenomenologically based failure criteria with separate

treatment of instability, shear and normal fracture. 8th European LS-DYNA Users Conference, Strasbourg, 2011 pp. 1–11.

91   Itabashi M, Kawata K. Carbon content effect on high-strain-rate tensile properties for carbon steels. International Journal of Impact Engineering 2000;24:117–131.

92   Jackson K, Allwood J. The mechanics of incremental sheet forming. Journal of Materials Processing Technology 2009; 209:1158–1174.

93   Jadhav DN, Maiti SK. Characterization of stable crack growth through AISI 4340 steel using cohesive zone modeling and CTOD/CTOA criterion. Nuclear Engineering and Design 2010;240:713–721.

94   Jie M, Cheng CH, Chan LC, Chow CL. Forming limit diagrams of strain-rate-dependent sheet metals. International Journal of Mechanical Sciences 2009;51:269–275.

95   Kang YL, Zhang ZF, Wang HW, Qin QH. Experimental investigations of the effect of thickness on fracture toughness of metallic foils. Materials Science and Engineering 2005;394:312–319.

96   Keeler SP, Backofen WA. Plastic Instability and Fracture in Sheets Stretched Over Rigid Punches. Transactions of the ASM, 1963;56:25–48.

97   Keeler SP. Determination of Forming Limits in Automotive Stampings. Society of Automotive Engineers, Technical paper No. 650535, 1965.

98   Kegg RL. A new test method for determination of spinnability of metals. Transactions of the American Society of Mechanical Engineers, Journal of Engineering for Industry 1961;B83:119–124.

99   Koa DC, Kim DH, Kim BM, Choi JC. Methodology of perform design considering workability in metal forming by the artificial neural network and Taguchi method. Journal of Materials Processing Technology 1998;80(81):487–492.

100   Koa DC, Kim DH, Kim BM. Application of artificial neural network and Taguchi method to preform design in metal forming considering workability. International Journal of Machine Tools and Manufacture 1999;39:771–785.

101   Krishnan N, Cao J. Estimation of optimal blank holder force trajectories in segmented binders using an ARMA model. Journal of Mechanical Engineering Science 2003;125:763–770.

102   Kulkarni DM, Prakash R, Kumar AN. Experimental and Finite Element Analysis of Fracture Criterion in General Yielding Fracture Mechanics. Sadhana, Indian Academy of Sciences 2002;27(6):631–642.

103   Kulkarni DM, Prakash R, Talan PS, Kumar AN. The Effect of Specimen Thickness on the Experimental and Finite Element Characterisation of CTOD in Extra Deep Drawn Steel Sheets. Sadhana, Indian Academy of Sciences 2004a;29(4):365–380.

104   Kulkarni DM, Prakash R. Experimental Analysis of Fracture Criterion in General Yielding Fracture Mechanics. Journal of Institute of Engineers 2003a;84:18–21.

105   Kulkarni DM. Study of fracture behaviour of extra deep drawn steel sheets, Phd thesis, BITS, Pinali, 2005.

106   Kumar AN, Bhattacharya S. Rotational Factor using Bending Moment Approach under Elasto-Plastic Situation – II Notch 3PB geometry. Engineering Fracture Mechanics 1995;50(4):507–517.

107   Kumar AN. Modeling of Fracture Process in Annealed Sheet of AISI 202 Stainless Steel. Scripta Materialia 1996;34:369–373.

108   Kumar AN. On the Accuracy of Crack Size Measurement. International Journal of Fracture 1988a;38:R27–R30.

109   Kumkum Banerjee. Evaluation of annealing texture in IF and EDD steel sheets. Materials and Manufacturing Processes 2007;22(4):462–468.

110   Landes JD, Begley JA. Experimental methods for elastic-plastic and post-yield fracture toughness measurements. Barking: Post-yield fracture mechanics, Applied Science Publication, 1979.

111   Lee SW. Study on the forming parameters of the metal bellows. Journal of Materials Processing Technology 2002;130(131):47–53.

112   Leu DK, The limiting drawing ratio for plastic instability of the cup drawing process. Journal of Materials Processing Technology 1999;86:168–176.

113   Lewis ID, Smith RF, Knott JF. On the a/W ratio in plane strain fracture toughness testing. International Journal of Fracture 1975;11:179–183.

114   Li Q, Fu Y, Xu X. A review of the Effect of a/W ratio on fracture toughness (II)-- experimental investigation in LEFM. Journal of Marine Science and Application, 2005;4(2):1–5.

115   Li Q, Jin G, Wang Y. A review of the effect of a/W ratio on fracture toughness (I)-- experimental investigation in EPFM, Journal of Marine Science and Application, 2005;4(1):1–7.

116   Li Q, Qiu BH, Cui XF. Effect of plastic constraint on ductile fracture in structural steels. Proceedings of IWMST02, Tokyo, 2002:83–85.

117   Li Q, Shi D. The effect of a/W ratio and crack shape on J_i, and δ_i, values in a ship plate steel Proceedings of the IOPE-91, Edinburgh, 1991:137–141.

118   Li Q, Zhang L. Effect of several variables on J-COD relationship and plastic rotational factor r_P. Engineering Fracture Mechanics 1986;53:473–480.

119   Li Q, Zhou LM, Li S. The effect of a/W ratio on crack initiation values of COD and J-integral. Engineering Fracture Mechanics 1986;23:925–928.

120   Li Q. A study about J_i and δ_i in three-point bend specimens with deep and shallow notches. Engineering Fracture Mechanics 1985;22:9–15.

121   Li Q. The effect of plastic constraint on the initiation of ductile tears in shipbuilding structural steel. Journal of Marine Science and Application 2003;2:1–4 .

122   Li W, Siegmund T. An analysis of crack growth in thin-sheet metal via a cohesive zone model. Engineering Fracture Mechanics 2002;69:2073–2093.

123   Lin J. A general formula of J-integral calculating for both shallow and deep cracks. Journal of Harbin Shipbuilding Engineering Institute 1987;8:68–73.

124   Liu HW, Ke JS. Thickness effect on crack tip deformation of fracture. Engineering Fracture Mechanics 1976;8:425–436.

125   Liu HW, Kuo AS. Fracture Toughness of Thin and Tough Plates. International Journal of Fracture 1978;14:R109–R112.

126   Liu HW, Kuo AS. Fracture toughness of thin and tough plates. International Journal of Fracture 1978;14:R109–R112.

127   Liu HW. Fracture Mechanics of Ductile and Tough Materials and its Applications to Energy Related Structures. Published by Martinus Nijhoff Publishers, the Hague, 1981.

128   Mahmoud S, Lease K. The effect of specimen thickness on the experimental characterization of critical crack-tip-opening angle in 2024-T351 aluminum alloy. Engineering Fracture Mechanics 2003;70:443–56.

129   Mai YW, Cotterell B. On essential work of ductile fracture in polymers. International Journal of Fracture 1986;32:105–125.

130   Majerus JN, Santhanam S. Anisotropy in Fracture Behavior of Thin Al-7075-T651 Plates. Engineering Fracture Mechanics 1997;56:437–442.

131   Marchal Y, Delannay F. In Buence of test parameters on the measurement of the essential work of fracture of zinc sheets. International Journal of Fracture 1996;80:295–310.

132   Merkle JG, Corten HT. Elastic-Plastic Fracture Toughness Testing with Compact Tension Specimens. Journal of Pressure Vessel Technology 1990;96:286–292.

133   Mizui N, Okamoto A. Effects of Mn content and Hot Band Coiling Temperature on Deep Drawability of Continuous Annealed Al-killed Sheet Steels. Proceedings of International Symposium on Developments in the Annealing of Sheet Steels, TMS Ferrour Metallurgy Committee, Cincinnati, OH, 1991: 247–259.

134   Mizui N, Okamoto A. The Effect of Carbon Content on the Mechanical Properties of Continuous Annealed Al-killed Sheet Steels. Sumitomo Search 1990;44:113–119.

135   Mourad AH I, Alghafri MG, Abu Zeid OA, Maiti SK. Experimental investigation on ductile stable crack growth emanating from wire-cut notch in AISI 4340 steel. Nuclear Engineering and Design 2005;235:637–647.

136 Mourad AH I, Aly ED, Chao YJ. Fracture toughness prediction of low alloy steel as a function of specimen notch root radius and size constraints. Engineering Fracture Mechanics (2012), http://dx.doi.org/10.1016/j.engfracmech.2012.05.010

137 Mourad AH I, Aly ED. Notch Radius and Specimen Size Effects on Fracture Toughness of Low Alloy Steel. Procedia Engineering 2011;10:1348–1353.

138 Mourad AH I. Assessment of the effect of the notch radius on ductile stable crack growth. In: Proceedings of ASTM PVP2008, Chicago, USA, July 27–31, 2008: 77–82.

139 Murakami Y. Stress Intensity Factors Handbook. Published by Pergamon Press, New York, 1987.

140 Murthy VRS, Gupta KP, Jena AK, Murty GS.Structure and Properties of Engineering Materials. 1st edition, The McGraw-Hill companies, India, 2005.

141 Nakazima K, Kikuma T, Hasuka T. Study on the formability of steel sheets. Yawata Technical Report 1968;284:140–141.

142 Needleman A. A continuum model for void nucleation by inclusion debonding. Journal of Applied Mechanics 1987;54:525–531.

143 Negre P, Steglich D, Brocks W. Crack extension at an interface: prediction of fracture toughness and simulation of crack path deviation. International Journal of Fracture 2005;134:209–229.

144 O'Donoghue PE, Kanninen MF, Leung CP, Demofonti G, Venzi S. The development and validation of a dynamic fracture propagation model for gas transmission pipelines. International Journal of Pressure Vessels and Piping 1997;70:11–25.

145 Obermeyer EJ, Majlessi SA. A review of recent advances in the application of blank-holder force towards improving the forming limits of sheet metal parts. Journal of Materials Processing Technology 1998;75:222–234.

146 Ortiz M, Pandolfi A, Finite-Deformation Irreversible Cohesive Elements for Three-Dimensional Crack Propagation Analysis. International Journal for Numerical Methods in Engineering 1999;44:1267–1282.

147 Ortiz M, Suresh S. Statistical Properties of Residual Stresses and Intergranular Fracture in Ceramic Materials. Journal of Applied Mechanics 1993;60:77–84.

148 Ozturk F, Toros S, Kilic S. Evaluation of tensile properties of 5052 type aluminum-magnesium alloy at warm temperatures. Archives of Material Science and Engineering 2008;34(2):95–98.

149 Padmanabhan R, Oliveira MC, Alves JL, Menezes LF. Influence of process parameters on the deep drawing of stainless steel. Finite Elements in Analysis and Design 2007;43:1062–1067.

150 Pandey AB, Majumdar BS, Miracle DB. Effects of Thickness and Precracking on the Fracture Toughness of Particle-Reinforced Al-Alloy Composites. Metallurgical and Material Transactions, 1997;29(A):1237–1243.

151 Pardoen T, Delannay F. A Method for the Metallographical Measurement of the CTOD at Cracking initiation and the Role of Reverse Plasticity on Unloading. Engineering Fracture Mechanics 2000;65:455–466.

152 Pardoen T, Ferracin T, Landis CM, Delannay F. Constraint effects in adhesive joint fracture. Journal of the Mechanics and Physics of Solids 2005;53:1951–1983.

153 Pardoen T, Hachez F, Marchioni B, Blyth PH, Atkins AG. Mode–I fracture of sheet metal. Journal of the Mechanics and Physics of Solids 2004;52:423–452.

154 Pardoen T, Marchal Y, Delannay F. Essential work of fracture versus fracture mechanics—towards a thickness independent plane stress toughness. Engineering Fracture Mechanics 2002;69: 617–631.

155 Pardoen T, Marchal Y, Delannay F. Thickness dependence of cracking initiation criteria in thin aluminum plates. Journal of the Mechanics and Physics of Solids 1999;47:2093–2123.

156 Park DH, Bae WR, Jeong HJ, So BS, Ko T.J, Yarlagadda PK DV. Applicability valuation for evaluation of surface deflection in automotive outer panels. Journal of Achievements in Materials and Manufacturing Engineering 2008;31(2):558–564.

157   Park K, Kim Y. The effect of material and process variables on the stamping formability of sheet materials. Journal of Materials Processing Technology 1995;51:64–78.

158   Qiu H, Enoki M, Hiraoka K, Kishi T. Effect of pre-strain on fracture toughness of ductile structural steels under static and dynamic loading. Engineering Fracture Mechanics 2005;72:1624–1633.

159   Qiu Y, Crisfield MA, Alfano G. An interface element formulation for the simulation of delamination with buckling. Engineering Fracture Mechanics 2001;68:1755–1776.

160   Rao KP, Mohan EV R. Direct Evaluation of Sheet Metal Forming Properties under Various Deformation Conditions. Key Engineering Materials 2000; 177(180):509–516.

161   Ravi Kumar D. Formability analysis of Extra-Deep Drawing Steel. Journal of Materials Processing Technology 2002;130:31–41.

162   Ravilson ACF, Herber CS, Paulo V, Prestes M. Revisiting single-point incremental forming and formability/failure diagrams by means of finite elements and experimentation. The Journal of Strain Analysis for Engineering Design 2009;44(4):221–234.

163   Ray KK, Patra1 A, Bhattacharjee D. A new methodology for estimating fracture criterion of thin sheets. Key Engineering Materials 2010;417(418):305–308.

164   Ray KK, Roy S, Bhaduri A. Fracture criteria of deep-drawn steel sheets. International Journal of Fracture 1995;70:R3–R8.

165   Rice JR, Beltz GE. The activation-energy for dislocation. Journal of the Mechanics and Physics of Solids 1994;42:333–360.

166   Rice JR, Paris PC, Merkle JG. Some Further Results of J-Integral Analysis and Estimates. ASTM STP 536, American Society of Testing and Materials, Philadelphia 1973: 231–245.

167   Rice JR, Rosengren GF. Plane Strain Deformation near a Crack Tip in a Power-Law Hardening Material. Journal of the Mechanics and Physics of Solids 1968;16:1–12.

168   Rice JR. A Path Independent Integral and the Approximate Analysis of Stress Concentration by Notches and Cracks. Journal of Applied Mechanics 1968;35:379–386.

169   Rice JR. Dislocation nucleation from a crack tip–an analysis based on the PIERLS concept. Journal of the Mechanics and Physics of Solids 1992;40:239–271.

170   Roy Y, Dodds RH Jr. Simulation of Ductile Crack Growth in Thin Aluminum Panels Using 3D Surface Cohesive Elements. International Journal of Fracture 2001;110:21–45.

171   Ruiz G, Pandolfi A, Ortiz M. Three-dimensional cohesive modeling of dynamic mixed-mode fracture. International Journal for Numerical Methods in Engineering 2001;52:97–120.

172   Schedin E, Melander A. On the Strain Distribution During Punch Stretching of Low and High Grades of Sheet Steel. Journal of Materials Processing Technology 1987;15:181–186.

173   Scheider I, Schodel M, Brocks W, Schonfeld W. Crack propagation analyses with CTOA and cohesive model: Comparison and experimental validation. Engineering Fracture Mechanics 2006;73: 252–263.

174   Scheider I, Brocks W. Simulation of cup-cone fracture using the cohesive model. Engineering Fracture Mechanics 2003;70:1943–1961.

175   Scheider I, Brocks W. The effect of the traction separation law on the results of cohesive zone crack propagation analyses. Key Engineering Materials 2003a;251(252): 313–318.

176   Scheider I, Schodel M, Brocks W, Schonfeld W. Crack propagation analyses with CTOA and cohesive model: Comparison and experimental validation. Engineering Fracture Mechanics 2006;73:252–263.

177   Scheider I. Brocks W. Cohesive elements for thin-walled structures. Computational Materials Science 2006;37:101–109.

178   Scheider I. Residual strength prediction of a complex structure using crack extension analyses. Engineering Fracture Mechanics 2009;76(1):149–63.

179   Schindler HJ. Determination of Fracture Mechanics Material Properties utilising Notched Test Specimens. Mechan Behaviour of Mater 1991;6:153–158.

180   Seshadri BR, Newman JC Jr, Dawicke DS, Young RD. Fracture Analysis of FAA/NASA Wide Stiffened Panels. Second Joint Conference on Aging Aircraft. Williamsburg, 1998: 513–524.

181   Shahani AR, Rastegar M, Dehkordi MB, Kashani HM. Experimental and numerical investigation of thickness effect on ductile fracture toughness of steel alloy sheets. Engineering Fracture Mechanics 2010;77:646–659.

182   Shen W. Single-point method of calculating J-integral. Journal of Huazhong Engineering Institute, 1978;2:20–24.

183   Sheng ZQ, Jirathearanat S, Altan T. Adaptive FEM simulation for prediction of variable blank holder force in conical cup drawing. International Journal of Machine Tools and Manufacture 2004;44:487–494.

184   Shukla A. Practical fracture mechanics in design. 2nd ed. New York: Marcel Dekker, 2005.

185   Siegmund T, Brocks W. Modeling crack growth in thin sheet aluminum alloys. ASTM STP 1389 2000:475–85.

186   Singh SK, Gupta AK, Mahesh KA. Study on the extent of ironing of EDD steel at elevated temperature. CIRP Journal of Manufacturing Science and Technology 2010b;3:73–79.

187   Singh SK, Mahesh K, Kumar A, Swathi M. Understanding formability of extra-deep drawing steel at elevated temperature using finite element simulation. Materials and Design 2010a;31:4478–4484.

188   Sorem WA, Dodds JR RH, Rolfe ST. Effects of crack depth on elastic-plastic fracture toughness. International Journal of Fracture 1991;47:105–126.

189   Srawley JE, Brown WF. Fracture Toughness Testing and its Applications. ASTM STP No. 381, Philadelphia, PA, 1975:133–198.

190   Srinivas M, Kamat SV, Rao PR. A fractographic technique for the estimation of initiation fracture toughness J_{Ic} for ductile materials. Journal of Testing and Evaluation 1994;22(4):302–308.

191   Srinivas M, Kamat SV. Effect of notch root radius on ductile fracture toughness of Armco Iron. International Journal of Fracture 1992;58:R15–R21.

192   Stoughton TB, Zhu X. Review of theoretical models of the strain-based FLD and their relevance to the stress-based FLD. International Journal of Plasticity 2004;20:1463–1486.

193   Sun PJ, Wang GZ, Xuan FZ, Tu ST, Wang ZD. Quantitative characterization of creep constraint induced by crack depths in compact tension specimens. Engineering Fracture Mechanics 2011;78:653–665.

194   Sutton MA, Michael L, Boone ML, Ma F, Helm JD. A combined modeling–experimental study of the crack opening displacement fracture criterion for characterization of stable crack growth under mixed mode I/II loading in thin sheet materials. Engineering Fracture Mechanics 2000;66:171–185.

195   Swaminathan K, Padmanabhan KA. Some Investigations on the Fracture Behaviour of an Indigenous Extra-Deep Drawing low Carbon Steel - Part I. Transactions of Indian Institute of Metals 1991;44:231–247.

196   Tan H, Liu C, Huang Y, Geubelle PH. The cohesive law for the particle/matrix interfaces in high explosives. Journal of Mechanics and Physics of Solids 2005;53:1892–1917.

197   Tejedor R, Rodríguez-Baracaldo R, Benito JA, Caro J, Cabrera JM. Influence of the carbon content on the strain rate sensitivity of nanocrystalline steels. Original Research Article Scripta Materialia 2008;59(6):631–634.

198   Toda H, Yamamoto S, Kobayashi M, Uesugi K, Zhang H. Direct measurement procedure for three-dimensional local crack driving force using synchrotron X-ray microtomography. Acta Materialia 2008;56:6027–6039.

199   Tomar V, Zhai J, Zhou M. Bounds for element size in a variable stiffness cohesive finite element model. International journal for numerical methods in engineering 2004;61:1894–1920.

200   Traversin M, Kergen R. Closed-loop control of the blank-holder force in deep-drawing: finite-element modeling of its effects and advantages. Journal of Materials Processing Technology 1995;50:306–317.

201   Turon A, Davila CG, Camanho PP, Costa J. An engineering solution for mesh size effects in the simulation of delamination using cohesive zone models. Engineering Fracture Mechanics 2007;74:1665–1682.

202   Turon A, Dávila CG, Camanho PP, Costa J. An Engineering Solution for Mesh Size Effects in the Simulation of Delamination Using Cohesive Zone Models. Engineering Fracture Mechanics 2007;74(10)1665–1682.

203   Turon A. Camanho PP, Dávila CG. A Damage Model for the Simulation of Delamination in Advanced Composites under Variable-Mode Loading. Mechanics of Materials 2006;38(11):1072–1089.

204   Tvergaard V, Hutchinson JW. The Relation between Crack Growth Resistance and Fracture Process Parameters in Elastic–Plastic Solids. Journal of the Mechanics and Physics of Solids 1992 40(6):1377–1397.

205   Verleysen P, PeirsJ, Slycken JV, Faes K, Duchene L. Effect of strain rate on the forming behaviour of sheet metals. Journal of Materials Processing Technology 2011;211:1457–1464.

206   Verma RK, Chandra S. An improved model for predicting limiting drawing ratio. Journal of Materials Processing Technology 2006;172:218–224.

207   Vratnica M, Pluvinage G, Jodin P, Cvijovic Z, Rakin M, Burzic Z. Influence of notch radius and microstructure on the fracture behavior of Al–Zn–Mg–Cu alloys of different purity. Materials and Design 2010;31:1790–1798.

208   Wang GZ, Liu XL, Xuan FZ, Tu ST. Effect of constraint induced by crack depth on creep crack-tip stress field in CT specimens. International Journal of Solids and Structures 2010;47:51–57.

209   Wang L, Lee TC. The effect of yield criteria on the forming limit curve prediction and the deep drawing process simulation. International Journal of Machine Tools and Manufacture 2006;46:988–95.

210   Wang ZX, Shi HJ, Lub J. Size effects on the ductile/brittle fracture properties of the pressure vessel steel 20 g. Theoretical and Applied Fracture Mechanics 2008;50:124–131.

211 Wells AA. Unstable Crack Propagation in Metals: Cleavage and Fast Fracture. Proceedings of the Crack Propagation Symposium, Cranfield, UK 1961;1:210-230.

212 Wilson CD, Landes JD. Inconsistencies between CTOD and J Calculations. Journal of Testing and Evaluation 1994;22:505–511.

213 Wilson DV, Acselrad O. Strain Localisation in Biaxially Stretched Sheets Containing Compact Defetcs – I. International Journal of Mechanical Sciences 1984;26:573–585.

214 Wu PD, Graf A, Jain M, MacEwen SR. On Alternative Representation of Forming Limits. Key Engineering Materials 2000;177(180):517–522.

215 Xie D, Waas AM. Discrete cohesive zone model for mixed-mode fracture using finite element analysis. Engineering Fracture Mechanics 2006;73:1783–1796.

216 Xin Chen, Xiaomin MA S. Simulation of stable tearing crack growth using the Cohesive Zone Model approach. Experimental and Applied Mechanics 2011;6:537–543.

217 Xu XP, Needleman A. Numerical Simulations of Fast Crack Growth in Brittle Solids. Journal of the Mechanics and Physics of Solids 1994;42(9):1397–1434.

218 Xu XP, Needleman A. Void Nucleation by Inclusion Debonding in a Crystal Matrix. Modeling and Simulation in Materials Science and Engineering 1993;1:111–132.

219 Yang S, Chao YJ, Sutton MA. Higher order asymptotic crack tip fields in power-law hardening materials. Engineering Fracture Mechanics 1993:1–20.

220 Yoda M. The effect of the notch root radius on the J-integral fracture toughness under modes I, II and III loading. Engineering Fracture Mechanics 1987;26(3):425–431.

221 Yoshihara S, Manabe KI, Nishimura H. Effect of blank holder force control in deep-drawing process of magnesium alloy sheet, Journal of Materials Processing Technology 2005;170:579–585.

222 Yuan H, Lin G, Cornec A. Verification of a cohesive zone model for ductile fracture. Journal of Engineering Materials and Technology 1996;118:192–200.

223 Zerbst U, Heinimann M, Donne CD, Steglich D. Fracture and damage mechanics modelling of thin-walled structures – An overview. Engineering Fracture Mechanics 2009;76:5–43.

224   Zhongqi Y, Zhongqin L, Yixi Z. Evaluation of fracture limit in automotive aluminium alloy sheet forming. International Journal of Material and Design 2007;28(1):203–207.

225   Zou Z, Reid SR, Li S, Soden PD. Modelling interlaminar and intralaminar damage in filament wound pipes under quasi-static indentation. Journal of Composite Materials 2002;36:477–499.

LIST OF PUBLICATIONS

List of publications based on present work

1   Chaudhari VV, Kulkarni DM, Prakash R. Determination of critical CTOD using crack flank opening angle method in general yield regime. Fatigue and Fracture of Engineering Structures and Materials 2011;34:260–269. **[Impact factor: 0.93]**

2   Chaudhari VV, Kulkarni DM, Prakash R. Three- dimensional finite element analysis of fracture behaviour in general yielding fracture mechanics. Journal of Mechanical Engineering, Strojnícky Casopis 2010;61(c. 3):131–148.

3   Chaudhari VV, Kulkarni DM, Prakash R. Study of Influence of Notch Root Radius on Fracture Behaviour of Extra Deep Drawn Steel Sheets. Fatigue and Fracture of Engineering Structures and Materials 2009;32:975–986. **[Impact factor: 0.93]**

4   Kulkarni DM, Chaudhari VV, Prakash R, Kumar AN. Effect of thickness on fracture criterion in general yielding fracture mechanics. International Journal of Fracture 2008;151:187–198. **[Impact factor: 1.485]**

5   Chaudhari VV, Kulkarni DM. Effect of Strain Rate on Fracture Toughness of Extra Deep Drawn Steel Sheets: Experimental and Finite Element Approach. International Conference on Advances in Mechanical Engineering (Communicated).

Other publications

1   Dhananjay M. Kulkarni and Vikas Chaudhari, "Failure Analysis and Prevention: A Course for Undergraduates", Bulletin of Marin Science and Technology. 2012;7(1):27–29.

2   Vikas Chaudhari, D. M. Kulkari, Ravi Prakash and Pravin Talan, "Experimental Characterization of Crack Growth Behaviour in Extra Deep Drawn Steel Sheets", Proceedings of the 50th Congress of the Indian Society of Theoretical and Applied Mechanics (ISTAM), December 2005

3   Vikas Chaudhari, Vinod Suryawanshi, "System Modeling Through Bond Graph", Proceedings of National Conference on Advances in Mechanical Engineering (NAME-2004), February 2004.

4   Vikas Chaudhari, Vinod Suryawashi, "Artificial Neural Network Modeling of Extrude Honing Process", Proceedings of National Conference on Development and Challenges in Mechanical Engineering, March 2004

5   Vikas Chaudhari, Vinod Suryawashi, "Modeling of Mechatronics System- A Bond Graph Approach", Proceedings of National Conference on Recent Advances in Mechatronics, July 2004.

APPENDICES

Appendix A

Tensile Test Data of EDD Steel Steels

A 1 Engineering stress – strain data: EDD 'A'

Sr. No.	Strain (mm/mm)	Stress (MPa)	Sr. No.	Strain (mm/mm)	Stress (MPa)
1.	0.0000	0.00	16.	0.1260	378.31
2.	0.0011	237.47	17.	0.1440	383.55
3.	0.0013	265.79	18.	0.1560	387.13
4.	0.0013	278.47	19.	0.1860	387.06
5.	0.0014	293.59	20.	0.1980	385.21
6.	0.0240	335.09	21.	0.2040	384.41
7.	0.0300	345.44	22.	0.2100	383.62
8.	0.0360	351.39	23.	0.2160	381.20
9.	0.0540	352.58	24.	0.2220	380.43
10.	0.0600	356.16	25.	0.2280	378.86
11.	0.0660	360.92	26.	0.2460	375.40
12.	0.0752	363.30	27.	0.2586	372.91
13.	0.0868	369.26	28.	0.2712	371.90
14.	0.0960	375.22	29.	0.2840	369.83
15.	0.1140	377.12	30.	0.2969	367.11

A 2 Engineering stress – strain data: EDD 'B'

Sr. No.	Strain (mm/mm)	Stress (MPa)	Sr. No.	Strain (mm/mm)	Stress (MPa)
1.	0.0000	0.00	25.	0.2039	309.14
2.	0.0008	167.86	26.	0.2100	314.13
3.	0.0009	188.83	27.	0.2160	316.71
4.	0.0010	209.79	28.	0.2220	318.32
5.	0.0012	245.41	29.	0.2280	321.20
6.	0.0013	259.19	30.	0.2460	326.11
7.	0.0015	261.61	31.	0.2600	329.56
8.	0.0016	263.48	32.	0.2640	330.04
9.	0.0180	264.30	33.	0.2820	328.27
10.	0.0240	266.95	34.	0.3000	327.14
11.	0.0300	270.43	35.	0.3180	326.42
12.	0.0360	273.38	36.	0.3360	325.15
13.	0.0540	275.58	37.	0.3540	324.80
14.	0.0600	278.15	38.	0.3720	323.10
15.	0.0660	283.92	39.	0.3900	322.46
16.	0.0752	284.30	40.	0.4080	321.40
17.	0.0868	288.27	41.	0.4260	320.15
18.	0.0960	289.21	42.	0.4440	319.14
19.	0.1260	291.11	43.	0.4620	318.24
20.	0.1341	294.29	44.	0.4799	317.16
21.	0.1440	296.56	45.	0.4980	316.43
22.	0.1560	299.12	46.	0.5160	315.23
23.	0.1860	302.13	47.	0.5340	314.10
24.	0.1936	307.12	48.	0.5519	312.97

A 3 Engineering stress – strain data: EDD 'C'

Sr. No.	Strain (mm/mm)	Stress (MPa)	Sr. No.	Strain (mm/mm)	Stress (MPa)
1.	0.0000	0.00	25.	0.2039	330.15
2.	0.0011	231.29	26.	0.2100	331.13
3.	0.0011	241.22	27.	0.2160	333.71
4.	0.0012	255.93	28.	0.2220	335.32
5.	0.0013	266.36	29.	0.2280	337.20
6.	0.0013	272.53	30.	0.2360	339.09
7.	0.0013	276.97	31.	0.2400	341.56
8.	0.0015	278.61	32.	0.2640	342.04
9.	0.0016	279.48	33.	0.2820	340.27
10.	0.0180	284.30	34.	0.3000	338.14
11.	0.0240	289.95	35.	0.3180	336.42
12.	0.0300	290.43	36.	0.3360	335.15
13.	0.0360	293.38	37.	0.3540	332.80
14.	0.0540	295.58	38.	0.3720	329.10
15.	0.0600	298.15	39.	0.3900	327.46
16.	0.0660	301.92	40.	0.4080	326.40
17.	0.0752	305.30	41.	0.4260	325.15
18.	0.0868	307.14	42.	0.4440	324.14
19.	0.0960	309.12	43.	0.4620	323.24
20.	0.1260	314.12	44.	0.4799	322.90
21.	0.1341	316.70	45.	0.4980	322.43
22.	0.1440	318.33	46.	0.5160	321.73
23.	0.1560	321.20	47.	0.5239	321.12
24.	0.1860	326.09	48.	0.5300	320.45

A 4 Engineering stress – strain data: EDD 'D'

Sr. No.	Strain (mm/mm)	Stress (MPa)	Sr. No.	Strain (mm/mm)	Stress (MPa)
1.	0.0000	0.00	19.	0.0766	320.00
2.	0.0002	48.89	20.	0.0847	330.19
3.	0.0005	101.86	21.	0.0996	345.06
4.	0.0007	150.91	22.	0.1056	350.15
5.	0.0009	180.74	23.	0.1122	355.04
6.	0.0038	190.60	24.	0.1202	360.13
7.	0.0135	200.21	25.	0.1287	365.02
8.	0.0187	210.07	26.	0.1398	370.12
9.	0.0253	220.59	27.	0.1535	375.00
10.	0.0289	230.16	28.	0.1606	377.04
11.	0.0327	240.14	29.	0.1756	380.10
12.	0.0370	250.13	30.	0.2030	381.93
13.	0.0416	260.11	31.	0.2081	381.32
14.	0.0462	270.09	32.	0.2082	381.12
15.	0.0513	280.28	33.	0.2106	380.71
16.	0.0567	290.26	34.	0.2122	380.51
17.	0.0626	300.04	35.	0.2142	379.89
18.	0.0693	310.02	36.	0.2152	379.69

Appendix B

True Stress – Logarithmic Plastic Strain Data of EDD Steel Steels

B 1 True stress – logarithmic plastic strain data: EDD 'A'

Sr. No.	Log Strain (mm/mm)	True Stress (MPa)	Sr. No.	Log Strain (mm/mm)	True Stress (MPa)
1.	0.0000	294.00	**14.**	0.1428	447.52
2.	0.0221	343.13	**15.**	0.1684	459.06
3.	0.0279	355.80	**16.**	0.1785	461.48
4.	0.0336	364.04	**17.**	0.1834	462.83
5.	0.0508	371.62	**18.**	0.1884	464.18
6.	0.0565	377.53	**19.**	0.1934	463.54
7.	0.0621	384.74	**20.**	0.1983	464.89
8.	0.0706	390.62	**21.**	0.2032	465.24
9.	0.0813	401.31	**22.**	0.2177	467.75
10.	0.0897	411.24	**23.**	0.2278	469.34
11.	0.1060	420.11	**24.**	0.2377	472.78
12.	0.1166	425.98	**25.**	0.2477	474.87
13.	0.1324	438.78	**26.**	0.2577	476.12

B 2 True stress – logarithmic plastic strain data: EDD 'B'

Sr. No.	Log Strain (mm/mm)	True Stress (MPa)	Sr. No.	Log Strain (mm/mm)	True Stress (MPa)
1.	0.0000	245.70	23.	0.1938	385.13
2.	0.0001	259.53	24.	0.1986	388.99
3.	0.0003	262.00	25.	0.2035	394.44
4.	0.0003	263.90	26.	0.2180	406.32
5.	0.0165	269.04	27.	0.2291	415.24
6.	0.0224	273.35	28.	0.2323	417.18
7.	0.0283	278.55	29.	0.2464	420.83
8.	0.0340	283.23	30.	0.2604	425.29
9.	0.0512	290.46	31.	0.2740	430.22
10.	0.0569	294.85	32.	0.2876	434.41
11.	0.0625	302.66	33.	0.3010	439.79
12.	0.0710	305.68	34.	0.3142	443.30
13.	0.0817	313.28	35.	0.3272	448.22
14.	0.0902	316.98	36.	0.3400	452.54
15.	0.1171	327.80	37.	0.3527	456.54
16.	0.1242	333.75	38.	0.3652	460.84
17.	0.1329	339.25	39.	0.3776	465.27
18.	0.1434	345.79	40.	0.3898	469.38
19.	0.1689	358.33	41.	0.4018	473.99
20.	0.1753	366.59	42.	0.4138	477.90
21.	0.1838	372.19	43.	0.4256	481.84
22.	0.1888	380.09	44.	0.4372	485.71

B 3 True stress – logarithmic plastic strain data: EDD 'C'

Sr. No.	Log Strain (mm/mm)	True Stress (MPa)	Sr. No.	Log Strain (mm/mm)	True Stress (MPa)
1.	0.0000	277.34	22.	0.1985	409.76
2.	0.0002	279.03	23.	0.2034	414.09
3.	0.0003	279.93	24.	0.2099	419.13
4.	0.0164	289.41	25.	0.2131	423.53
5.	0.0223	296.91	26.	0.2322	432.35
6.	0.0282	299.15	27.	0.2463	436.21
7.	0.0340	303.95	28.	0.2603	439.59
8.	0.0511	311.54	29.	0.2740	443.40
9.	0.0568	316.05	30.	0.2876	447.77
10.	0.0624	321.84	31.	0.3010	450.62
11.	0.0709	328.26	32.	0.3141	451.54
12.	0.0816	333.79	33.	0.3271	455.17
13.	0.0901	338.80	34.	0.3400	459.58
14.	0.1170	353.71	35.	0.3527	463.68
15.	0.1241	359.16	36.	0.3652	468.06
16.	0.1328	364.16	37.	0.3775	472.57
17.	0.1432	371.32	38.	0.3897	477.88
18.	0.1688	386.75	39.	0.4018	482.98
19.	0.1751	393.36	40.	0.4138	487.76
20.	0.1837	397.48	41.	0.4190	489.37
21.	0.1887	400.66	42.	0.4230	490.30

B 4 True stress – logarithmic plastic strain data: EDD 'D'

Sr. No.	Log Strain (mm/mm)	True Stress (MPa)	Sr. No.	Log Strain (mm/mm)	True Stress (MPa)
1.	0.0000	180.89	**17.**	0.0932	379.44
2.	0.0029	191.32	**18.**	0.0986	387.14
3.	0.0124	202.91	**19.**	0.1045	394.89
4.	0.0175	214.00	**20.**	0.1116	403.44
5.	0.0239	226.17	**21.**	0.1191	412.00
6.	0.0273	236.80	**22.**	0.1288	421.85
7.	0.0310	248.00	**23.**	0.1407	432.56
8.	0.0351	259.38	**24.**	0.1468	437.58
9.	0.0395	270.94	**25.**	0.1597	446.85
10.	0.0439	282.58	**26.**	0.1826	459.47
11.	0.0486	294.66	**27.**	0.1868	460.67
12.	0.0537	306.72	**28.**	0.1870	460.48
13.	0.0592	318.80	**29.**	0.1889	460.87
14.	0.0654	331.51	**30.**	0.1903	461.27
15.	0.0721	344.50	**31.**	0.1919	461.28
16.	0.0796	358.16	**32.**	0.1927	461.39

Appendix C

Validation of Cohesive Zone Model (CZM)

1. **Thickness effect:** validation of cohesive zone model (CZM)
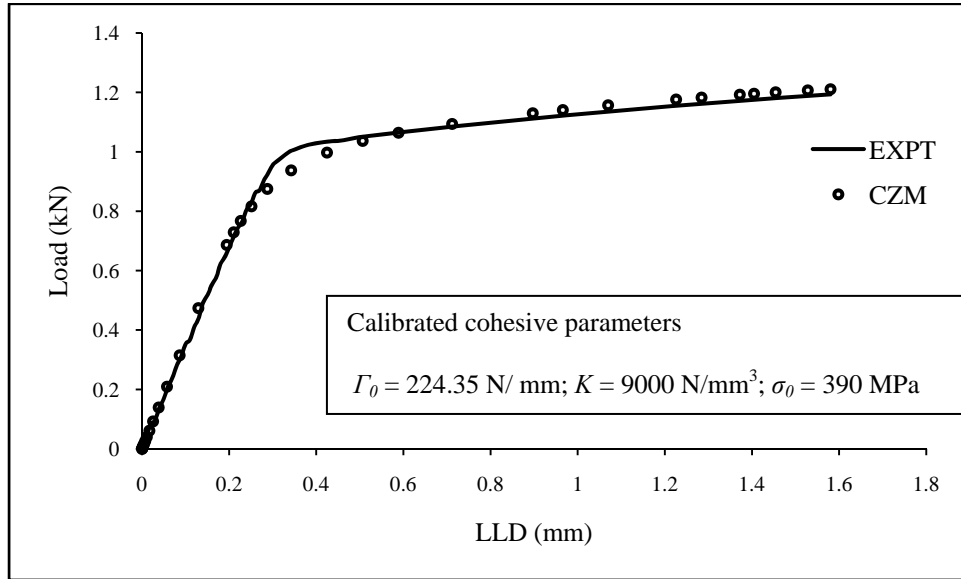
Fig C 1 Thickness effect (Specimen code T1; *B*=1.2 mm)
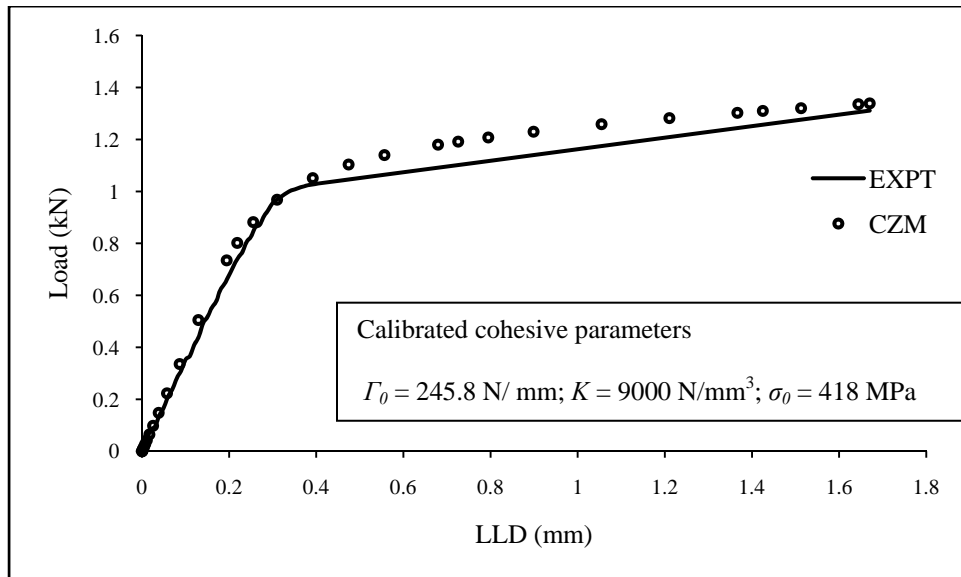
Fig C 2 Thickness effect (Specimen code T2; *B*=1.3 mm)
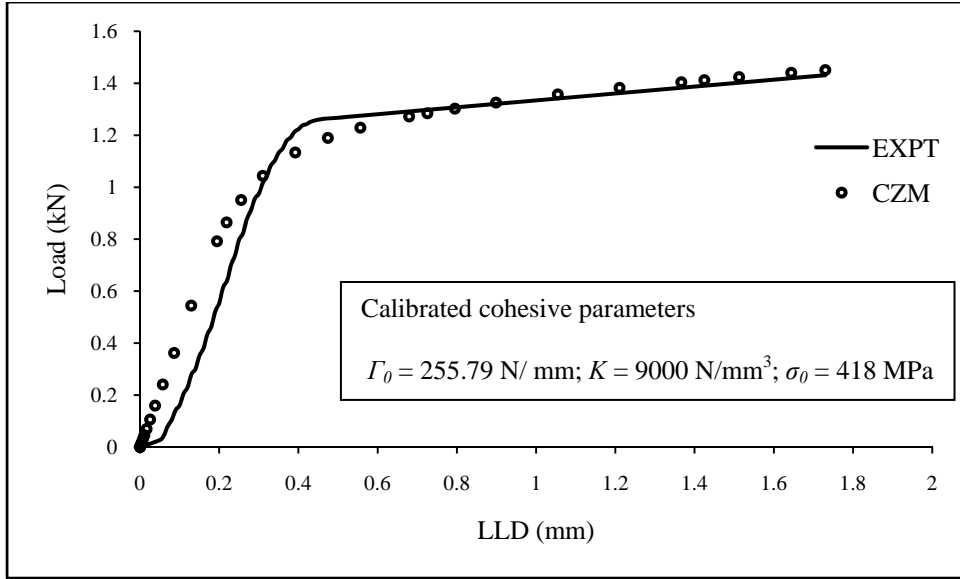
Fig C 3 Thickness effect (Specimen code T3; B=1.4 mm)
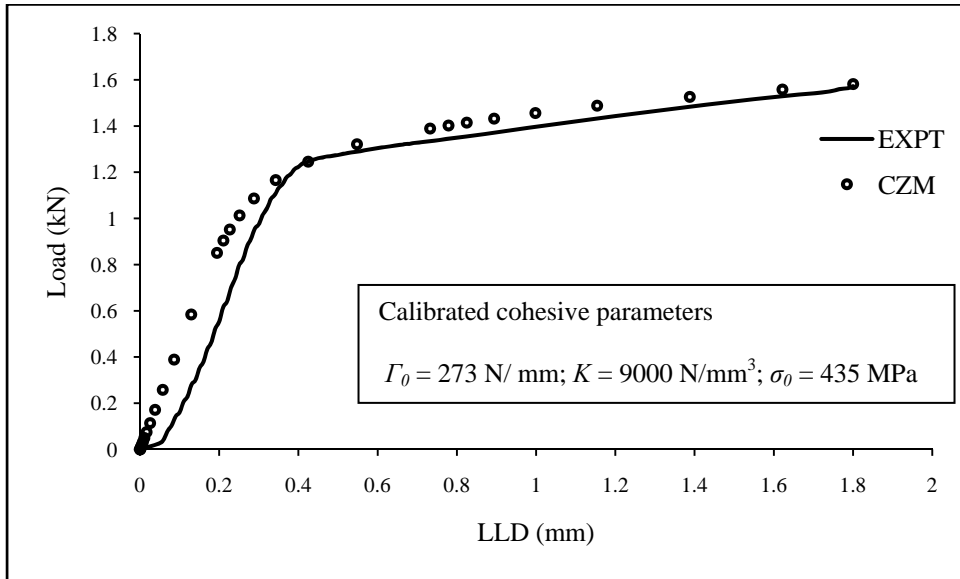
Fig C 4 Thickness effect (Specimen code T4; B=1.5 mm)
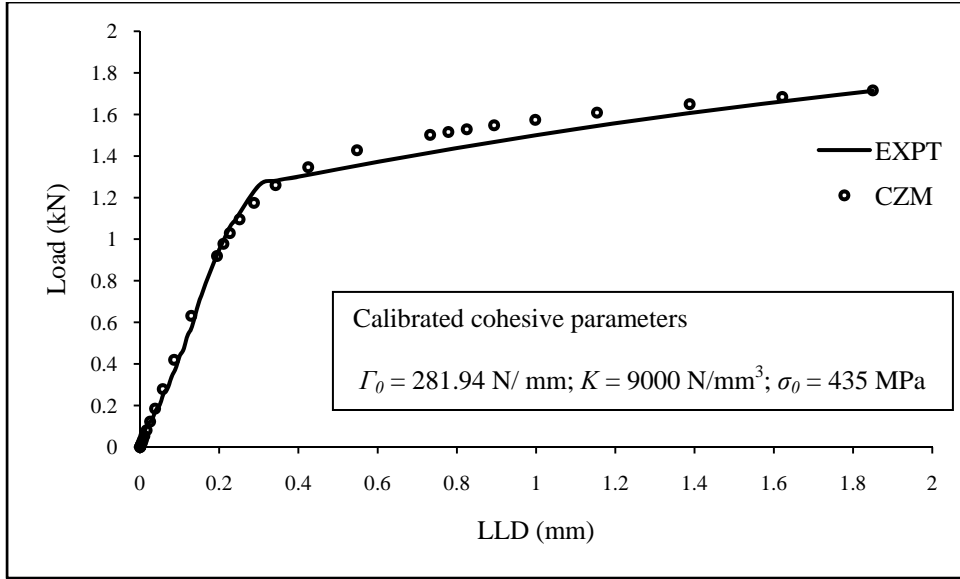
Fig C 5 Thickness effect (Specimen code T5; *B*=1.6 mm)
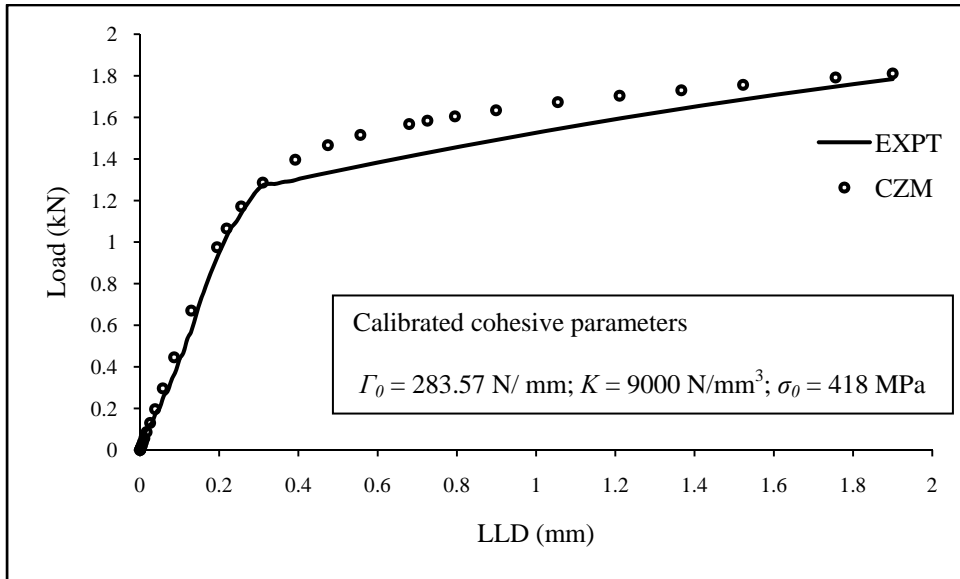
Fig C 6 Thickness effect (Specimen code T6; *B*=1.7 mm)

2. **Notch radius effect:** validation of cohesive zone model (CZM)

Calibrated cohesive parameters

$\Gamma_0 = 698.3$ N/ mm; $K = 10000$ N/mm^3; $\sigma_0 = 350$ MPa

Fig C 7 Notch radius effect (Specimen code N1; ρ=0.07 mm)

Calibrated cohesive parameters

$\Gamma_0 = 653.84$ N/ mm; $K = 10000$ N/mm^3; $\sigma_0 = 350$ MPa
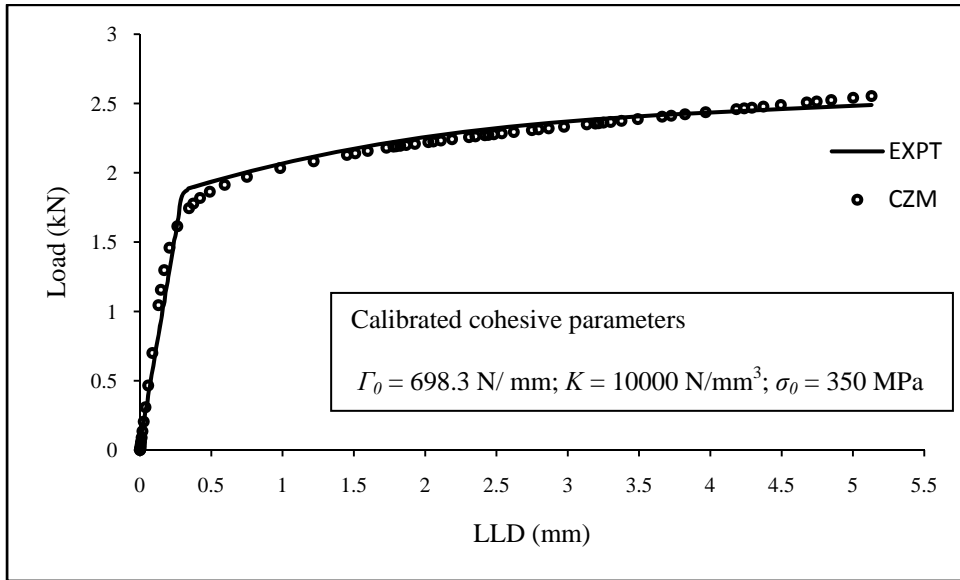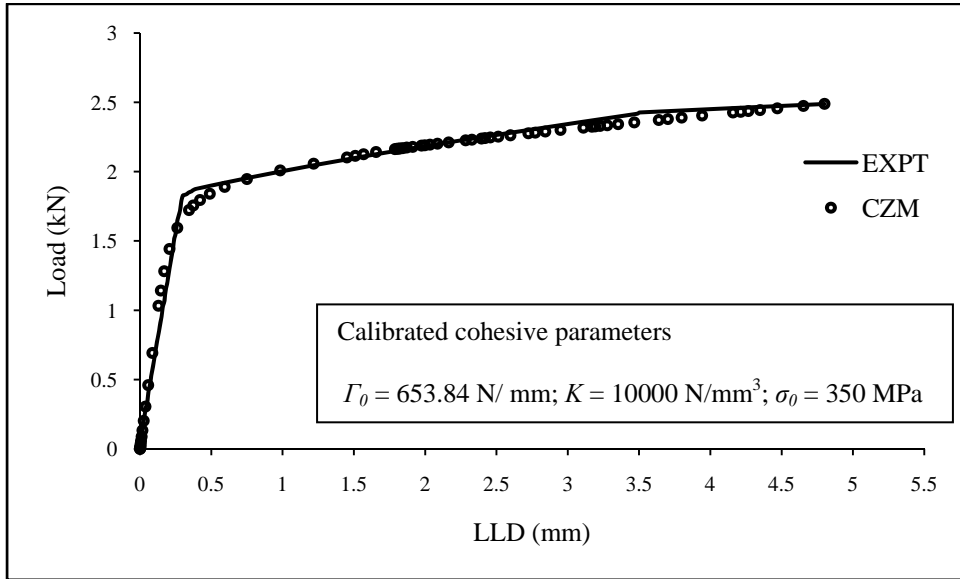
Fig C 8 Notch radius effect (Specimen code N2; ρ=0.085 mm)
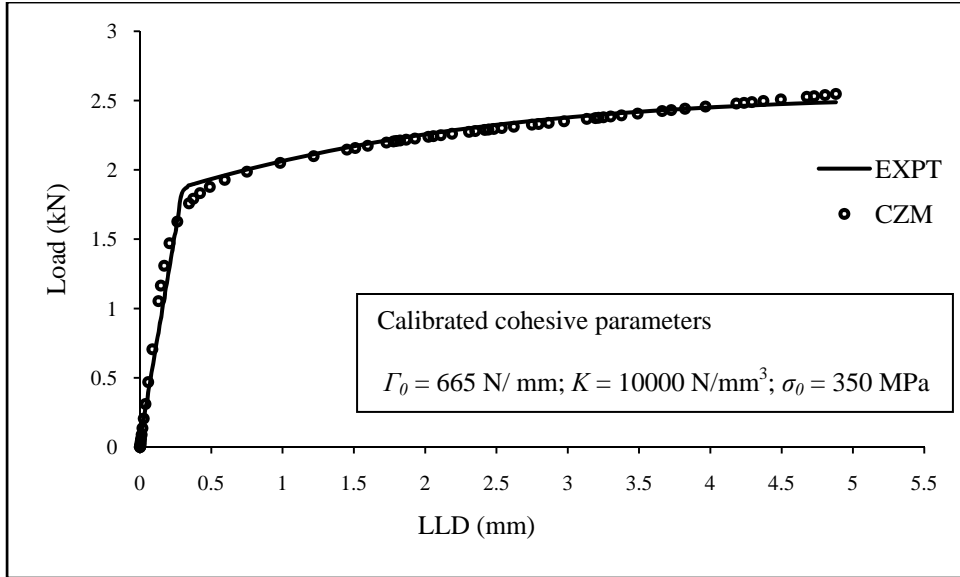
Fig C 9 Notch radius effect (Specimen code N3; ρ=0.1 mm)
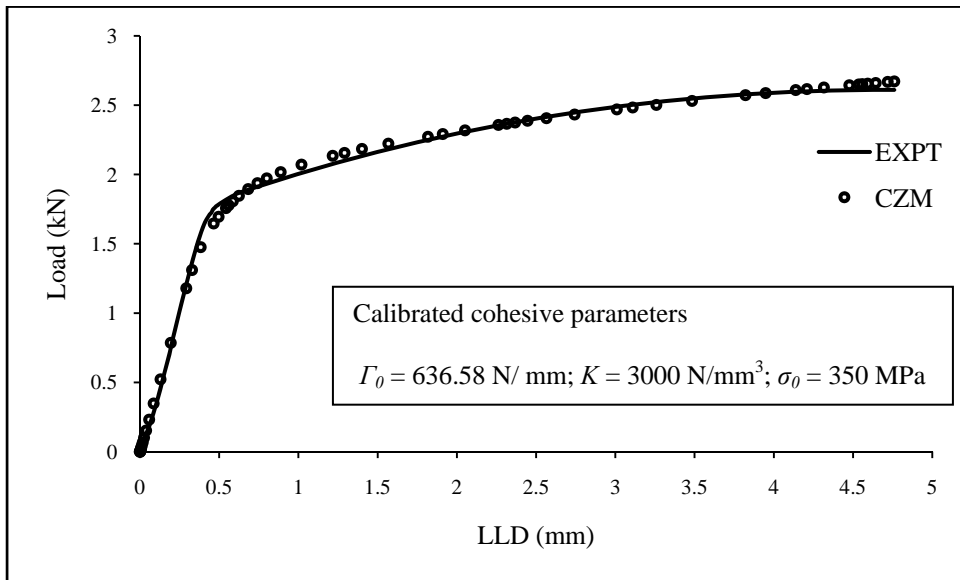
**Fig C 10** Notch radius effect (Specimen code N4; ρ=0.11 mm)
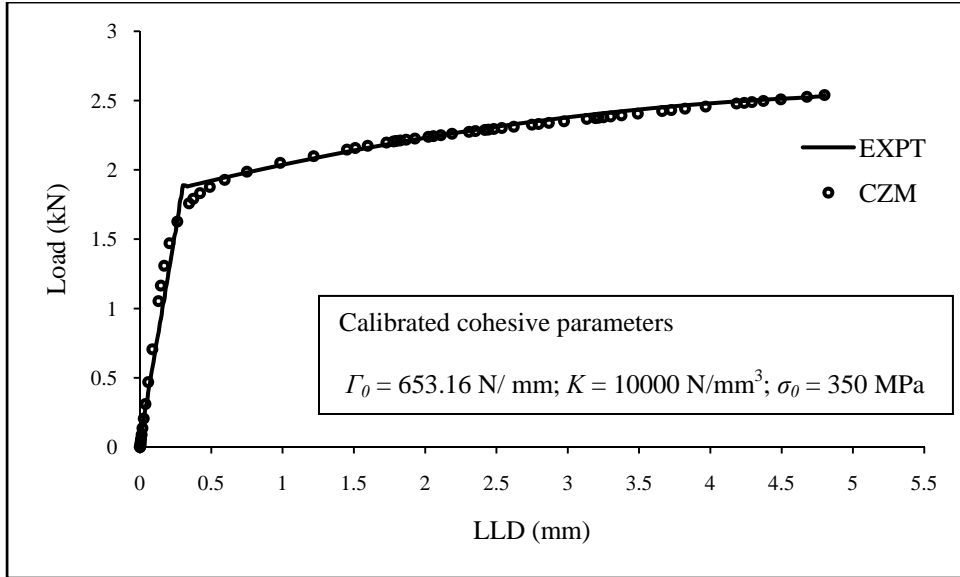
**Fig C 11** Notch radius effect (Specimen code N5; ρ=0.12 mm)
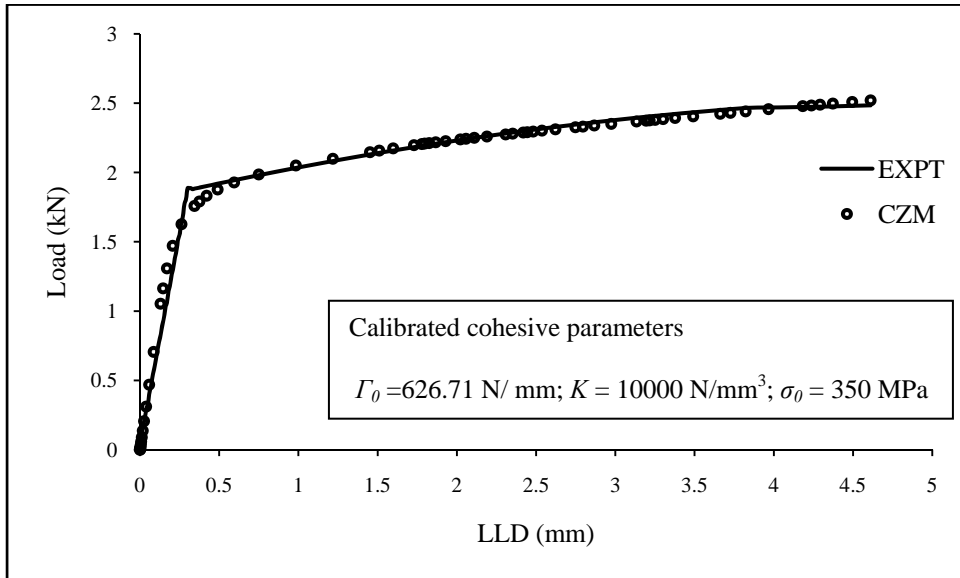
Fig C 12 Notch radius effect (Specimen code N6; ρ=0.13 mm)
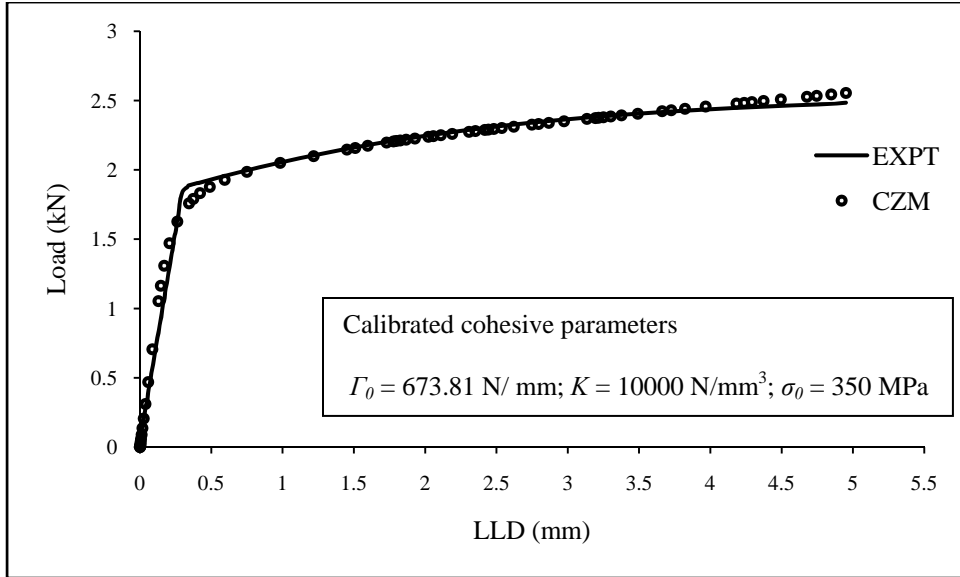
Fig C 13 Notch radius effect (Specimen code N7; ρ=0.14 mm)
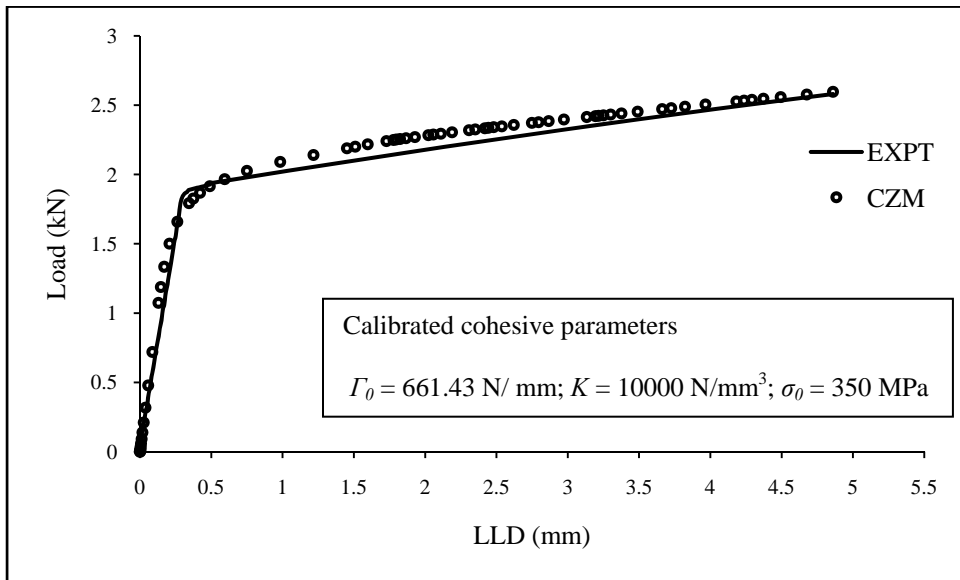
Fig C 14 Notch radius effect (Specimen code N8; ρ=0.15 mm)
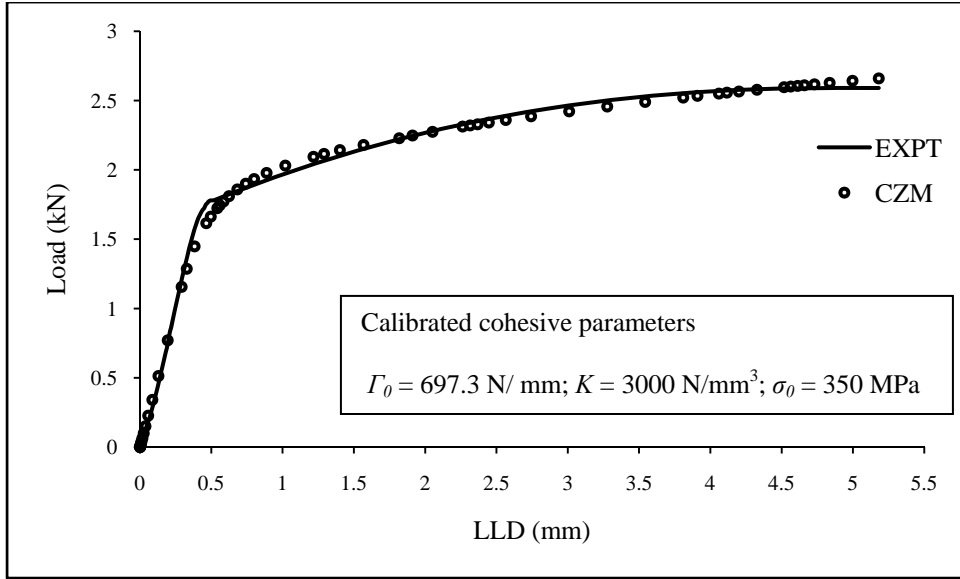
Fig C 15 Notch radius effect (Specimen code N9; ρ=0.16 mm)
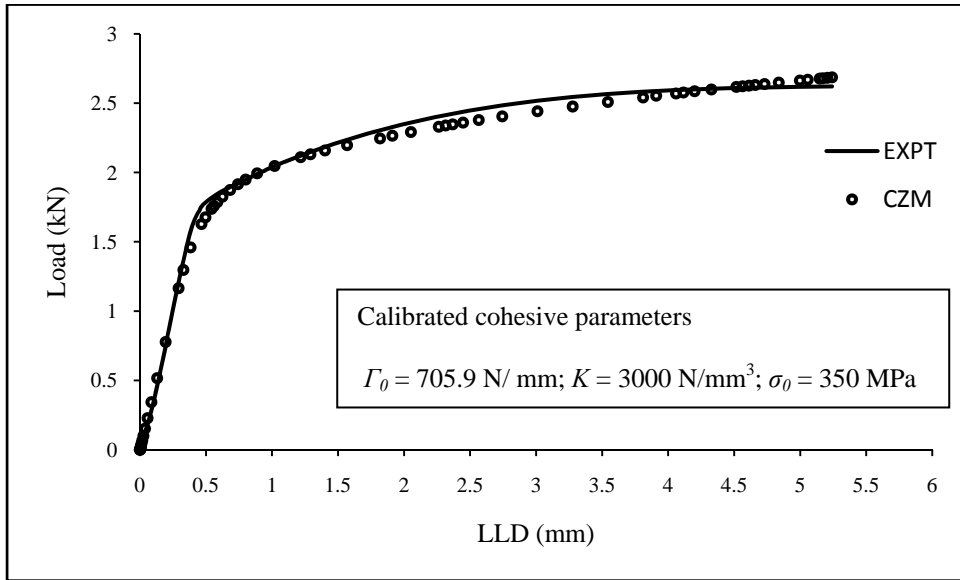
Fig C 16 Notch radius effect (Specimen code N10; ρ=0.17 mm)
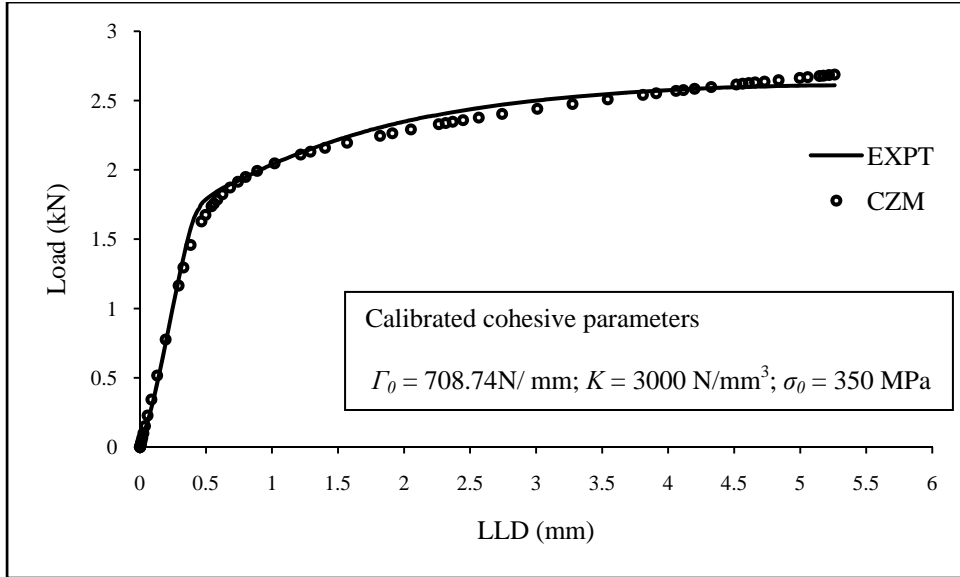
Fig C 17 Notch radius effect (Specimen code N11; ρ=0.18 mm)
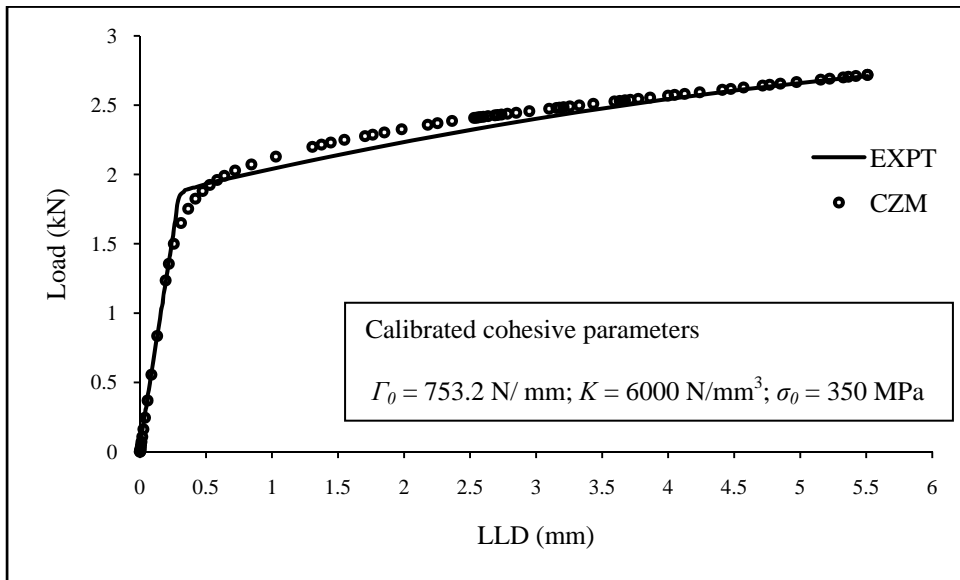
Fig C 18 Notch radius effect (Specimen code N12; ρ=0.25 mm)
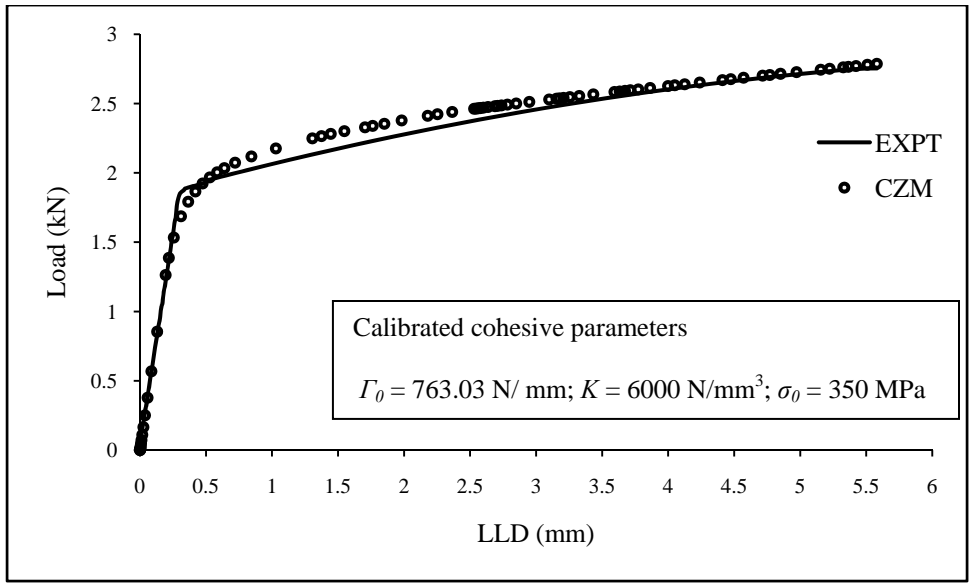
Fig C 19 Notch radius effect (Specimen code N13; ρ=0.4 mm)
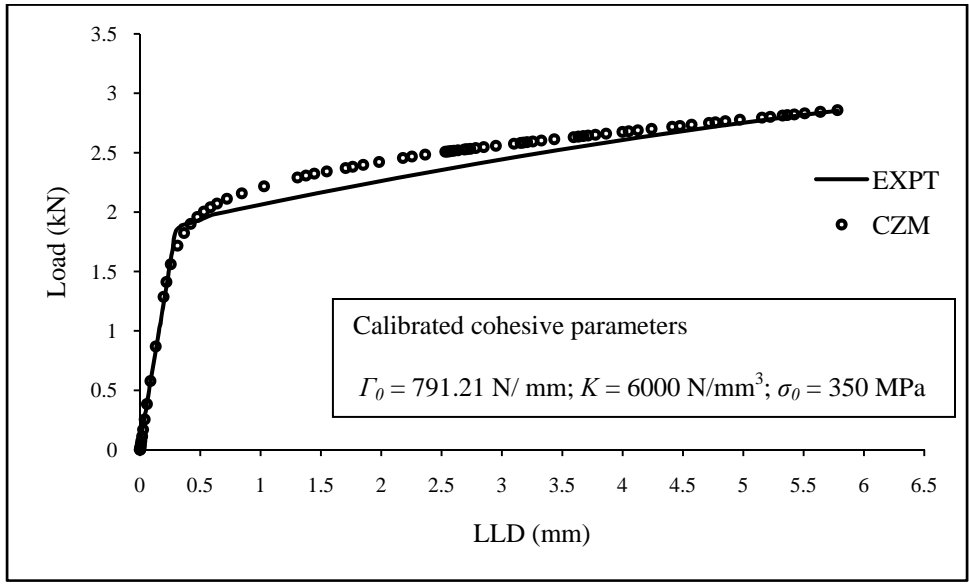
Fig C 20 Notch radius effect (Specimen code N14; ρ=0.6 mm)

132
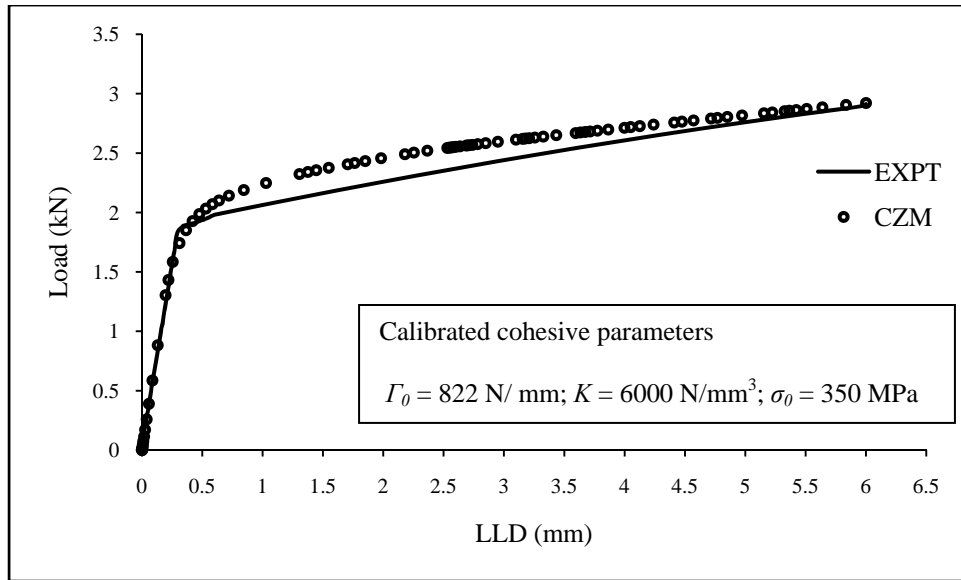
Fig C 21 Notch radius effect (Specimen code N15; ρ=0.75 mm)

3. **Strain rate effect:** validation of cohesive zone model (CZM)
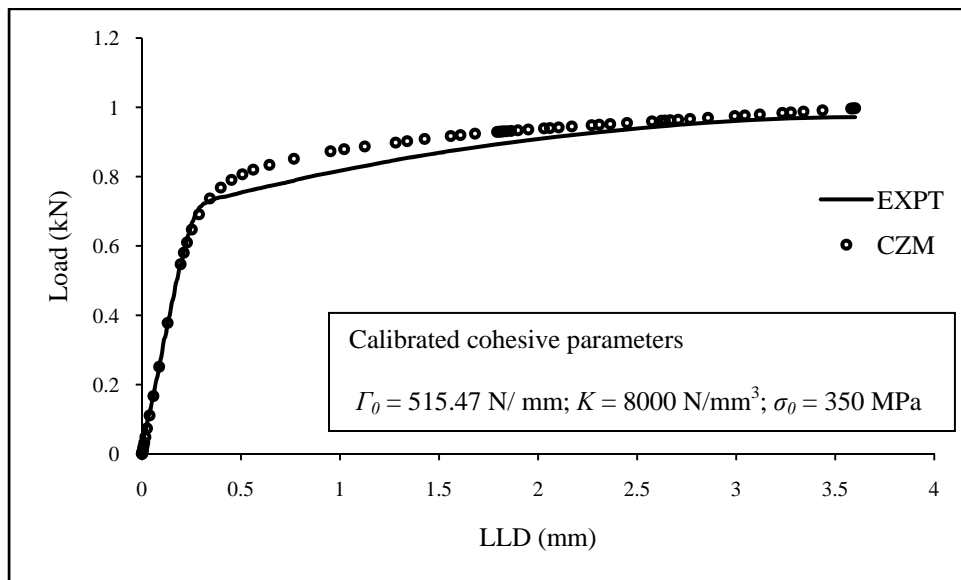
Fig C 22 Strain rate effect (Specimen code S1; 0.2 mm/min.)
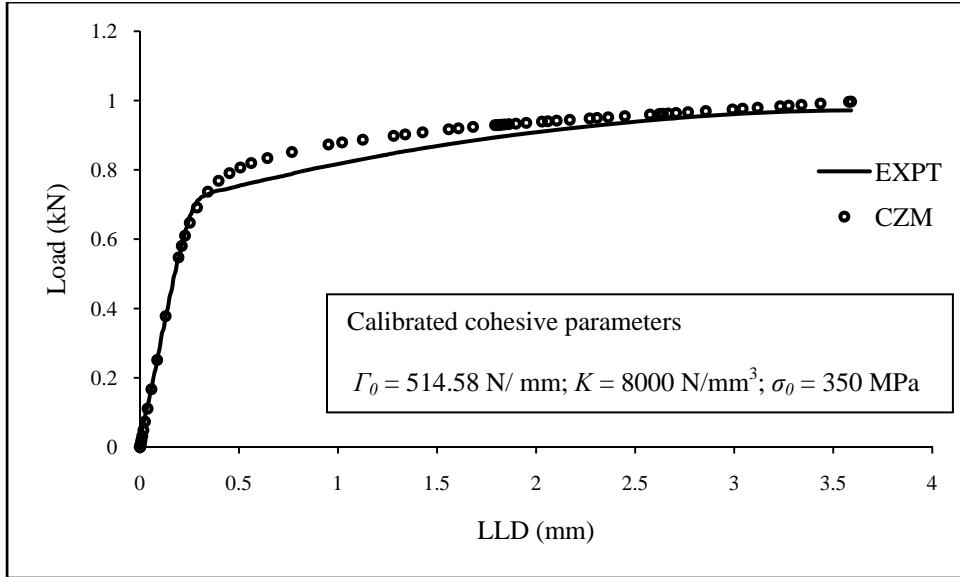
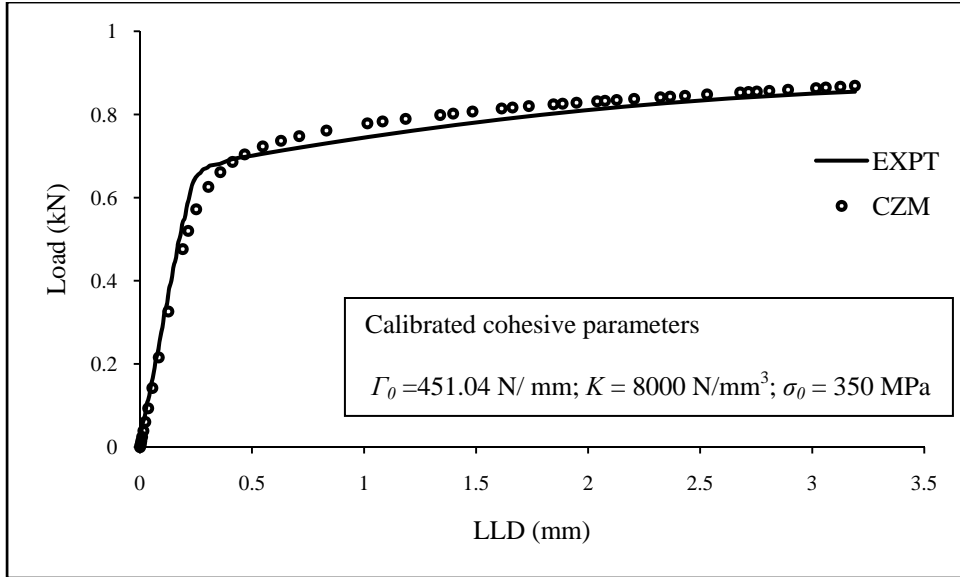**Fig C 23** Strain rate effect (Specimen code S2; 0.2 mm/min.)
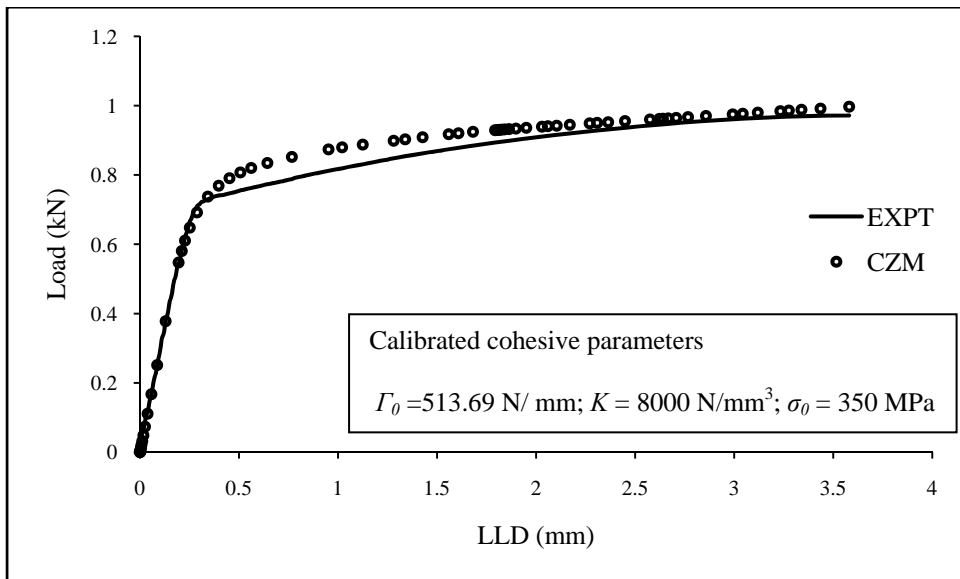
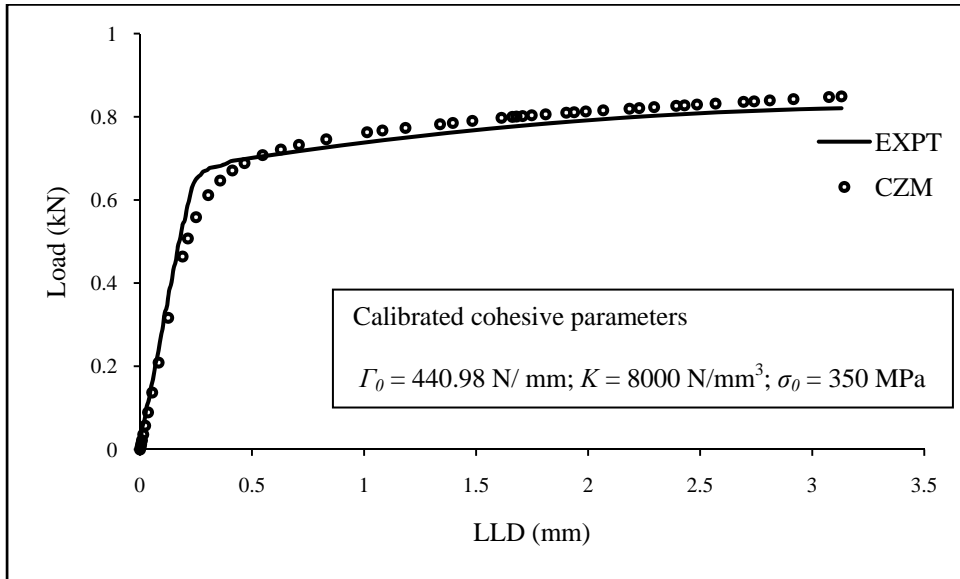**Fig C 24** Strain rate effect (Specimen code S3; 0.4 mm/min.)
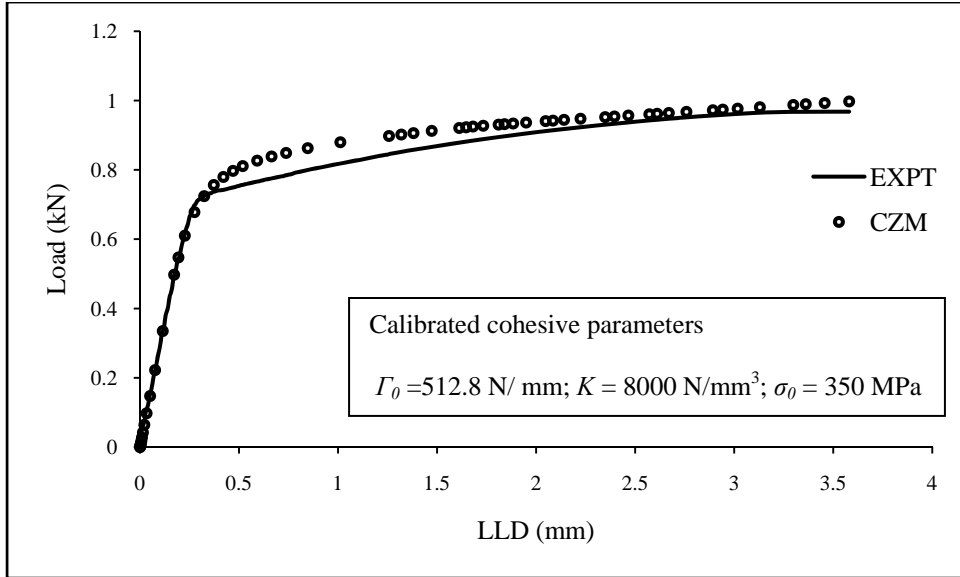
Fig C 25 Strain rate effect (Specimen code S4; 0.4 mm/min.)
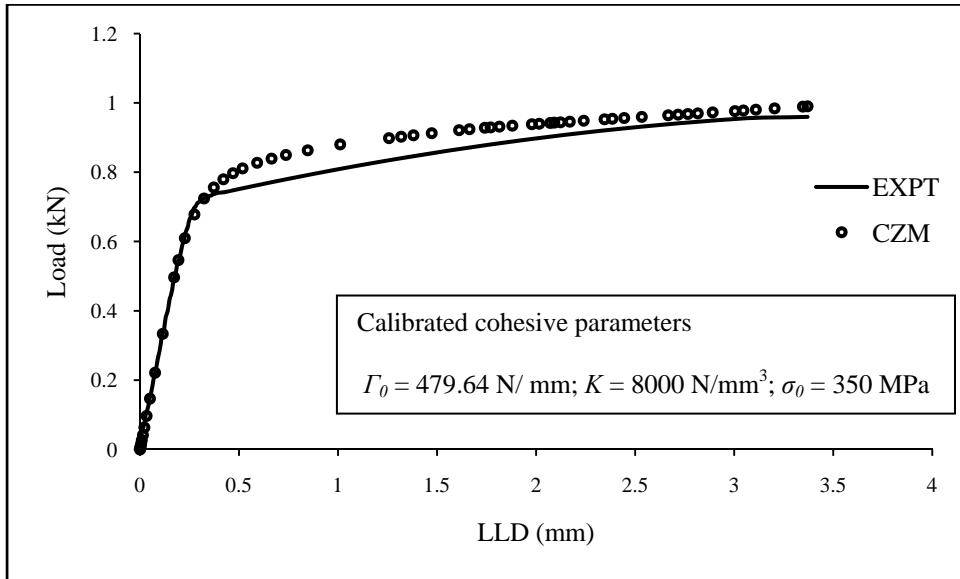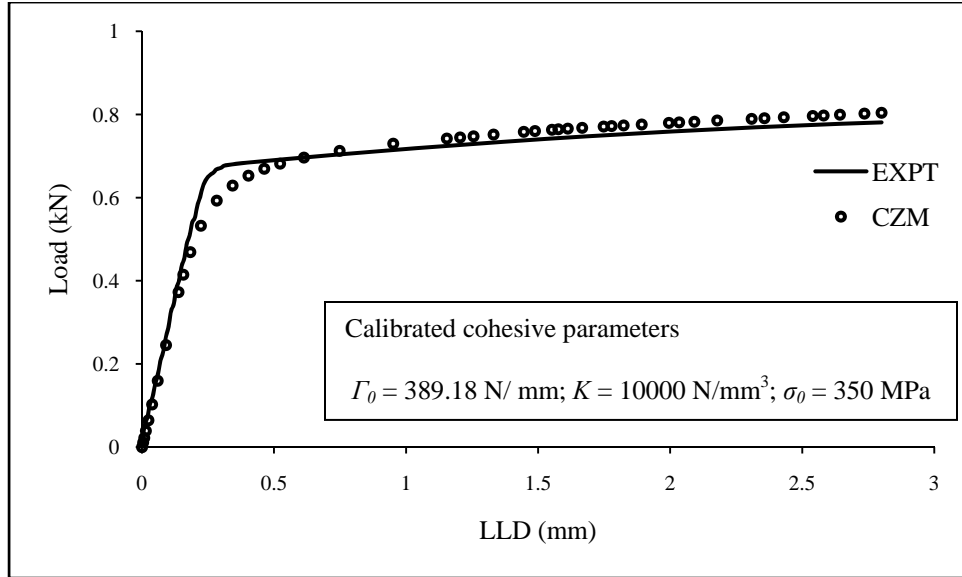

Fig C 26 Strain rate effect (Specimen code S5; 0.6 mm/min.)

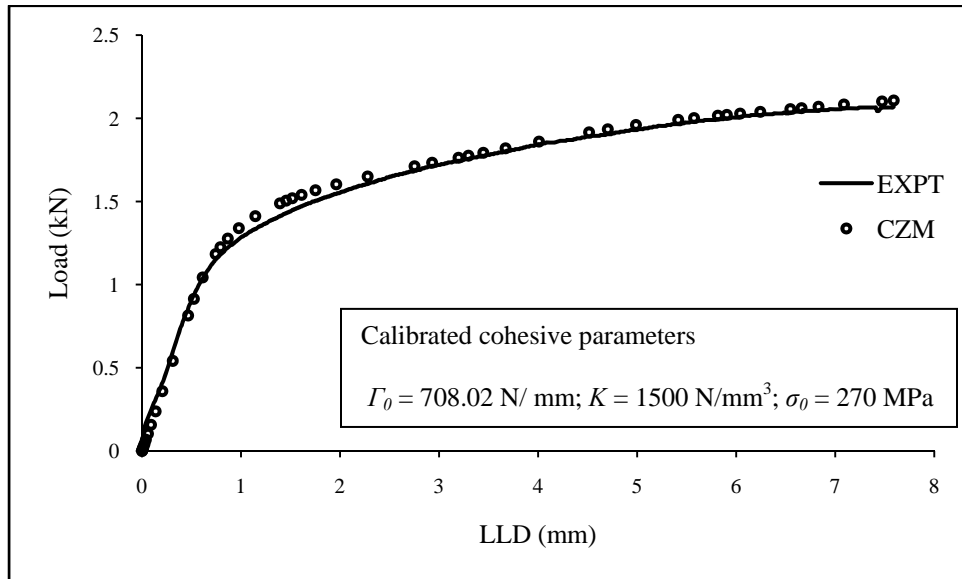**Fig C 27** Strain rate effect (Specimen code S6; 1 mm/min.)

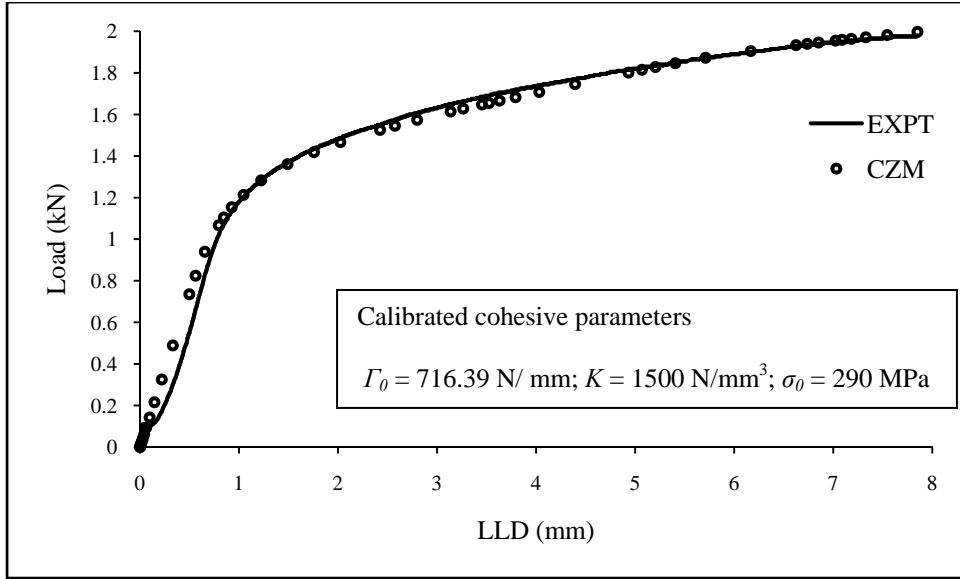**Fig C 28** Strain rate effect (Specimen code S7; 1.5 mm/min.)

136

Fig C 29 Strain rate effect (Specimen code S8; 2.5 mm/min.)

4. *a_0/W* **ratio effect:** validation of cohesive zone model (CZM)
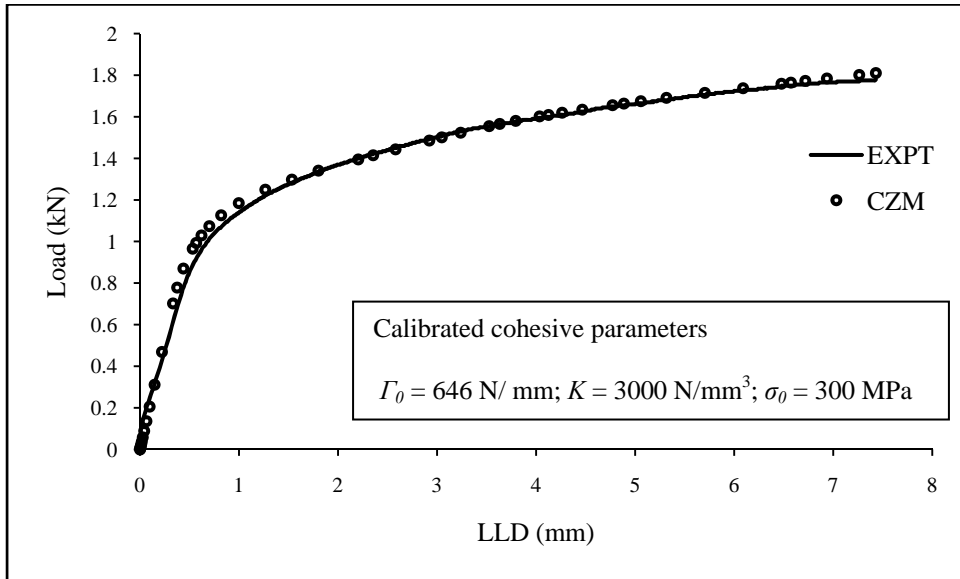

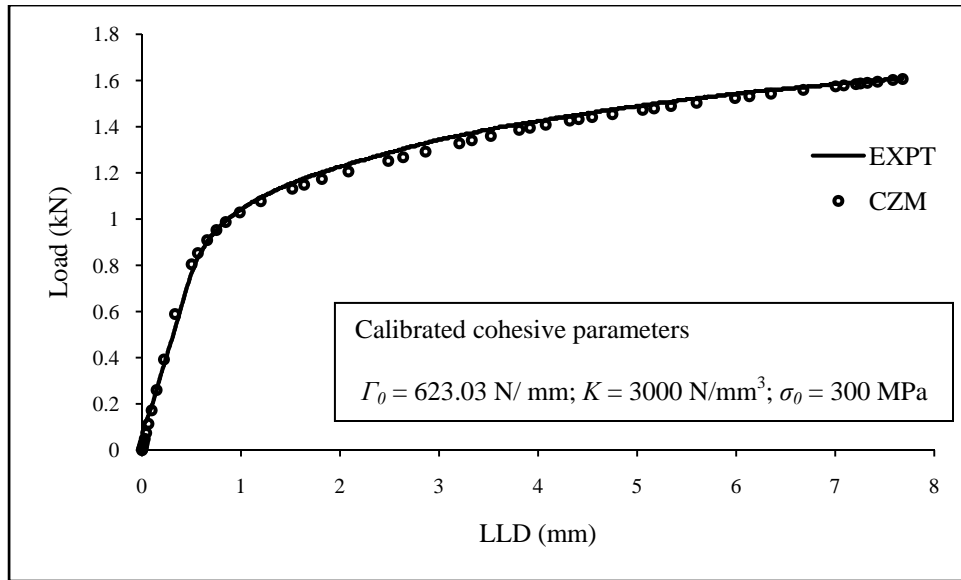**Fig C 30** *a_0/w* ratio effect (Specimen code A1; *a_0/w* =0.5)

Fig C 31 a_0/w ratio effect (Specimen code A2; a_0/w =0.525)
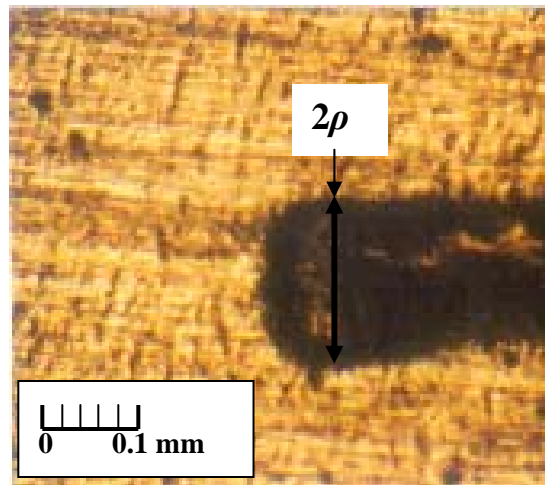

Fig C 32 a_0/w ratio effect (Specimen code A3; a_0/w =0.55)

138

Fig C 33 a_0/w ratio effect (Specimen code A4; a_0/w =0.575)

Appendix D

Measurement of notch radius using a micrograph (100X)

Appendix E

Specifications of machines and equipments used for the thesis work

1.   Computerised Universal Testing Machine

    Make   FIE, Kolhapur (INDIA)

    Model   UTS S10

    Capacity   100 kN

2.   CMOD Gauge

    Make   WAZAU, Germany

    Model   WAC 07.02.01 (for CT type specimens)

    Specifications   Measuring range   3-13 mm

3.   Microscope

    Make   KYOWA GETNER

    Specifications   Trinocular Inverted Metallurgical Microscope with 1200X with Material plus Image analysis software

4.   Polishing Machine

    Make   PYROMATIC

    Specifications   Cutt-off Machine- 100mm cut off wheel Dia 6"/ 8" 3 HP Motor

                          Polishing Machine- 10" Dia double Disc 0.5 HP Dc Motor

                          Mounting Press- Dia 32 mm 5Ton capacity with pressure guage

                          Belt Grinder- 500 X 100 mm wet and dry type 0.25 HP Ac Motor

5.   Chemical Analyser

    Make   Worldwide Analytical System WAS, USA

    Model   Model Foundry Master

6.   Gas Analyser

    Make   LECO Corporation, USA

    Model   CS-244

BRIEF BIOGRAPHY OF THE SUPERVISOR

Prof. D M Kulkarni is Associate Prof in Mechanical Engineering Department and Faculty In–charge in BITS Pilani, K K Birla Goa Campus. He has his Masters from IIT Kharagpur and PhD from BITS Pilani. He has 16 years of teaching and 2 years of industrial experience. His research area is Fracture Mechanics, Biomechanics and Advanced Finite Element Analysis. He has research grants from Industry and DST in the area of BioMechanics. He has published over 20 research papers in the international journal / conferences of repute. He has also published a book on Engineering Graphics with AutoCAD, which is implemented by many autonomous Universities. He has also published a chapter in a research book in the Bio-Medical Tribology Axisymmetric Contact Stress Analysis for Artificial Hip Joint. He is certified Instructor of American Society of Mechanical Engineering (ASME) to design the courses and train the industrial professionals in India. He has conducted hands-on training sessions in Advanced Finite Element Analysis at industrial sites in Maharashtra and Gujrath. He has been awarded 2 times (2011 & 2012) for Faculty Excellence for his contribution in Teaching, Research and Administration. He was also awarded by BITS alumni for 'Distinguished Faculty Award (2010). He is senior Membership of International Association of Computer Science and Information Technology (IACSIT) and member of Editorial Board, Intellectuals Society for Socio-Techno Welfare (ISST) Journal of Mechanical Engineering

BRIEF BIOGRAPHY OF THE CANDIDATE

Chaudhari Vikas Vinayak is a lecturer in the Mechanical Engineering department at the Birla Institute of Technology and Science, Pilani, KK Birla Goa campus, Goa, India. He has over 9 years of teaching experience. He has been teaching core mechanical courses like Fracture mechanics, Mechanics of solids, Materials technology and testing, Structure and properties of material etc. He completed his graduation in Mechanical Engineering from University of Pune in 2000. He obtained M. Tech degree in Machine Design from Institute of Technology, Banaras Hindu University (IT-BHU), Varanasi, India, in 2003. His area of research is Fracture Mechanics. He has published over 8 research papers in the international journal / conferences of repute (International Journal of Fracture, Fatigue and Fracture of Engineering Materials and Structures).